MODELING AND ANALYSES OF ELECTROLYTIC IN-PROCESS DRESSING (ELID) AND GRINDING

K. FATHIMA PATHAM

NATIONAL UNIVERSITY OF SINGAPORE

2004

ACKNOWLEDGEMENTS

Firstly, I would like to thank my supervisors Professor M. Rahman and A/P A. Senthil Kumar for their invaluable guidance, support, motivation and encouragement. I am indebted to them for their patience and the valuable time that they have spent in discussions.

I would also like to thank Dr. Lim Han Seok for his great support and positive critics which made my project successful.

Special thanks to Professor B.J. Stone (Western University of Australia), Professor Stephan Jacobs (Rochester University) and Mr. Miyazawa (Fuji Die Co.,) for their encouragement and support.

I would also like to thank all the staff of Advanced Manufacturing Laboratory, especially Mr. Lim Soon Cheong for his technical support. Finally, I would like to thank all my student friends in NUS for their support and help. I am indebted to my family members for their support provided to achieve my ambition.

Last but not least, I give all the glory to GOD who provided me sound health and mind to finish my project.

TABLE OF CONTENTS

Summary

The applications of hard and brittle materials such as glass, silicon and ceramics have been increasing due to their excellent properties suitable for the components produced in the newer manufacturing industries. However, finishing of those materials is a great challenge in the manufacturing industries until now. Several new processes and techniques have been implemented in order to finish the difficult-to-machine materials at submicron level. Grinding is a versatile and finishing process, which is generally used for finishing hard and brittle work surfaces up to several micrometers. The greater control realized on the geometry (geometrical accuracy) of the work during the fixed abrasive processes replenish the old grinding process into newer manufacturing. Finishing of non-axi-symmetric components with the aid of finer abrasive grinding wheels eliminates the necessity of polishing, which also increases the geometrical accuracy because the final shape could be achieved in a single machining setup and process. However, several difficulties have been experienced while manufacturing and machining with nanoabrasive (size of the abrasive in nanometers) grinding wheels and hence the fixed abrasive grinding process such as nanogrinding is not used as a robust method for finishing components made of hard and brittle materials. Grinding wheels made of harder metal bonds provide sufficient strength to hold the micro/nanoabrasives, but the wheels need a special dressing process in order to establish self-sharpening effect for uninterrupted grinding.

The Electrolytic In-process Dressing (ELID) is a new technique that is used for dressing harder metal-bonded superabrasive grinding wheels while performing grinding. Though the application of ELID eliminates the wheel loading problems, it makes grinding as a hybrid process. The ELID grinding process is the combination of an electrolytic process

and a mechanical process and hence if there is a change in any one of the processes this may have a strong influence on the other. The ambiguities experienced during the selection of the electrolytic parameters for dressing, the lack of knowledge of wear mechanism of the ELID-grinding wheels, etc., are reducing the wide spread use of the ELID process in the manufacturing industries. There were no general rules or procedures available to choose the electrical parameters for good association with the grinding parameters. Therefore, fundamental analyses are necessary in order to understand the hybrid process and to minimize the difficulties arise during its implementation.

This project is mainly focused on the fundamental studies on the ELID grinding. A wide variety of experiments were conducted by varying the electrical parameters and grinding parameters in order to analyze the influence of one process to the other (influence of the electrolytic process on grinding and vise versa). The analysis strongly evident that the oxidized layer produced during the ELID influences the grinding forces, the wear mechanism and the quality of the ground surface, which lead for a detailed analysis on the ELID-layer (oxidized layer). The investigations show that the thickness and the micro/nanomechanical properties of the ELID-layer were found to be different when the grinding wheel was dressed using different electrolytic dressing parameters. When grinding is performed using micro/nanoabrasive grinding wheels, the oxidized layer acts as a binder for the active grits, which produces the discrepancies during the mico/nanoELID grinding. An analytical model has been developed for ELID grinding and it has been substantiated by the experimental investigations. The research work conducted in this project will be more helpful to promote better understanding while implementing the ELID, and to improve its robustness in the field of precision manufacturing.

Nomenclatures

a – Depth-of-cut in μm

a_c – The area of contact between the asperities

A_a – The apparent area of contact between the wheel and work

A_e – Area of the electrode in mm^2

A_g – Grinding area (grinding width x contact length) in mm^2

A_r – The real area of contact between the wheel and work

b – Grinding width in mm

d – Distance between the contact planes

d_c – The critical-depth-of-cut of the work

d_g – Mean grit size in μm

dR – Radial wear in mm

D_{sum} – The surface density of summits on the brittle surface

D_w – Wheel diameter in mm

E_w – The Modulus of elasticity of the work material

E_s – The Modulus of elasticity of the ELID layer.

f_h – Holding force per grit

f_g – Grinding force per grit

F_h – Total holding force

F_N – Normal force

F_T – Tangential force

F_n' – Normal specific force in N/mm

f_v – The volume percentage of the diamond grits

G – Grinding ratio

$g(z)$ is the probability of height distribution

H – Hardness of the work material

h_{eq} – Equivalent-chip-thickness

h_{max} – Maximum chip thickness or grit depth of cut in µm

$\overline{h_s}$ - The summit height normalized by summit rms

I_d – The current density in A/cm^2

I_p - Input power in A

K_c – Fracture toughness of the work material

k – ELID dressing constant

k_1 – Constant related to wheel topography

k_2 – Constant related to material properties

l_c – Contact length in *mm*

L_s - Distance between the adjacent grits

L_w – Circumference of the wheel in *mm*

m – Material removal by electrolysis in mm^3/min

N – Numbers of active grits per unit area

N_{g1} – Number of active particles in unit area of the diamond layer in cm^2

N_{av} – The active grit density or Number of active grits per unit area of the wheel

N_g – The number of grits per unit area

N_a – The number of active grit per unit area

N_i – The number of inactive grits per unit area of the grinding wheel

N_{cont} – The number of contact between the asperities

N_s – The spindle rotation in *rpm*

N_v – number of diamond particle in the diamond layer

R –The composite or effective curvature

R_a – Average surface roughness

R_c – Current duty ratio (T_{on} / (T_{on} + T_{off}))

R_s – The radius of the asperity on the wheel surface

R_p – Radius of the plastic zone

R_t – Peak to valley roughness

R_w – the radius of the asperity on the work surface

S – Sharpness factor depends on condition of the grit (size and sharpness)

T – Period in μs

T_c – Charging time of the double layer

T_d – Charging time of the double layer

T_{on} – Pulse on time in μs

T_{off} – Pulse off time in μs

v_w – Feed rate in *mm/min*

v_s – Velocity of the grinding wheel *mm/min*

V_m – Volume of material removal from the workpiece in mm^3

V_w – Volume of material removal from the wheel in mm^3

V_l - the volume of the diamond layer

V_p – Peak voltage

W is the load applied on perpendicular to the surface in contact

W_l – The ratio of the electrode to the wheel perimeter in mm

$\bar{z}_m$ is the non-dimensional mean height

Greek letters

α,β – The normal force components of f_g

δ - the displacement within the contact between the asperities

μ – Frictional co-efficient depends on the work/bond material

ρ – Constant related to the topography of the grinding wheel

Δh – The height difference between the active grits

γ_w - The Poisson ratio of the work material

γ_s - The Poisson ratio of the ELID layer

σ - The standard deviation and

σ_s – Yield strength of the layer

LIST OF FIGURES

List of Tables

Appendix

Chapter 1

Introduction

1.1 The requirement of the micro/nanogrinding

Applications of hard and brittle materials have been increasing in the recent years due to their excellent properties suitable for the optical, electrical and electronics industries. High geometrical accuracy and mirror surface finish are the main requirements for components produced in the optical industries. Machining with either fixed or loose abrasives with decreasing abrasive sizes are generally used to establish the desired shape and surface finish. This conventional finishing process requires several processing steps such as microgrinding, lapping and polishing. Microgrinding is used to produce the required geometry, and then the final finish is obtained using lapping and polishing processes. However, this method of finishing is limited to the geometrical shapes such as plain and spherical surfaces. Aspheres are the recent interest in the optical industries, which may be difficult to produce using the existing conventional processes. Automobile and aeronautic industries use ceramics for producing components such as automobile engine parts and turbine blades, which also find difficult to manufacture using the conventional methods [Blaedel et al., 1999].

Grinding is a versatile finishing process which is normally used for finishing components up to a surface roughness of few micrometers. However, it is possible to

produce various geometrical shapes using grinding with the aid of CNC (Computerized Numerical Control) machines and fixed abrasive tools (grinding wheels). The surface produced by grinding usually produces two different types of layers on the ground surface. The layer in which the roughness is measured is known as the surface relief layer and the layer beneath is known as the damaged layer. An array of microcracks beneath the finished surface leads to strength degradation, which reduces the life of the finished components. Therefore, the damaged layer should be removed using a process which does not make an additional damage on the surface. Loose abrasive polishing can be used to eliminate the surface defects but it is only suitable for limited applications, and it also experience difficulties such as poor geometrical accuracy and undetermined polishing time. Finally, the micro/nanogrinding was found to be an alternative and an efficient process because it removes the damaged layer without producing any additional subsurface damages and controls the final geometry [Blaedel et al., 1999].

1.2 Difficulties encountered during micro/nanogrinding

Although grinding with micro/nanoabrasive grits is an efficient method to finish the brittle materials, the method is not robust due to several difficulties experienced during real applications. There are many difficulties associated when manufacturing superabrasive grinding wheels. The major problem is the preparation of the bonding matrix for the superabrasives. The superabrasives should be held firmly by the bonding system while grinding. The grit holding ability can be increased using harder metal-bond, but self-sharpening ability of the grinding wheel become very poor and, truing and dressing of harder metal-bonded grinding wheels also become difficult. Because of

the smaller protrusion height of the superabrasives the problem of wheel loading and glazing increases, which diminishes the effectiveness of the grinding wheel. Periodical dressing is essential to eliminate the difficulties such as wheel loading and glazing, which makes the grinding process very tedious.

1.3 Remedies

Different dressing methods have been proposed for continuous dressing of superabrasive wheels. One method is introducing loose abrasives into the grinding fluid and the other is using a multi-point diamond dresser. Some in-process methods like passing the grinding wheel on an alumina stick during grinding are also used [Blaedel et al., 1999]. Among the dressing processes, the Electrolytic In-process Dressing (ELID) is found to be a simple and efficient technique that utilizes electrolysis for dressing metal-bonded grinding wheels. During the ELID, the metal-bond is slowly corroded and the corrosion product is then mechanically removed by abrasion during the grinding process. This method removes the swarf from the bonding matrix as well as produces enough grain protrusion. In some grinding wheels such as cast iron-bonded wheels, a protective layer is formed on the grinding wheel during electrolysis and it resists the current flow. So, the conductivity of the grinding wheel is reduced after every dressing due to the oxidized layer deposition, which also prevents the bonding material from further oxidization. The grinding wheels that can produce such a protective layer during electrolysis are more suitable for in-process dressing.

Different grinding wheels made of metals and alloys such as cast iron, cobalt, copper, bronze, cast iron-cobalt, etc., can be dressed using the ELID. However, the thickness of the protective oxide layer and its resistance to current depends on the bond material of the wheel, the power supplied and the electrolyte chosen. When the protective oxide layer is removed during grinding by the chip/wheel interactions the in-process dressing is stimulated. Thus the condition of the grinding wheel topography is maintained throughout the grinding process that encourages the continuous application of the metal-bonded grinding wheels.

1.4 Objective of this study

Grinding is the finishing process which mainly depends on the operator skill when compared to other machining processes. Finishing components of complicated shapes using fine grinding process requires more skills. However, grinding with the aid of the ELID increases the complicateness of the process though it is an efficient method for finishing brittle materials. There is a great difficulty of selection of the ELID parameters with respect to the grit size of the grinding wheel, bond-material, and the grinding parameters, which restrict the application of the ELID. This may be apparently one of the reasons some industries still using resin-bonded grinding wheels for fine grinding. Therefore, the main objective of this project is to increase the robustness of the ELID by eliminating the ambiguities encountered during ELID grinding.

A study on the fundamental mechanism of the ELID becomes necessary for better understanding, which includes the influences of the ELID parameters on the grinding

forces; surface finish and the wheel wear. The influence of the grinding parameters on the ELID must be evaluated for selecting suitable grinding conditions. The wear mechanism of the ELID-grinding wheels should be experimented in order to achieve better geometrical accuracy and tolerance. Investigation of the ELID-layer is inevitable for better understanding and controlling of the ELID grinding.

Model for micro/nanogrinding with the aid of the ELID has been proposed in order to reduce the cumbersome grinding experiments. The model should be useful to predict the grinding forces for a particular work surface and a particular bond dressed at a defined conditions. The simulated grinding forces at different dressing conditions will be more useful in order to choose the efficient dressing and grinding conditions during ELID grinding.

1.5 Thesis organization

This thesis consists of nine chapters. Chapter 1 gives an introduction to the work done in this research. In chapter 2, the literature review of the ELID techniques, principles of the ELID, different techniques and the applications of the ELID are presented.

Chapter 3 explains the basic principle and the classifications of the ELID. The principle of the electrolysis, the basic components of the ELID, classification and the mechanism of the ELID are described. The description of experimental setup, grinding experiments, measuring equipments and the measuring techniques have been explained in Chapter 4.

Chapter 5 explains the fundamental studies conducted on ELID grinding. The influence of the ELID parameters on the grinding forces, surface finish and wheel wear are investigated.

The wear mechanisms of the ELID-grinding wheels are discussed in the Chapter 6. The characters of the ELID-grinding wheels, the wear of wheels during pre-dressing and during in-process dressing have been explained in detail. The influence of the wear of grinding wheels for different geometrical surfaces has been experimented. The wear reduction strategies are also proposed.

Chapter 7 contains the investigations on the ELID-layer. The mechanical properties of the ELID-layer are investigated, which provides necessary information about the layer needed for achieving defect free grinding.

Chapter 8 proposes a model for Micro/nanoELID grinding. This model helps to predict the bond material and suitable dressing conditions for a particular work material by comparing the simulated grinding forces at various ELID dressing conditions.

Chapter 9 contains the main conclusions and main contributions drawn from this project. The suggestions for future work is also presented and discussed in this chapter.

Chapter 2

Literature review

The ELID technique originated from Japan, and most of the works reviewed were reported from Material Fabrication Lab, RIKEN, Japan. The previous relevant reports are systematically arranged, classified and presented in this chapter. This chapter covers the development and mechanism of ELID, different methods of ELID grinding and various applications of the ELID grinding in the field of precision manufacturing. The advantages and drawbacks of the ELID grinding is analyzed and presented at the last section of this chapter.

2.1 Development and mechanism of the ELID grinding

Murata et al. [Murata et al., 1985] introduced ELID in 1985 for the application of abrasive cut-off of ceramic. The structural ceramics are highly difficult to grind due to its hard and brittle nature. Normally for grinding harder materials, the softer grade grinding wheels have been used. But, the softer grinding wheels have the problem of large diameter decrease due to wheel wear. Therefore, stronger bond with harder abrasives have been selected for grinding hard and brittle materials. When the grits are worn out, a new layer in the outer surface is electrolyzed and necessary bonding is removed from the grinding wheel surface in order to realize grit protrusion. The experiments were performed using metal bonded grinding wheels (not specified) of grit size #80, #100, #150 and #400. The results showed that the grinding force was reduced

to a significant amount when the in-process dressing was done. Even though the surface finish is not a major criterion in abrasive cut-off, the surface roughness also improved due to the application of the ELID. The experiments show that ELID is an effective process of increasing surface quality even though it has some problems like rust formation due to electrolyte application [Murata et al., 1985].

Ohmori et al. [Ohmori and Nakagawa, 1990] further improved ELID suitable for superabrasive grinding wheels. Different types of grinding wheels have been used along with ELID grinding [Ohmori et al., 1999, 2000]. The grinding wheels used in ELID are broadly classified into the following:

- Metal-bonded diamond grinding wheels and
- Metal-resin-bonded diamond grinding wheels

Normally cast iron or copper is used as the bonding material. Some amount of cobalt can also be included in the bonding material for better grinding performance. Metal and resin are mixed into a definite ratio in order to get a good grinding performance. Normally copper is used as a bonding material for metal-resin bonded grinding wheels. The grades of the grinding wheels are ranging from #325 to #300,000, which has an average grit size from 38 μm to 5 nm. The basic ELID system consists of a metal bonded diamond grinding wheel, an electrode, a power supply and an electrolyte [Ohmori and Nakagawa, 1990].

2.2 Different methods of ELID grinding

ELID is classified into four major groups based on the materials to be ground and the applications of grinding, even though the principle of in-process dressing is similar for all the methods. The different methods are as follows:

1. Electrolytic In-process Dressing (ELID – I),
2. Electrolytic Interval Dressing (ELID – II),
3. Electrolytic Electrode-less dressing (ELID – III) and
4. Electrolytic Electrode-less dressing using alternate current (ELID – IIIA).

2.2.1 Electrolytic in-process dressing (ELID – I)

The basic ELID system consists of an ELID power supply, a metal-bonded grinding wheel and an electrode. The electrode used could be 1/ 4 or 1/6 of the perimeter of the grinding wheel. Normally copper or graphite could be selected as the electrode materials. The gap between the electrode and the grinding wheel was adjusted up to 0.1 to 0.3 *mm*. Proper gap and coolant flow rate should be selected for an efficient in-process dressing. Normally arc shaped electrodes are used in this type of ELID and the wheel used is either straight type or cup type.

2.2.2 Electrolytic Interval Dressing (ELID – II)

Small-hole machining of hard and brittle materials is highly demanded in most of the industrial fields. The problem in micro-hole machining includes the following:

- Difficult to prepare small grinding wheels with high quality,

- Calculation of grinding wheel wear compensation and
- Accuracy and surface finish of the holes are not satisfactory.

The existing ELID grinding process is not suitable for micro-hole machining because of the difficulty of mounting of an electrode. Using the combination of sintered metal bonded grinding wheels of small diameter, Electric Discharge Truing (EDT) and Electrolytic Interval Dressing (ELID–II) could solve the problems in micro-hole machining. The smallest grinding wheel for example 0.1 *mm* can also be trued accurately by using EDT method, which uses DC-RC electric power. The small grinding wheels can be pre-dressed using electrolysis in order to gain better grain protrusions. The dressing parameters should be selected carefully to avoid excessive wear of grinding wheel. The grinding wheel is dressed at a definite interval based on the grinding force. If the grinding force increases beyond certain threshold value, the wheel is re-dressed [Ohmori and Nakagawa, 1995; Qian et al., 2000; Zhang et al., 2000].

2.2.3 Electrode-less In-process dressing (ELID– III)

Grinding of materials such as steel increases the wheel loading and clogging due to the embedding of swarf on the grinding wheel surface and reduces the wheel effectiveness. If the size of swarf removal is smaller, the effectiveness of the grinding wheel increases. For machining conductive materials like hardened steels, metal-resin-bonded grinding wheels have been used. The conductive workpiece acts as the electrode and the electrolysis occurs between the grinding wheel and the workpiece. Normally the bonding material used for grinding wheel is copper or bronze. The electrolytic layer is formed on the workpiece and it is removed by the diamond grits. Thus the swarf production is controlled by using electrode-less in-process dressing (ELID–III). During

electrolytic dressing, the base material is oxidized and the wheel surface contains resin and diamond grits. Theoretically the metal bond is removed by electrolysis, but the experimental results showed that the grinding wheel surface contains cavities, which is caused due to electric discharge. When high electric parameters are elected, the amount of electric discharge increases and it causes damage on both the wheel and ground surfaces. For better surface finish, low voltage, low current, low duty ratio and low in-feed rate should be selected [Ohmori et al., 2000].

2.2.4 Electrode-less In-process dressing using alternative current (ELID–IIIA)

The difficulties of using electrode-less in-process dressing could be eliminated with the application of ELID-IIIA. The alternative current produces a thick oxide layer film on the surface of the workpiece, which prevents the direct contact between the grinding wheel and the workpiece. Thus the electric discharge between the wheel and workpiece is completely eliminated and the ground surface finish is improved [Lim et al., 2000; 2001].

2.3 Applications of ELID grinding process

This section explains the applications of the ELID for different difficult to grind materials used for various applications.

2.3.1 The structural ceramic components

Structural ceramic has been used widely because of its excellent properties such as high wear resistance, high thermal resistance and high resistance to chemical degradations. Cutting tools, automobile parts and aerospace turbocharger are the most important

components that use structural ceramic materials. However grinding of ceramic becomes difficult and costlier due to the lower material removal rates (MRR). Cast iron–bonded diamond grinding wheels with the aid of ELID produces high material removal rates since the grain protrusion from the wheel size is maintained constantly using ELID. The results show that the normal grinding force was reduced when there is an increase of MRR using ELID grinding. The final surface roughness obtained from conventional and ELID grinding processes were found to be 0.211 μm and 0.117 μm, respectively [Bandyopadyay et al., 1996; Fujihara et al., 1997; Bandyopadhyay and Ohmori, 1999; Zhang Bi et al., 2000].

2.3.2 Bearing steel

The applications of cylindrical surfaces are wider in manufacturing industries. The surface roughness and the waviness are the two major factors, which affects the performance of rolling surfaces, because it induces noise and vibration of the components. Precision grinding of bearing steel was carried out using ELID and the surface finish, waviness and the roundness of the samples are compared with the conventional methods. The experiments were performed using both cast iron-bonded diamond wheels and CBN grinding wheels. The surface finish obtained using ELID was with an average surface roughness of 20 *nm* with #4000 grinding wheel. A comparison of waviness obtained using different processes shows that the waviness of the surface obtained using ELID was smaller than the maximum allowable level (MAX) [Qian et al., 2000].

2.3.3 Chemical vapor deposited silicon carbide (CVD- SiC)

The application of CVD-SiC has been increasing in recent years because of its excellent physical and optical properties. It is an ideal material for making reflection mirrors, but finishing of this material is very difficult due to its hard and brittle nature. Nanosurface finish could be possible only when the material removal have done at ductile mode. ELID grinding using cast iron-bonded diamond wheel of grit size #4000 produced an average surface roughness of 7.2 *nm*. The reason for better surface finish using ELID was found due to the thickness of the insulating layer, which acts as a damper during ELID [Zhang et al., 2001; Kato et al., 2001].

2.3.4 Precision internal grinding

Precision cylindrical surfaces are widely used in manufacturing industries. Finishing of internal cylindrical holes for a hard and brittle material becomes difficult because the accuracy and the tolerance mainly depend on the profile of the grinding wheel. The wheel profile should be perfect in order to get good tolerance. Cast iron-fiber-bonded grinding wheels using ELID-II method is highly suitable for internal grinding. The wheel profile is further improved by using Electro Discharge Truing (EDT) [Ohmori et al., 1999].

2.3.5 Mirror surface finish on optical mirrors

Finishing of larger X-Ray mirrors is highly difficult using the conventional grinding processes. Superabrasive diamond grinding wheels and ELID are used to produce a mirror of 1 *m* length with an average surface finish less than 10 *nm*. It indicates that by using ELID grinding, high accuracy also can be obtained because roughing to finishing

processes could be performed in the same machining setup [Zhang et al., 2000; Wang et al., 2000].

2.3.6 Micro lens

Micro optical components are more useful in fiber optics, optical storage systems and portable information devices. Fabrication of micro components needs smaller grinding wheels, low grinding speed and sufficient wheel-workpiece stiffness. A new grinding method known as one-pass method was implemented, in which larger depth of cut and lower feed rate were used. The produced micro-lens of diameter 250 μm shows good profile accuracy using cast-iron bonded grinding wheel with the aid of ELID [Ohmori and Qian, 2000].

2.3.7 Form grinding

Micro thread production is an important process in micro machining. The produced threads should be of good form accuracy and tolerance. Small and hard diamond bonded grinding wheels are highly suitable for machining micro threads. Cast iron-bonded diamond grinding wheels with the aid of ELID produces high profile accuracy. Special forms of wheels were prepared based on the shape requirement [Zhang et al., 2000].

2.3.8 Die materials

Finishing of harder die materials such as SKDII and SKII51 with fine surface finish and accuracy is a great challenge in the manufacturing industries. The grinding ratio for such harder materials is lower, and the wheel wear rate will be increasing significantly. ELID–IIIA technique has been implemented successfully for grinding of this kind of harder conductive materials. The workpiece is connected to the positive pole and the

metal-resin bonded grinding wheel is connected to the negative pole. The electrolysis occurs between the workpiece and the grinding wheel, and a passive layer is formed on the workpiece surface, which reduces the effective depth of cut and improves the ground surface and the shape accuracy of the grinding wheel [Lim et al., 2000; 2001].

2.3.9 Precision grinding of Ni-Cr-B-Si composite coating

Surface coatings are necessary to prevent the material surface from wear and corrosion. Stephenson et al. used CBN grinding wheels with the aid of ELID to finish the coated surface. They found that the surface finish using ELID shows limited damage to primary and secondary carbides. The surface ground without ELID shows damages in the form of carbide pullout and localized fracture due to the removal of large WC particles. The reason is ELID produces good protrusion of CBN grits that eliminates the carbide pullout. The ground surface measured shows an average surface roughness of 5-10 *nm* and 60-80 *nm* for with ELID and without ELID, respectively [Stephenson et al., 2001; 2002].

2.3.10 Micro-hole machining

Machining of micro-hole in a hard and brittle is a great challenge in manufacturing industries. Micro-hole of diameter 250 *μm* was produced on ceramic material. The micro-holes were produced using two types of grinding wheels such as cobalt-cast iron compound diamond grinding wheel and cast iron-bond diamond grinding wheel. The grit sizes of the grinding wheels used in the experiments are #325, #500, and #1200. Three different grinding fluids were also used to compare the efficiency of the grinding process.

The experimental results show that the coolant selection also has a strong influence on the grinding forces. The proportion of oxide layer thickness and the etched layer thickness are varying with the application of grinding fluid. Normally two kinds of electrodes such as arc and tube have been selected for interval dressing based on the grinding applications [Bandyopadhyay and Ohmori, 1999].

2.3.11 ELID-lap grinding

High flatness and mirror surface finish are the requirements in many industries nowadays. ELID-lap grinding is a constant pressure grinding which uses metal-bonded grinding wheels finer than #8000. This method is highly efficient to ground surfaces of different hardness at the same time. Experiments were conducted on two different materials such as silicon and cemented carbide. At first, the materials were ground separately and then ground together. The result shows that the surface finish is improved when they are ground together than ground separately [Itoh et al., 1998].

2.3.12 Grinding of silicon wafers

Finishing of silicon wafers with nano accuracy and mirror surface finish is a great demand in semiconductor industry. Grinding with superabrasive metal-bonded grinding wheels using ELID was found to be a good choice of producing mirror surface finish on silicon wafers [Ohmori and Nakagawa, 1990; Venkatesh et al., 1995].

2.4 ELID-EDM grinding

Truing of metal bonded grinding wheel is highly difficult due to its high bonding strength. Recent development of Electro Discharge Truing (EDT) shows good truing

accuracy. A new rotating truing device is also developed for the purpose of truing metal bonded grinding wheels. Nagakawa [Suzuki et al., 1997] introduced on-machine EDT that eliminates the difficulty of truing. In this method the grinding wheel can be trued after mounting on the machine spindle, which reduces the mounting errors and increases better truing accuracy. The grinding wheel profile obtained after truing using on-machine truing shows an accuracy of 3 μm. Recent studies show that the combination of ELID and EDM process could be successfully used for nanogrinding, because the grinding wheel profile is corrected during grinding. [Okuyama et al., 2001; Ohmori and Nakagawa, 1997].

2.5 Summary and problem formation

From the literature survey it is clear that the application of the ELID is wider, and the process is used to finish a variety of hard metals and non-metals. However, several factors are not clearly reported elsewhere in those reports. For example the selection of bond materials, electrode materials, selection of electrolytic parameters, etc., this makes the ELID users difficult to implement the process. The wheel wear mechanism of the ELID-grinding wheel, which is more essential for precision finishing of the non-axis-symmetric components has not been reported. Though the importance of the oxidized layer was indicated in some articles, the information such as the phenomena of the layer, wear rate and the mechanical properties of the layer are not discussed in detail. Therefore, with these limitations and insufficient data it is highly difficult to implement the ELID for precision finishing. Therefore, the major objective of this thesis is to reduce the ambiguities experienced while grinding with the aid of the ELID, and promotes the robustness of the process in the precision manufacturing field.

Chapter 3

The basic principle and classifications of the ELID

3.1 Introduction

The micro/nanogrinding is a motion copying method, which mainly depends on the wheel-work interactions [Yoshioka et al., 1987]. Periodic dressing of grinding wheels is cumbersome and also produces inaccuracy during the process. The main requirement for a grinding wheel is its ability to replenish the topography and promotes an uninterrupted grinding (or with minimum interruptions). When grinding is performed with conventional grinding wheels (other than metal-bonded), the worn out grits are removed automatically by the grinding force and the grits beneath come into contact with the workpiece. This is known as the 'self-sharpening' effect [Figure 3.1], which makes the in-process dressing unnecessary, and grinding becomes continuous. The conventional wheels are also prepared with certain porosity in order to provide space for chip and coolant [Malkin, 1987; Shaw, 1996]. However, the wheels have the properties described above are suitable for machining metals or materials with less hardness, and they are not recommended for grinding harder material because of intense diminution of wheel diameter. Therefore, wheels with high bonding strength are quite suitable in order to withstand higher grinding forces generated during grinding.

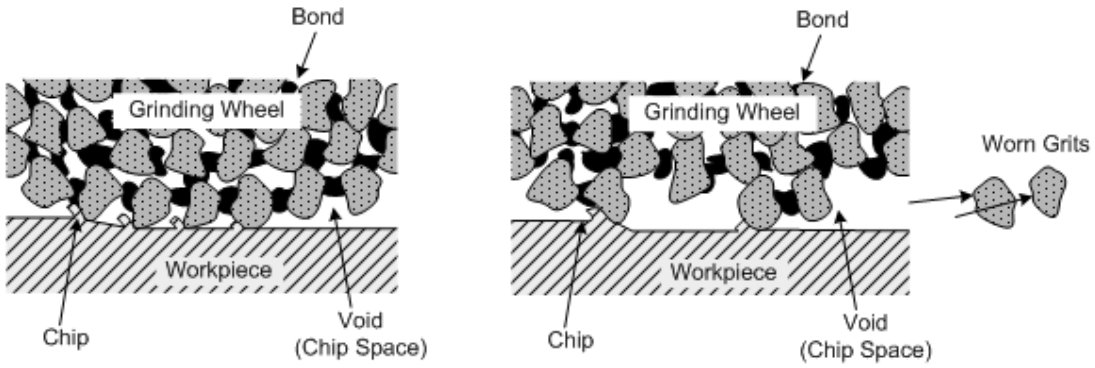

(a) Grinding (b) Self-sharpening effect

Figure 3.1 Self-sharpening effect of the conventional grinding wheel.

Though the metal-bonded grinding wheels possess excellent properties (such as high bond strength, high stability and high grindability) its usage was not widespread because they are not suitable for continuous usage due to their poor self-sharpening effect, and there is no space for chip and coolant because the grits are bonded in the metal matrix. The metal bond around the grit should be removed to a certain amount in order to produce grain protrusion as well as space for coolant and chip flow. The necessary bond material is removed electrochemically by anodic dissolution, but when the grit size of the grinding wheel becomes smaller, problems such as wheel loading and glazing are encountered which impedes the effectiveness of the grinding wheel. Therefore, an additional process is necessary in order to rectify the above problems and promotes uninterrupted grinding using metal-bonded grinding wheels.

The concept of the ELID is to provide uninterrupted grinding using harder metal-bonded wheels. The problems such as wheel loading and glazing can be eliminated by introducing an ‘electrolyze cell’ (anode, cathode, power source and electrolyte) during grinding, which stimulates electrolysis whenever necessary. The electrolyze cell

required for the in-process dressing is different from the cell used for standard electrolysis or electroplating. Therefore, attention should be focused on the selection of factors such as the bond-material for the grinding wheels, electrode material, the electrolyte and the power source. If any one of the parameters is not chosen properly, the result obtained from the electrolysis will be different. Therefore, an adequate knowledge about the electrolysis is necessary before incorporate with the machining process. This chapter provides the necessary information about the ELID, selection of bond material for the ELID, the electrode material selection for the grinding wheels, electrolyte and the power source selections.

3.2 The principle of electrolysis and the ELID

Electrolysis is a process where electrical energy is converted into chemical energy. The process happens in an electrolyte, which gives the ions a possibility to transfer between two electrodes. The electrolyte is the connection between the two electrodes which are also connected to a direct current as illustrated in Figure 3.2, and the unit is called the electrolyze cell. When electrical current is supplied, the positive ions migrate to the cathode while the negative ions will migrate to the anode. Positive ions are called cations and are all metals. Because of their valency they lost electrons and are able to pick up electrons. Anions are negative ions. They carry more electrons than normal and have the opportunity to give them up. If the cations have contact with the cathode, they get the electrons they lost back to become the elemental state. The anions react in an opposite way when they contact with the anode. They give up their superfluous electrons and become the elemental state. Therefore the cations are reduced and the anions are oxidized. To control the reactions in the electrolyze cell various electrolytes

(the electrolyte contains the ions, which conduct the current) can be chosen in order to stimulate special reactions and effects. The ELID uses similar principle but the cell is varied by using different anode and cathode materials, electrolyte and the power sources suitable for machining conditions.

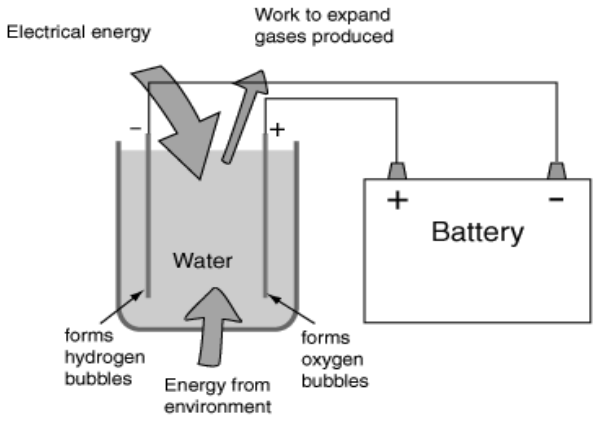

Figure 3.2 Electrolytic cell.

3.3 The basic components of the ELID

As discussed earlier, an electrolyze cell is necessary in order to facilitate the self-sharpening effect on the grinding wheels. The cell is created using a conductive wheel, an electrode, an electrolyte and a power supply, which is known as the ELID system. Figure 3.3 shows the schematic illustration of the ELID system. The metal-bonded grinding wheel is made into a positive pole through the application of a brush smoothly contacting the wheel shaft. The electrode is made into a negative pole. In the small clearance of approximately 0.1 to 0.3 *mm* between the positive and negative poles, electrolysis occurs through the supply of the grinding fluid and an electrical current. The descriptions of different components are discussed in the subsequent sections of this chapter.

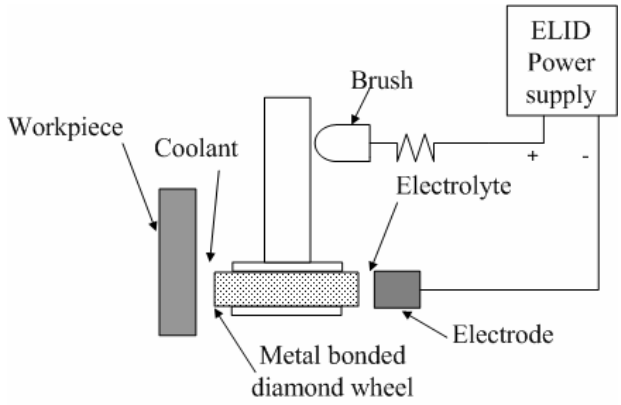

Figure 3.3 Schematic illustration of the ELID system.

3.3.1 The ELID-grinding wheels

The ELID grinding wheels are made of conductive materials *i.e*. metals such as cast iron, copper and bronze (the properties of the metal-bonds are tabulated in Table A.1). The diamond layer is prepared by mixing the metal and the diamond grits with certain volume percentage, and the wheels were prepared by powder metallurgy. The prepared diamond layer is attached with the steel hub as shown in Figure 3.4. The grinding wheels are available in different size and shapes. Among them the straight type and the cup shape wheels are commonly used.

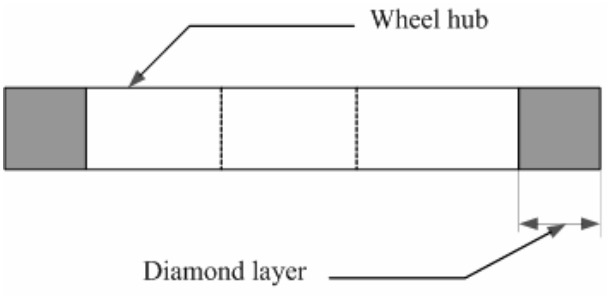

Figure 3.4 Metal bonded grinding wheel.

3.3.2 The electrode

The dimension of the electrode depends on the size and shape of the grinding wheel. The size of the electrode can be chosen in such a way that there is no hindrance for the machining process. However, the spindle speed (spindle rotation of the machine) of the grinding wheel is higher and it reduces the effect of electrolysis. Hence the size of the electrode should be sufficient to produce the effect of in-process dressing. Generally the size of the electrode can be chosen from 1/6 th to 1/4 th of the grinding wheel perimeter. The thickness of the electrode is made by 1 – 2 *mm* more than the width of the grinding wheel [Ohmori and Nakagawa, 1990].

3.3.3. Material for the ELID electrodes

Material such as copper, graphite and stainless steel are commonly used as the electrode materials. The metal ions of the anode migrate to the cathode and become a thin layer on the surface, which needs to be galvanized. Therefore, care should be taken when selecting the cathode material. To predict the reactions during electrolysis, the "electrochemical electromotive series" is used. Metals with a more noble character than copper will not react, but fall down as an anode mud. However, metals with a standard potential less than copper will also be electrolyzed and migrate at the cathode. The elements ordered by their standard potentials (E_0) are tabulated in Table A.2. The standard potential shows the capability, with regard to hydrogen ions, to give up electrons. In this table the standard potential of hydrogen is zero. The other elements have a positive or a negative standard potential. That means elements with a negative potential were easier to oxidate than hydrogen and elements with a positive potential were more difficult to oxidate than hydrogen. From the table, it is clear that copper can be used as the electrode material for all type of ELID-grinding wheels.

When grinding with copper bonded grinding wheels, the Cu^{2+} ions in solution is precipitated on the cathode, and a more pure copper layer is formed than before. The pollution from the grinding wheel will not react but fall down to the ground as the anode mud. Therefore, the cathode is always pure and conductive when used with copper or bronze bonded wheels.

3.3.4 The gap between the electrodes

The gap between the electrodes should be more than the oxidized layer formed on the grinding wheel surface and also sufficient for electrolyte flow. It is recommended that the gap between the electrodes can be adjusted to 100 – 300 μm. However, the gap between the electrodes can not be maintained throughout the process because of the wheel wear. The gap should be measured using the gap sensor and it is adjusted by an automatic gap adjustment system [Lee, 2000].

3.3.5 The function of the Electrolyte

The electrolyte plays an important role during in-process dressing. The performance of the ELID depends on the properties of the electrolyte. If the oxide layer produced during electrolysis is solvable, there will not be any oxide layer on the wheel surface and the material oxidized from the wheel surface depends on the Faraday's law. However, the ELID (developed by Ohmori, 1990) uses an electrolyte in which the oxide is not solvable and therefore the metal oxides are deposited on the grinding wheel surface during in-process dressing. The performance of different electrolytes has been studied by Ohmori et al., which shows the importance of the selection of the electrolyte [Ohmori, 1997]. The electrolyte is diluted (2%) with water and used as an electrolyte and coolant for grinding. The amount of chlorine presents in the water should be

considered because it has a positive potential, which has a significant influences on electrolysis.

3.3.6 Power sources

Different power sources such as AC, DC and pulsed DC have been experimented with the ELID. The applications and the advantages of different power sources were compared, and the results were described in the previous studies [Ohmori, 1995, 1997]. However, the recent developments show that the pulsed power sources can produce more control over the dressing current than other power sources. When the DC-pulsed power source is used as the ELID power supply, it is essential to understand the basics of pulsed electrolysis in order to achieve better performance and control.

3.4 Basic concepts of pulse electrolysis

The rate of reaction and the change of magnitude of the driving force are the two main factors that control the electrolysis. The reaction rate can be controlled by changing the current density, and the driving force can be changed by adjusting the electrode potential. Modern electronic enhanced the advantage of allowing the current and voltage to be applied as the function of time. The control of pulsed voltage during electrolysis needs a third electrode as a reference electrode, which makes the control very tedious. Therefore the control of pulse current is more suitable for electrolysis [Puippe, 1986]. There are varieties of pulses such as unipolar, bipolar and reversed pulses have been used for pulsed electrolysis, but for simplicity, unipolar cathodic pulses followed by zero current have been analyzed in this study. Figure 3.5 shows the schematic

illustration of a glavanostatic pulse train and its nomenclatures. The duty ratio of the pulse current can be expressed as

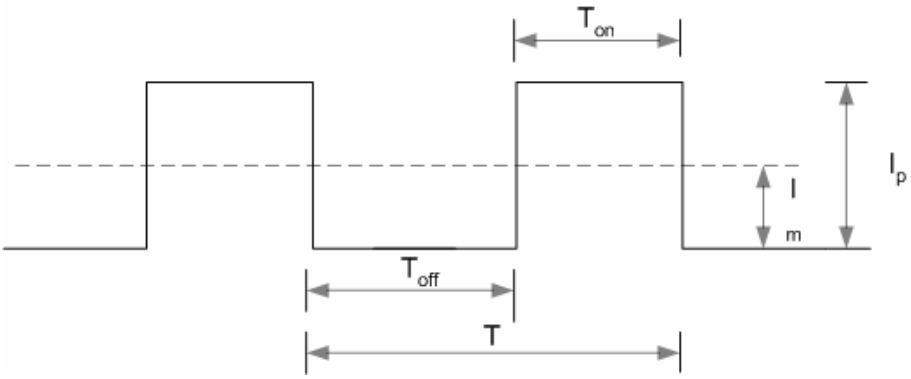

Figure 3.5 Galvanic pulse train and its nomenclatures.

[T_{on} – Pulse ON-time, T_{off} – Pulse OFF-time, T – time of the cycle, I_p – Peak current and I_m – Mean current]

$$R_c = \frac{T_{on}}{T} \tag{3.1}$$

where T is the period, $T = T_{on} + T_{off}$

The current density of the pulse current is expressed as shown below

$$I_d = \frac{I_p}{A_e} \tag{3.2}$$

where A_e - Area of the cathode, the value of the average current can be expressed as

$$I_m = I_d . R_c \tag{3.3}$$

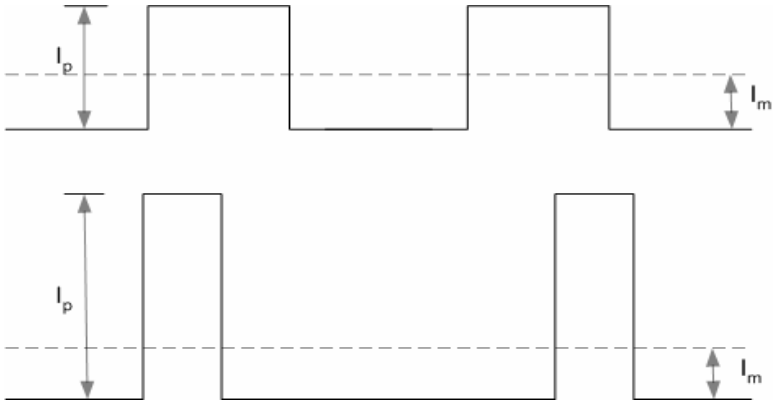

Figure 3.6 Pulse with similar current density.

The average current density can be maintained either changes the pulse width or the peak current as illustrated in Figure 3.6. However, the advantage of pulse electrolysis cannot be fully utilized due to the natural phenomena, which produces some limiting factors. They are the electrical double layer at the metal/electrolyte interface and the mass transfer considerations.

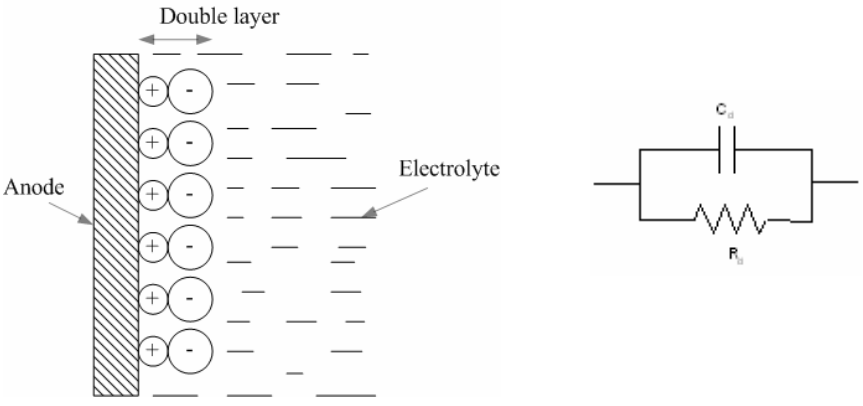

(a) Electrical double layer (b) Circuit diagram for double layer

Figure 3.7 Electric double layer and its equivalent electric circuit.

The concept of double layer is an important phenomenon in pulse electrolysis. If a solid phase is in contact with a liquid phase, the positive and negative charges on the solid/liquid interface oppose each other that form an electric condenser. This condenser is called as electric double layer, which is represented schematically in Figure 3.7 (a). The electrical double layer at the electrode/electrolyte interface can be approximated to a plate capacitor with an interface distance of few angstroms. The capacitance is inversely proportional to the distance between the parallel plates, and hence the capacitance at the interface is considered as high capacitance. The equivalent diagram of electrode can be represented as a capacitor connected with a resistance in parallel as schematically illustrated in Figure 3.7 (b). The selection of T_{on} and T_{off} should be greater than the T_c (charging time of the double layer) and T_d (discharging time of the double layer), respectively, otherwise there will be a heavy distortion of the pulse current. Figure 3.8 (a) and 3.8 (b) shows an ideal pulse and pulse with small damping, respectively. Figure 3.8 (c) shows the condition of heavy damping and the pulse oscillates around an average value and it never reach the value of zero, which violets the concept of pulse current.

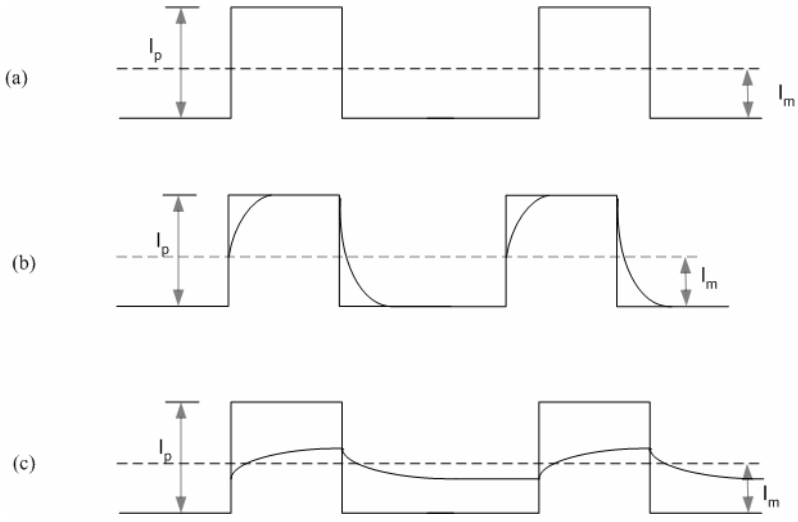

Figure 3.8 Pulse train with damping.

The limitation of the useful range of pulse conditions due to mass transport effects arise from the reduction of cations in the diffusion layer. Pulse electrolysis using short pulses creates a second diffusion layer instead of one as in DC. The layer near the cathode is called as pulsated diffusion layer (T_p) and the layer next to that is known as stationary diffusion layer (T_s) as seen in Figure 3.9. The concentration of the electrolyte surrounding the cathode pulsates with the same frequency of the pulse current. The concentration decreases during the OFF-time. If shorter pulse is used for electrolysis, the diffusion layer does not have time to extend very far into the solution where convection takes over the mass transport, which creates concentration gradient into the electrolyte [Puippe, 1986].

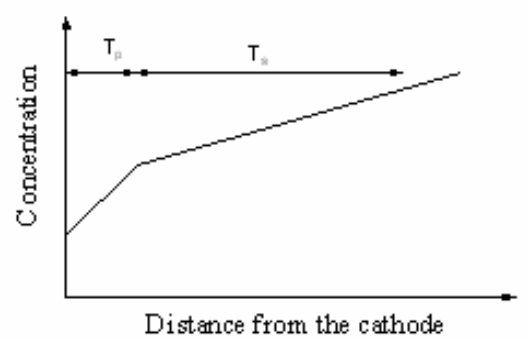

Figure 3.9 Pulsation layer.

Diffusion occurs as a result of the inhomogeneity of the system, i.e., when its separate parts contains either different substances or the same substances but in different concentrations. The transport processes of diffusion can be expressed quantitatively with the aid of Fick's law (Appendix B).

Finishing of brittle materials at submicron level with good control of final geometry is the attraction of fixed abrasive process. For precision finishing, the replenishment of the

grinding wheel topography is very important, which could be achieved by the precision control of electrolysis. For better control of current, the pulsed current has been preferred than the DC current. Pulsed current has various control parameters such as pulse ON-time, OFF-time, pulse width, and pulse frequency. The change of any one of these parameters affects the electrolysis.

3.5 Classification of ELID based on grit size of the grinding wheel

The application of the grinding process can be broadly classified into two different types such as the rough grinding (macrogrinding) and the micro/nanogrinding. The requirements for the above processes are entirely different [Hans et al., 1997]. However, the application of the ELID is unavoidable for uninterrupted grinding for both the processes, and hence the application of ELID can be classified into two types based on the requirements:

1. The application of the ELID using courser grit wheels, and
2. The ELID using superabrasive wheels

When grinding with courser grits, the requirement of the wheels are high grinding ratio and self-sharpening ability. The ELID uses to dress the grinding wheels in a method known as ‘slow corrosion’ of the bond material using low current (I_p – 5 A) and low voltage (V_p – 20-30 V). This method can be useful for abrasive cutting and stock removal processes.

The ‘slow corrosion’ method is not suitable for grinding with superabrasive grinding wheels of grit sizes smaller than 10 μm. The grit protrusion or the protrusion height of the superabrasive wheels are very smaller and hence controlling electrolysis within the small scale is difficult. If the control is not appropriate it leads to excessive bond erosion and the grits are removed along with the bond material. Therefore the bond erosion should be controlled as fast as possible as in the case of grinding with superabrasives. The in-process dressing method for superabrasive (introduced by Ohmori,1990) uses a different method which produces a self-protective oxide layer as the fastest rate, which can be possible when using higher voltage and current. Generally current 10 A and voltage 60 – 90 V can be used for the purpose of speed up the electrolysis.

3.6 Mechanism of the ELID grinding

Based on the analysis, the mechanism of the ELID grinding can be explained as shown in Figure 3.10. After truing, the grains and bonding material of the wheel surface are flattened. It is necessary for the trued wheel to be electrically pre-dressed to protrude the grains on the wheel surface. When pre-dressing starts, the bonding material flows out from the grinding wheel and an insulating layer composed of the oxidized bonding material is formed on the wheel surface. This insulating layer reduces the electrical conductivity of the wheel surface and prevents excessive flow out of the bonding material from the wheel. As grinding begins, diamond grains as well as the layer gradually wears out. As a result, the electrical conductivity of the wheel surface increases and the electrolytic dressing restarts with the flow out of bonding material from grinding wheel. The protrusion of diamond grains from the grinding wheel

therefore remains constants. This cycle is repeated during the grinding process to achieve stable grinding.

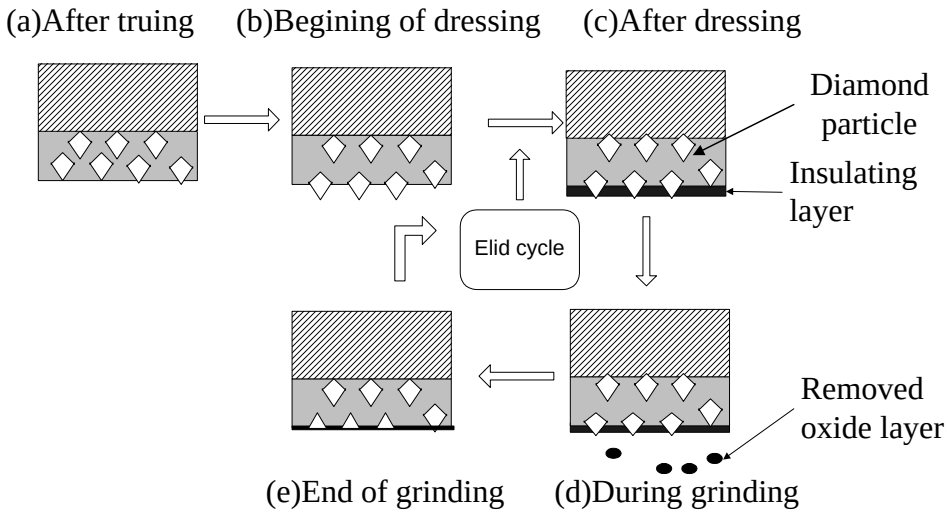

Figure 3.10 Mechanism of the ELID grinding.

3.7 Concluding remarks

The knowledge about the ELID system and its different components are necessary for efficient control of the process. The ELID improves the 'self-sharpening' effect of the harder metal-bonded grinding wheels with the aid of an electrolyze cell, and hence the wheel loading and glazing problems are eliminated. The information provided regarding the mechanism of ELID and the pulse electrolysis are useful to understand the experiments conducted on the fundamental studies and wheel wear mechanism.

Chapter 4

Experimental setup and procedures

This chapter describes the details of the experimental setup and the experimental procedures used in this study. Grinding methods and procedures implemented for different investigations, the configurations of the measuring equipments and measuring methods are described in detail.

4.1 Description of the grinding machine

The experiments were conducted on a five axis CNC machining center – DECKEL MAHO: DMU 50 V. The motor power of the machine is 10 kW. The feed drive resolution and position tolerance for the three axes (X, Y and Z) are 1 μm and 10 μm, respectively.

4.2 Workpiece material

4.2.1 Workpiece properties

Glass has been chosen as the workpiece material mainly for two reasons. Firstly, glass, which is uniform without any grain, slip or twin, is an ideal material for ultraprecision grinding. Secondly, the BK7 glass is a widely used material in optical industries due to its excellent properties such as transparency, homogeneity, isotropy, hardness, durability and high chemical resistance. However, BK7 is highly hard and brittle, and that makes

the finishing process very difficult. The properties and of the glass workpiece are tabulated in Table A.3.

4.2.2 Mounting of specimens

The method of specimen attachment and the alignment of the specimen are important aspects, which affects the flatness of the ground specimen. The specimens were attached by a thin layer of wax (NX-AF/EW: NEXSYS) to a steel mounting plate. The adhesive chosen have superior strength to withstand high force and temperature during grinding. The mounting plate was attached on a dynamometer, and the assembly was mounted vertical on the machine table.

4.2.3 Sample preparation

The samples were prepared from the BK7 glass block of diameter 80 *mm* and thickness 10 *mm*. The glass pieces were ground using #325 grit size grinding wheel in order to make it flat. The average surface roughness of the brittle surface produced on the workpiece was less than 1 μm, which was used as the workpiece for the grinding experiments.

4.3 Grinding wheels

Grinding wheels consists of abrasive grains known as grits, and the bonding material that holds the grits together. Diamond or CBN grits are generally preferred as superabrasive grit material for their extreme hardness suitable for machining brittle material like glass, silicon and ceramics. The ELID-grinding wheels are made of metal or metal-resin bonded. The grinding wheels are produced from powder-metallurgy

methods. The bonding-materials used are cast iron, cast iron-cobalt, copper, bronze and copper-resin bonded.

4.3.1 Measurement of wheel Profile

The active-surface of the ELID-grinding wheel is covered by oxidized layer after pre-dressing, and hence a non-contact profile measurement is necessary for measuring radial wear. A profile sensor was developed based on the principle of photoelectric effect. The schematic illustration and the photographic view of the profile sensor are shown in Figures 4.1 (a) and 4.1 (b), respectively. When the grinding wheel moves in between the LED and phototransistor, the light from LED is interrupted and the change of light intensity is measured in the form of electric current by the phototransistor. The calibrated displacement output characteristic of the sensor is shown in Figure 4.1 (c). The liner range from 3 ~ 9 volts have been chosen for measurements, and the reference point was always set at the output range of 4 – 6 volts.

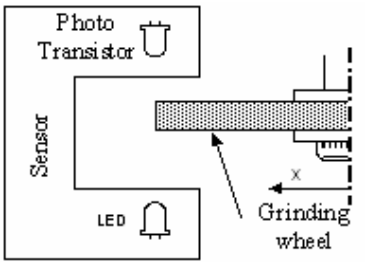

(a) Schematic illustration of the sensor

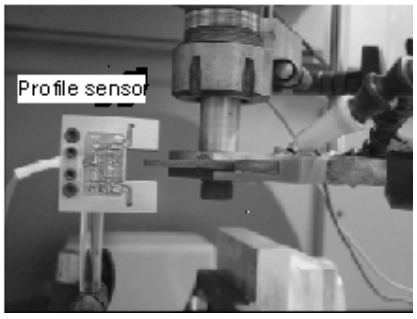

(b) Photographic view

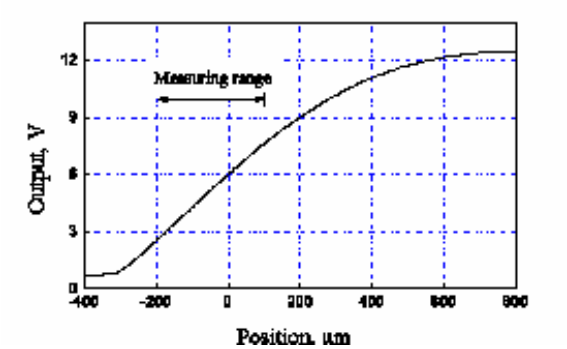

(c) The calibration curve for the sensor

Figure 4.1 Measurement of wheel profile using the developed profile sensor.

4.3.2 Preparation of the grinding wheel

The method of preparation of the ELID-grinding wheels is different from the conventional grinding wheels. For conventional metal-bonded grinding wheels, truing and dressing are performed in a single operation. A single point diamond truing tool is used for truing and dressing of conventional wheels. However, the conventional method of preparation is not suitable for superabrasive grinding wheels and hence the ELID-grinding wheels are prepared using two different operations as described below:

4.3.2.1 Truing process

The wheel profile should be free from irregularities or eccentricity before start grinding. Spark erosion methods are more suitable for the removal of unwanted material from harder grinding wheels. An electric spark is created in between the work and an electrode that removes the unwanted material from the workpiece. This process is known as Electro Discharge Truing (EDT) or plasma truing.

The EDT method is simple and highly accurate, and therefore it is more suitable for preparing grinding wheels for precision grinding. The truing process has been performed after mounting the grinding wheel in the machine spindle which reduces the inaccuracies created during wheel mounting. The grinding wheel is connected to the positive pole of the power supply. A steel bar clamped on the machine table was made as electrode. The thickness of the electrode should be at least twice of the grinding wheel thickness. The circuit diagram and the photographic view of the truing setup are shown in Figure 4.2 (a) and 4.2 (b). The grinding wheel profile was measured using the profile sensor before performing the truing operation. The eccentricity of the grinding wheel was measured and, the resistance and the capacitance were selected based on the requirement of material removal. The required accuracy can be obtained by choosing suitable resistance and capacitance. The capacitances used were 0.1 μF, 1 μF and 100 μF. The resistances used were 100 Ω - 1000 Ω.

Figures 4.2 (a) and (b) show the grinding wheel (diameter 100 *mm* and thickness 5 *mm*) profile before and after truing. The eccentricity was measured about 50 μm and it was reduced to 3 μm P-V after truing. The truing conditions were: spindle rotation: 1000 *rpm*, feed: 50 *mm/min* and in-feed: 1 μm for five passes. The profile of the grinding wheel was measured at equal intervals in order to avoid excessive bond wear.

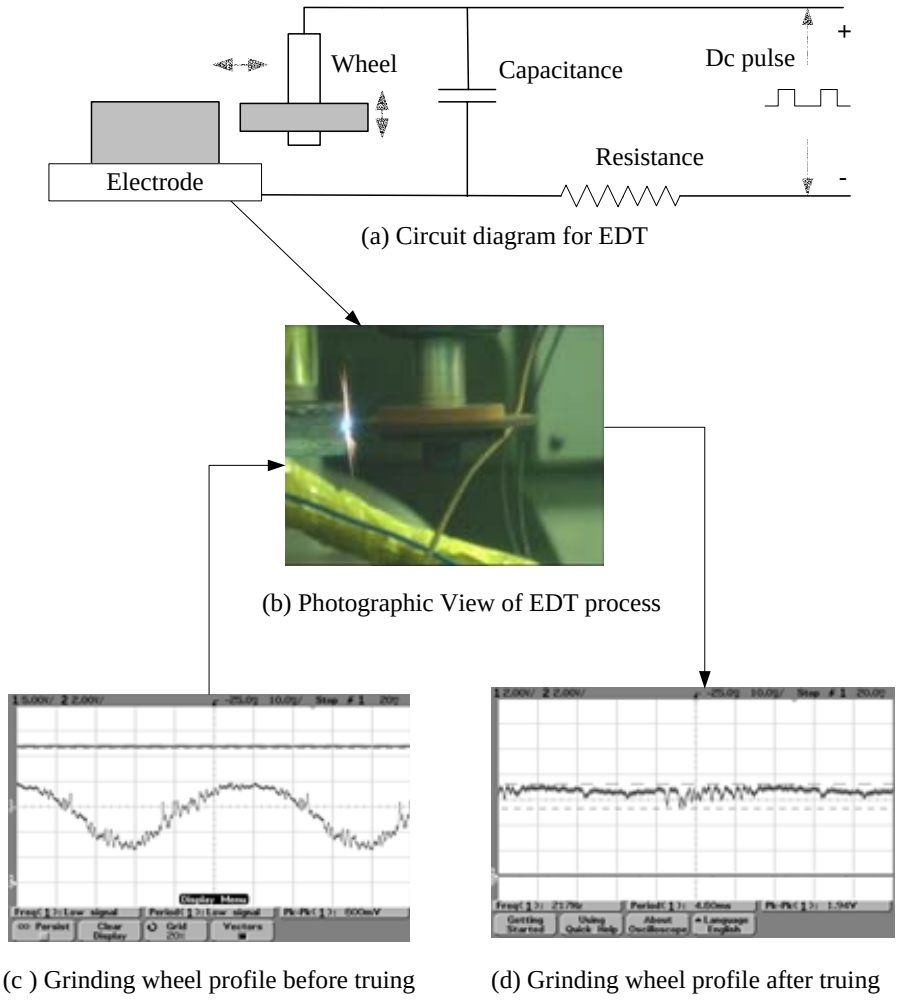

(a) Circuit diagram for EDT

(b) Photographic View of EDT process

(c) Grinding wheel profile before truing

(d) Grinding wheel profile after truing

Figure 4.2 The Electro Discharge Truing of ELID-grinding wheel.

4.3.2.2 Pre-dressing

Pre-dressing is the process of producing grin protrusion on the grinding wheel active-surface. After truing, the grinding wheel surface is flat and without any grain protrusion, and hence pre-dressing is essential to produce grain protrusion by eroding the bond material around the grits. The grinding wheel was mounted on the machine spindle, the electrode was placed in position and the gap was adjusted to 100 – 300 μm. Then the electrolysis was started with the supply of electrolyte and current. The pre-dressing conditions used in this study were 90 V, 10 A, R_C – 50% (ON-time – 5 μs and OFF-time

– 5 μs) and spindle rotation of 1000 *rpm*. At the beginning, an increase of current and a decrease of voltage were noticed. After some time, the current started reducing and almost the voltage rose approximately equal to the applied voltage. However, the above mentioned conditions were noticed after 20 – 30 *min* of pre-dressing.

4.3.3 Wear measurement of the grinding wheel

An unavoidable result from the grinding process is the wear of grinding wheel. The wear rate of the grinding wheels should be minimized in order to achieve better tolerance. Faster wheel wear influences the ground surface integrity. The wheel wear can be quantified by the volumetric loss of material from the grinding wheel during grinding. The radial grinding wheel wear was measured using the profile sensor. The volume removed from the grinding wheel (V_w) is calculated as

$$V_w = dR\ b\ L_w \tag{4.1}$$

where, dR – Radial wear in *mm*,

b – Grinding width in *mm* and

L_w – Circumference of the wheel in *mm*

When the wheel was moved in between the photodiode and LED; the voltage started increasing related to the light blocked by the grinding wheel which was monitored by a digital oscilloscope. When the voltage was between 4 – 6 *V*, the X, Y and Z co-ordinates of the machine was set to zero, which was used as the reference point. After grinding, the grinding wheel was brought into the same position, and the new profile was measured as illustrated in Figure 4.3. The difference in voltage measured was converted into micrometers, which is equal to the radial wheel wear. The grinding ratio is a

common measure used to characterize the resistance to wheel wear. The grinding ratio is generally indicated as '*G*' ratio, which can be expressed as

$$G = \frac{V_m}{V_w} \tag{4.2}$$

where,

V_m – Volume of material removal from the workpiece in mm^3

V_w – Volume of material removal from the wheel in mm^3

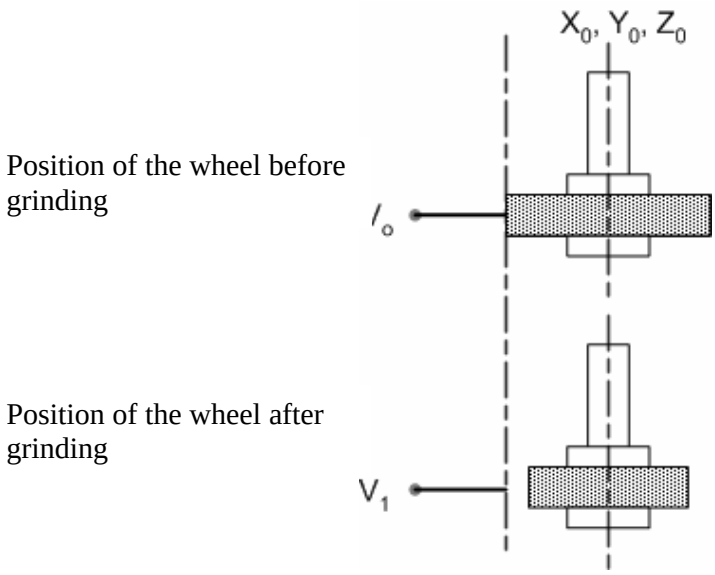

Figure 4.3 Measurement of radial wear.

4.4 Coolant and electrolyte

The electrolyte GC-7 supplied from NEXSYS Corporation, Japan, was diluted with water in the ratio of 1:50 and used as an electrolyte and coolant for the experiments. The pH value and the electric conductivity for the electrolyte were measured as 11 and

2300-2800 micro-Siemens after dilution, respectively. Basically, ELID coolant consists of some corrosion inhibitor such as triethanol amine and alkaline salts.

4.5 ELID power supply

The power supply used for ELID is FUJI ELIDER: 921. The ELID power supply produces DC pulsed current. The current and voltage can be varied from 1 – 30 A and 30 – 90 V, respectively. The pulse ON-time and OFF-time can be varied from 1 – 10 μs. The output current and voltage during the ELID process can be recorded through an output channel provided.

4.6 Force measurement system

A data-acquisition instrument was used to monitor and record normal and tangential grinding forces. The four major components of the force measurement system were Kistler three component piezoelectric dynamometer (model: 9256A1), a set of three Kistler 5007 dual-mode charge amplifiers and an interface PCIF 260 EP, a digital oscilloscope and a data recorder (PC208Ax: Sony). The grinding forces were recorded using a data recorder and the digital oscilloscope was used to monitor the grinding forces while recording. The drip value of the grinding forces was compensated using a software program written using Borland C++.

4.6.1 Force calibration

Calibration is the process of converting raw date into meaningful values of the appropriate unit. The calibration process provides a relationship between the raw output

voltage recorded by the data-acquisition system and force encountered by the workpiece during grinding. The grinding forces recorded were digitized using an Analog to Digital converter. The grinding forces were recorded with respect to every rotation of the grinding wheel. Figure 4.4 shows a plot of normal grinding force with respect to a rotation of the grinding wheel. Every wheel rotation was divided into 200 data points. An average value from four rotations was calculated for minimizing the error.

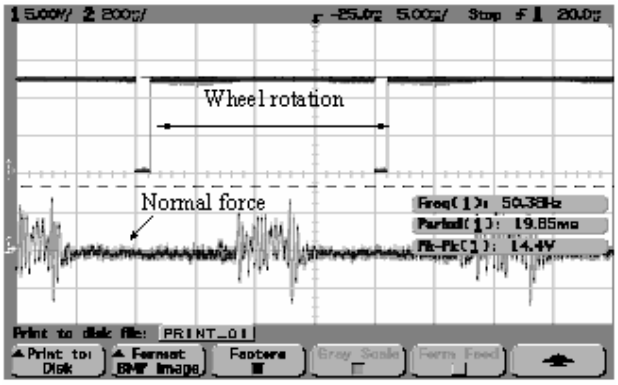

Figure 4.4 Measurement of grinding force.

4.7 Experimental setup

The schematic illustration of the experimental setup is shown in Figure 4.5. This setup consists of three main systems such as the ELID system, force measurement system and the wear monitoring system. The ELID system consists of an ELID-grinding wheel, an electrode, an electrolyte and a power supply. The force measurement system consists of a dynamometer, a fiber optical sensor to deduct the spindle rotation, a digital scope and a data acquisition system. The wear monitoring system consists of the profile sensor and a digital oscilloscope. The electrode for the grinding wheel was attached near the

grinding wheel and the gap between the grinding wheel and the electrode was adjusted to 0.1 – 0.3 *mm.* The pulse current was supplied from the ELID power supply. The positive pole of the power supply was connected to the metal-bonded grinding wheel and the negative pole was connected to the electrode. A carbon brush was used for smooth contact with the machine spindle through which the current passing. The electrolysis began at the small gap between the electrodes with the application of pulse current and the supply of electrolyte.

The workpiece was pasted on a metal piece and mounted vertically on the angle plate. The dynamometer was mounted in between the workpiece and the angle plate, and the assembly was mounted on the machine table. The developed profile sensor was mounted on the table which was used to measure the wheel profiles before and after grinding. The normal force, tangential force, wheel rotation and the dressing current were recorded using a data recorder and stored in a PC through a data acquisition system.

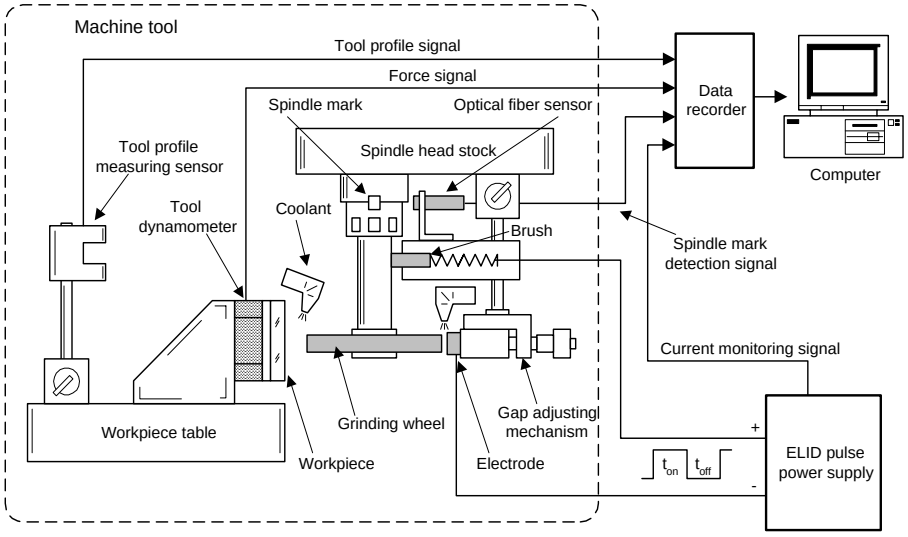

Figure 4.5 Schematic illustration of the experimental setup.

4.8 Grinding methods

Three types of grinding methods have been used based for the investigations. They were surface grinding, vertical groove grinding and creep feed grinding. The above methods produced flat surfaces, deep convex grooves and horizontal slots. The grinding methods are illustrated in Figures 4.6 (a), (b) and (c). For studying the phenomenon of the oxide layer and for the fundamental analysis, vertical grooving method had been used. During vertical groove grinding, the contact area between the grinding wheel and the workpiece was increasing at every depth of cut/pass. The increase of grinding area within a small volume of material removal made it easy to study the topographical changes of the grinding wheel. Creep feed grinding was used to study the behavior of the oxide layer and the cutting stability of the ELID-grinding wheels dressed at different current densities. There are two general parameters that influence the ground surface finish; they are the grinding parameters and the ELID parameters. The change of grinding parameters was obtained by changing the feed rate or the depth-of-cut. The feed rate can be chosen from 100 mm/min, and the maximum feed rate that can be feasible was determined by the experiments. The depth-of-cut can be varied from 1 μm to 5 μm for superabrasive wheels from mesh size #4000.

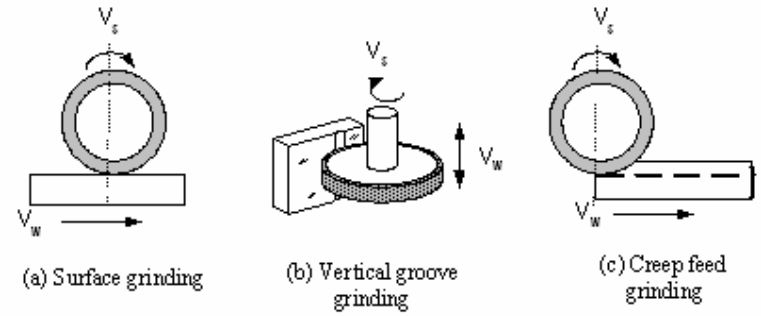

Figure 4.6 Different grinding methods.

The change of ELID conditions were obtained by changing the average current supplied for the electrolysis. The average current supplied can be varied by simply changing the ON and OFF time of the pulse. The pulse width for the experiments was set to 10 μs, which was the maximum pulse width obtained from the ELID-power supply. The change of ON and OFF-times vary the current duty ratio and the average current. Thus different in-process dressing conditions were achieved by the current variations. The current duty ratio (R_c) is defined as the ratio between ON-time of a cycle to the total time of a cycle as shown in Eq. (4.3).

$$Current\ Duty\ Ratio(R_c) = \frac{T_{on}}{T_{on} + T_{off}} \times 100(\%) \tag{4.3}$$

where,

T_{on} - ON-time of a cycle,

T_{off} - OFF-time of a cycle.

Table 4.1 shows the different pulses at different current duty ratios. The pulse frequency can be varied by changing the ON and OFF time. Different grinding methods have been used for the investigations based on the requirements. The surface grinding has been used to compare the surface finish of the ELID and without ELID processes.

Table 4.1 The Current duty ratio and the pulse width

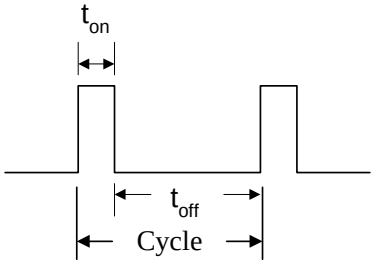

Duty ratio %	t_{on} µs	t_{off} µs
30	3	7
40	4	6
50	5	5
60	6	4

4.9 Measuring methods and measuring instruments

4.9.1 Surface measurements

Measurement of the ground surface is an importance measure to evaluate the grinding process. The surface roughness was measured perpendicular to the grinding direction. Surface roughness and the waviness of the workpiece were measured using Form Talysurf – 120 series. The measuring probe was 2 μm in diameter, the measuring speed chosen was 0.5 *mm/min* and the measured data were filtered using Gaussian filter. Normarski illuminated microscope was used to study the ground surface obtained from various grinding processes. The surface texture, surface roughness and the subsurface damages have been measured using Atomic Force Microscope (AFM). The grinding wheel surfaces were examined under Scanning Electron Microscope (SEM).

4.9.2 Microhardness

Microhardness of the grinding wheel samples were studied using Matsuzawa MXT 50 digital microhardness tester. Specimens were tested under varying loads from 20 *g* to 200 *g*. The dwelling period for the load application was 15 *s*. The sample was placed on the table and the microscope is focused on the spot where the microhardness to be measured, and then the indenter was placed on the spot. After the application of load, the indentation diagonals were measured, and the microhardness of the specimen was displayed on the digital display. The table movements (X, Y) were measured using the micrometer provided.

4.9.3. Microconstituents

The microconstituents of the grinding wheel samples at different spots were analyzed using Energy Dispersive X-ray (EDX) analysis.

4.9.4 Nanoindentation

The mechanical properties of the oxidize layers were analyzed using nanoindentation technique. A Triboscope of Hysitron Inc. was used to for the nanoindentation experiments.

Chapter 5

Fundamental analysis of the ELID

5.1 Introduction

The ELID grinding is used to establish nano-surface finish on difficult to machine materials. This fixed abrasive finishing process is highly suitable for components with varying cross sections such as aspheres. These components need better geometrical accuracy as well as free from subsurface damages. The finishing process should be controlled very accurately in order to achieve the requirements. For better process control, the mechanism of the process should be well known. The ELID grinding is a hybrid process, which consists of an electrochemical and a mechanical process. The change of ones parameter may influence the other but, there were no such previous studies reported so for, which promotes the fundamental analysis of the ELID grinding. It is evident that the fundamental studies will be more helpful to understand the importance of the selection of the ELID parameters and its influences.

The mechanism of the ELID grinding has been studied by comparing the grinding forces, the stability of the forces, the surface finish and the wheel wear with the conventional method. The fundamental studies were conducted by

1. Changing the ELID parameters at similar grinding process parameters,
2. Changing the grinding process parameters with similar ELID parameter and

3. Changing the grinding process parameters and the ELID parameters.

In addition, the advantage of the ELID can be examined using a comparison between the ELID and without ELID processes. The phenomena of the oxide layer can be studied by comparing the grinding forces pattern reordered during ELID and without ELID grinding. The following sections explain how the oxidized layer formed during ELID will facilitate to promote good surface finish.

5.2 A comparison between conventional and ELID grinding processes

The mechanism of material removal from a brittle surface is entirely different from the material removal mechanism of metals. The material removal from the brittle surface can be performed using anyone of the following material removal modes

1. Brittle mode,
2. Semi-ductile mode and
3. Ductile mode.

Every component almost uses all the above three modes in order to achieve the requirements. Therefore it is necessary to investigate the effectiveness of the ELID at different grinding modes. The experiments were performed by grinding the optical glass (BK7) specimens using three different grinding wheels of grades #325, #1200 and #4000 for producing brittle, semi-ductile and ductile mode, respectively. The bond material of the above grinding wheels was cast iron-cobalt hybrid bonding (FCI-X), which are mostly recommended with the ELID [Ohmori and Nakagawa, 1990]. The mean grit sizes of the grinding wheels are 40/60 μm, 8/20 μm and 2/6 μm for the above grade wheels, respectively. The grinding conditions for the brittle mode grinding were spindle speed: 3000 *rpm*, feed rate: 200 *mm/min* and depth-of-cut: 5 μm. The grinding

conditions for the semi-ductile mode grinding were spindle speed: 3000 *rpm*, feed rate: 200 *mm/min* and depth-of-cut: 2 μm, and for the ductile mode grinding spindle speed: 3000 *rpm*, feed rate: 200 *mm/min* and depth-of-cut: 1 μm. The ELID parameters for all the above grinding modes were I_p = 10 *A*, V_p = 90 *V* and current duty ratio of 50% (T_{on} – 5 μs, T_{off} – 5 μs).

Experiments were conducted at two different grinding modes: without ELID (conventional) and ELID. The average surface roughnesses of the above grinding modes measured perpendicular to the grinding direction were 1.533 μm, 0.567 μm and 0.026 μm for without ELID, and 0.563 μm, 0.161 μm and 0.006 μm for the ELID, respectively. The improvement in surface finish shows clear evidence that the ELID is an efficient process for finishing hard and brittle material, and it is also found that the ELID works efficiently in all grinding modes. Figures 5.1(a), (b) and (c) show the Normarski interference micrographs of ground glass surface at brittle, semi-ductile and ductile modes using the ELID, respectively.

Better performance of ELID process compared to conventional grinding (without ELID) can be easily observed at the semi-ductile mode when the ground surfaces are investigated under Normarski microscope. Figures 5.1 (d) and (e) show the Normarski micrograph of the ground surfaces machined using #1200 grade wheels without and with ELID respectively. The ground surface obtained using the ELID grinding technique contains less crashed parts (produced due to the interruption of grinding steaks) than that without ELID.

(a) Brittle mode (#325 , R_a : 0.215 μm)

(b) Brittle & Ductile (#1200, R_a: 0.112 μm)

(c) Ductile mode (#4000, R_a: 0.009 μm)

(d) Without ELID (#1200, R_a: 0.184 μm)

(e) With ELID (#1200, R_a: 0.099 μm)

Figure 5.1: Normarski micrographs of ground glass surfaces [50 X].

5.3 The phenomenon of the oxide layer

The main difference between the conventional grinding and the ELID grinding is the application of current to facilitate the self-sharpening effect of the harder metal bonded grinding wheels. However, the application of current oxidizes the wheel-active-surface (where the active grits are bonded), and the produced oxide deposited on the wheel surface. The oxide layer is named as 'self-protecting layer' of the ELID, which controls the bond material from further oxidation. The bond material of the ELID-grinding wheels is subjected to a hybrid process of electrolytic corrosion and mechanical etching (wheel/work interface), which may cause the change of topography of the grinding wheel while grind. If there is any change in the wheel topography, the effect will be reflected in the grinding forces. Therefore, the phenomena of the oxide layer can be explained by the deviation of grinding forces from the conventional grinding forces. The grinding parameters chosen for the experiments were spindle speed: 3000 *rpm*, feed rate: 200 *m/min*, depth-of-cut: 1 μm/pass. The ELID conditions were I_p = 10 *A*, V_p = 90 *V* and current duty ratio of 50% (T_{on} – 5 μs, T_{off} – 5 μs).

The normal and tangential forces obtained during conventional grinding are shown in figures 5.2 (a) and 5.2 (b), respectively. It can be observed that the normal and tangential forces almost remain constant although the grinding time increases. There is no much difference between the force recorded at the beginning and the end of the process. The normal force at the beginning and the end of the process were 60.13 *N* and 62.44 *N*, respectively. Figure 5.3 shows the normal and tangential forces, and dressing current information of the ELID grinding. Here the normal force increases gradually and reduces after reaching a peak point. Repeation of the increase and decrease of force occurs throughout the ELID grinding process and creates periodic

patterns on the normal force diagram. From Figure 5.3 (a) it is observed that the normal force gradually increases to 50.75 *N* and decreases to 19.73 *N*. After reaching a minimum force, the normal force starts to increase and forms a periodic pattern.

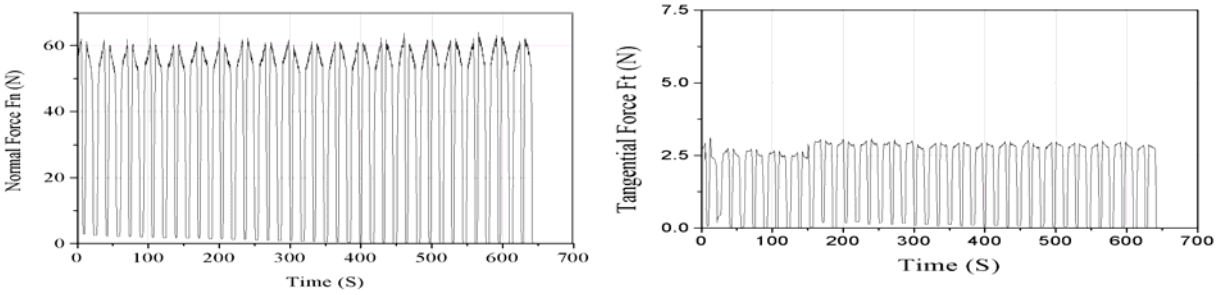

(a) Normal grinding force (b) Tangential grinding force

Figure 5.2: The Normal and tangential forces during conventional grinding.

The analysis of the normal and the tangential forces, and the dressing current explain the phenomena of the oxide layer. Figure 5.3 (b) shows the sudden increase of tangential force which may be due to the breakage of the insulating layer from the wheel surface, which was verified by the behavior of the dressing current. During that period an increase of dressing current to a maximum of 1.617 *A* was noticed, and then it reduced to 1.242 *A*. This kind of phenomena was observed throughout the grinding process [Figure 5.3(c)]. The breakage of the oxide layer increases the conductivity of the wheel surface that stimulates the electrolysis, which causes an increase of current and gradually decreases when the layer was formed. The behavior of insulating layer is characterized by comparing the phase relations between the grinding forces and current. The dressing current and the tangential force increases when the normal force decreases as can be seen in Figures 5.3 (c), 5.3 (b) and 5.3 (a), respectively. From

these periodic patterns, it is clear that the oxide layer is not fully worn out, but breaks suddenly after reaching a certain condition. The condition of breakage of the insulating layer is not clear but the factors influencing the layer breakage may be the thickness of the insulating layer, the contact area between the workpiece and the wheel, and the grinding parameters. The study on the phenomena of the insulating layer provides important information about the ELID. They are the reduction of forces and the instabilities. Therefore, it is necessary to examine the force instabilities at different ELID conditions.

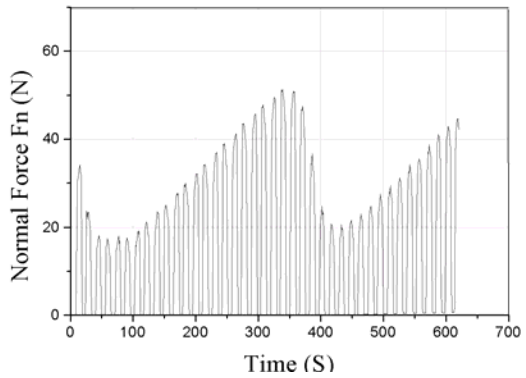

(a) Normal force

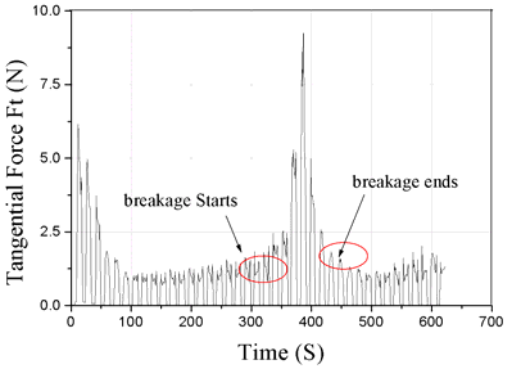

(b) Tangential force

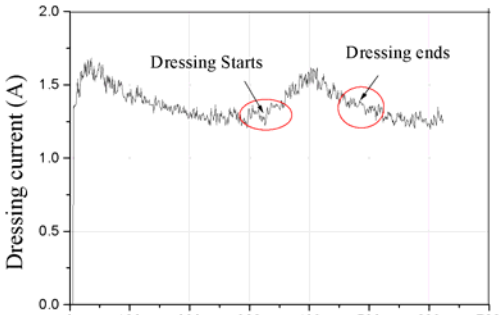

c) Dressing current

Figure 5.3: Normal and tangential forces and dressing current during the ELID grinding.

5.4 The effect of the ELID parameters

The effect of the change of the ELID parameters on the grinding forces, the surface finish and the wear of wheels has been presented in this section. The influence of T_{on} and T_{off} on pulsed plating has been reported by Ibl et al [Ibl et al., 1978; Ibl, 1980]. However, there were no such studies reported on ELID. Varying the current duty ratio is the easiest way of varying the average current (I_m) supplied for the electrolysis.

5.4.1 Effect of current duty ratio on the grinding forces

The stability of the grinding forces is an important factor in the grinding process. Therefore it is essential to analyze the stabilities of the forces at different in-process dressing conditions. The experiments were performed at similar grinding conditions (similar feed rate, spindle speed and depth-of-cut), and the in-process dressing conditions were varied by changing the current duty ratio from 30% to 60%.

The grinding forces were recorded with respect to the wheel rotation, and four rotations of the grinding wheel makes 900 points. An average force was calculated from every four rotations of the grinding wheel in order to minimize the error. The glass surface was ground using FCI-X – #325 wheels and an average surface roughness of 0.564 μm was achieved. The vertical grooves were ground on the glass surface using FCI-X – #4000 wheel. Each groove was ground to a depth of 250 μm. The grinding parameters for the above experiments were spindle speed: 3000 *rpm*, feed rate: 200 *mm/min* and depth-of-cut: 1 $\mu m/pass$.

Average values for every 200 *sec* are taken to show the overall changes during the whole grinding process. A comparison of grinding forces between conventional grinding and ELID (current duty ratio of 50%) are shown in Figures 5.4 (a) and (b), respectively. The normal grinding force obtained during the ELID grinding was less than the normal force of the conventional grinding at any instant, for example at 2000 *sec* for conventional and ELID grinding process were found to be 59.6 *N* and 21.1 *N* respectively. The normal cutting force was reduced almost three times by the application of the ELID.

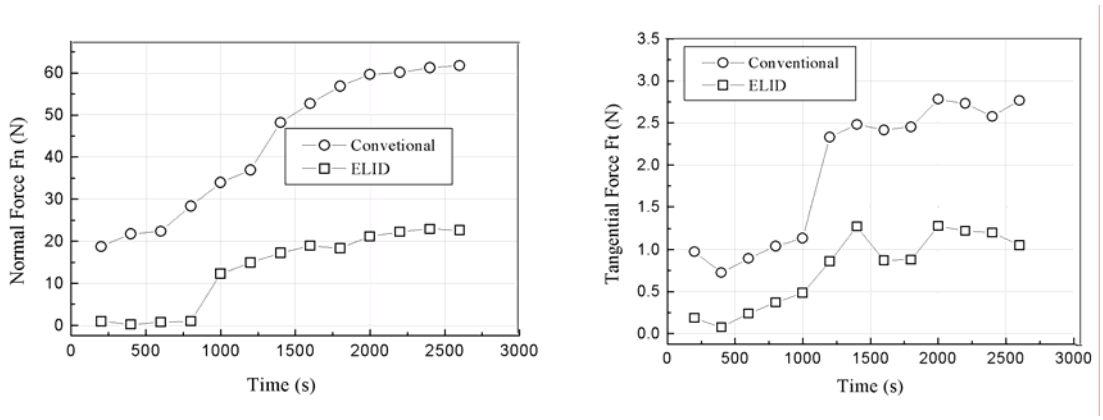

(a) Normal grinding force (b) Tangential grinding force

Figure 5.4: Normal and tangential grinding forces during conventional and the ELID grinding.

Figures 5.5 (a) and (b) show the comparison of normal and tangential forces at different current duty ratios. Figure 5.5 (a) shows that the normal cutting forces are minimum and more stable when the current duty ratio increases. The normal cutting forces at 2000 *sec* were found to be 28.7, 26.4 and 20.43 *N* for current duty ratios of 30, 40 and 60%, respectively. Figure 5.5 (b) shows that the tangential force is unstable

irrespective of current duty ratio. The instability of tangential force is due to the breakage and formation of the insulating layer from the grinding wheel that is unavoidable during in-process dressing. In-process dressing with high current duty ratio can minimize the tangential force even though it is unstable. The normal grinding force was found to be more stable and minimum when grinding with current duty ratio more than 40%.

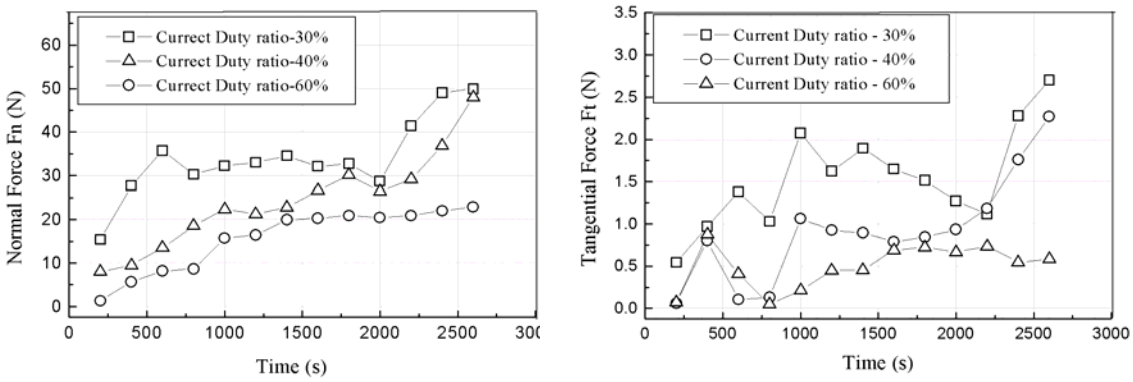

(a) Normal grinding force (b) Tangential grinding force

Figure 5.5: Normal and tangential grinding forces during ELID grinding at different current duty ratios.

The current recorded during in-process dressing at 50% and 60% current duty ratios are shown in figures 5.6 (a) and 5.6 (b), respectively. From the comparison, it was found that at 60% duty ratio the dressing frequency was more as compared to that of the 50% duty ratio. The increase of the dressing frequency with the increase of current duty ratio explains that the layer on the wheel-active-surface is softer, which causes the breakage of the layer often. From the above result it can be thought that higher the current duty ratio thicker the oxidized bond material or produces more oxide on the surface of the wheel. The oxidized layer thickness varies the grit holding strength. The grit holding strength can be related to the grit protrusion height to the thickness of the

oxidized bond material. It is difficult to measure the actual thickness of the bond material oxidized, but a comparison can be done by the oxide layer deposition on the grinding wheel. Thinner oxidized layer can hold the worn diamond grains for a longer duration than the thicker layer. When the surface is ground with a thinner layer, it has more chance of grinding using worn diamond particles and hence there is an increase in the normal force. The breakage and the formation of layer take longer time, which make the force unstable at very low current duty ratios.

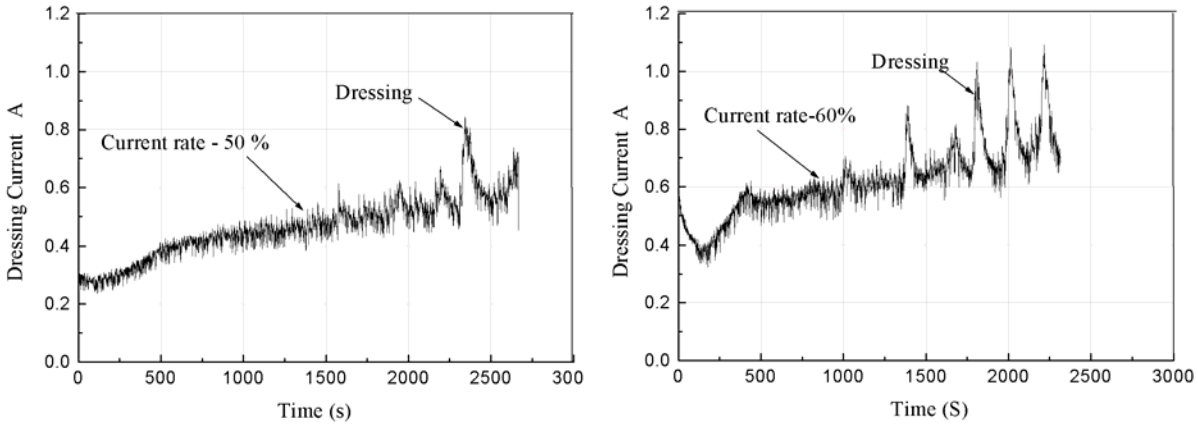

(a) Dressing current at 50% current duty ratio

(b) Dressing current at 60% current duty ratio

Figure 5.6: Comparison of frequency of dressing between 50% and 60% current duty ratios.

5.4.2 Influence of in-process dressing conditions on surface roughness and tool wear.

The surface finish and the wheel wear are other two important results obtained at different in-process dressing conditions. The radial wear of the grinding wheel was measured using the profile sensor. The surface roughness and the tool wear ratio with

respect to different current duty ratios are shown in Figure 5.7. The tool wear ratio is defined as the reciprocal of the grinding ratio as indicated in the Eq. (5.1).

$$Tool\ wear\ ratio(W_t) = \frac{Vol.of\ material\ removal\ from\ tool\ (V_t)}{Vol.of\ material\ from\ workpiece(V_m)} \tag{5.1}$$

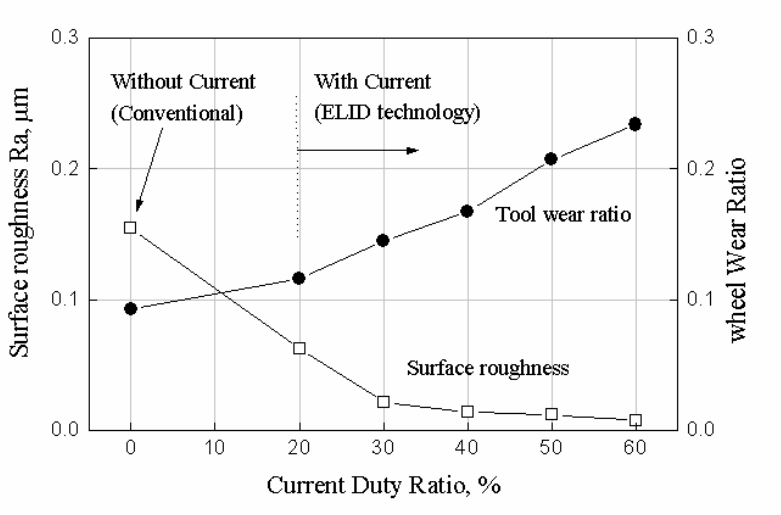

Figure 5.7: Effect of duty ratio on surface finish and tool wear ratio.

The average surface roughness *(R_a)* and the Tool wear ratio *(W_t)* obtained from conventional grinding were 0.154 *μm* and 0.093, respectively. The R_a and W_t from ELID grinding process at 50% current duty ratio were found to be 0.012 *μm* and 0.207, respectively. The average surface roughness improved more than 12 times and the tool wear ratio increased more than 2.23 times when applying the ELID grinding technique. Comparison between the in-process dressing at 50% and 60% current duty ratio shows the average surface roughness improved 1.5 times and tool wear ratio increased 13%. From the above results it is clear that when the current duty ratio is more than 50%, the wheel wear increases without much improvement in surface finish. From the results it is clear that the average current supplied for the electrolysis has a strong influence on

the surface finish and wheel wear. There is a remarkable improvement of surface roughness when the wheel is dressed up to an average current of 2 - 3 *A* than the conventional grinding. The grinding ratio decreased from 22 to 15 when dressed more than the average current of 4 *A*, and if it is more than 5 *A* the grinding ratio was dropped to 5. The results obtained show that there should be significant changes taking place on the active-wheel-surface when varying average current.

The wheel surface was assumed to have been ground by three types of grit. The first type of grit is tightly held by the bonding material and partially held by the oxide layer. The second type of grits is fully held by the oxide layer and the third type are worn diamond particles held by the layer. If the cutting pressure exceeds the holding pressure of a diamond grit, the worn diamond particles come out of the bonding matrix and become like loose abrasives and do the polishing process (if the grit size is more than depth of cut). The grit held by the oxide layer is loosely held in the bond and the process is same as the lapping process. The oxide layer holding the diamond grit is like the lapping pad and the bonding material acts like a supporting pad. The real grinding process is done by the grit which is tightly held by the bonding material. Thus, during ELID a smoother surface can be obtained. When the thickness of the oxide layer increases, the abrasives are loosely bonded and the grinding process becomes almost like polishing process. From the experiments it was observed that the surface roughness is much better when the current duty ratio increases. The oxide layer formed on the grinding wheel surface also acts as a damper and minimizes grinding chatter.

The rigidity of the machine is also important to get a fine surface finish. But ELID minimizes machine stability problems because the oxide layer formed on the surface of

the wheel improves the quality of protrusion height of grain cutting edge and mirror surface finish is possible with low rigidity machines [Zhang et al., 2001]. If the grinding wheel is dressed more frequently, the work surface is always ground with freshly protruded diamond particles, which can produce smoother surface.

5.4.3 The surface defects and the ELID parameter

Figures 5.8 (a), (b) and (c) show the Normarski micrographs of ground glass surfaces at current duty ratios of 20%, 40 % and 60%, respectively. The ground surface machined at 20% shows a sudden failure of ductile surface in the form of cracks that originated beneath the surface. There is a visible microcrack observed in the ground surface obtained using 40% current duty ratio. The surface free from visible microcracks was observed when grinding with 50% and more. Though, the subsurface damage (SSD) of the ground surface surfaces was not examined in this analysis it is clear that the grinding defects can be minimized when grinding using 50% current duty ratio.

(a) Surface defects (b) Surface cracks (c) Defect free surface

(Current duty ratio: 20%) (Current duty ratio: 40%) (Current duty ratio: 60%)

Figure 5.8: Normarski micrographs [50 X] of ground surfaces at different duty ratios.

5.5 The effect of the grinding parameters

5.5.1 Effect of feed rate on ELID grinding

When the grinding wheel is dressed at various conditions, the grinding forces, the surface roughness and the wheel wear differ though the grinding conditions are similar as discussed in the previous section. Now the influence on change of grinding parameters at similar dressing condition has been experimented. The experiments were conducted by varying the feed rate from 200 – 600 *mm/min* without varying the spindle speed and the depth-of-cut. Cast iron-cobalt bonded grinding wheel of diameter 75 *mm*, width 3 *mm* and grade #4000 was used for the experiments. The grinding parameters were spindle speed: 3000 rpm and depth-of-cut: 1 μm/pass; the ELID parameters were I_p – 10 A, V_p – 90 V and R_c – 50% (T_{on} – 5 μs, T_{off} – 5 μs).

Figures 5.9 (a) and (b) show the normal and tangential grinding forces at different feed rates. When the feed rate increases, the normal and the tangential forces also increase. However, the process was stopped due to the appearance of the black strips on the work surface. There was no defective surface reported up to 400 *mm/min*, and the process was stopped at 150 μm and 100 μm for the feed rates 500 *mm/min* and 600 *mm/min*, respectively.

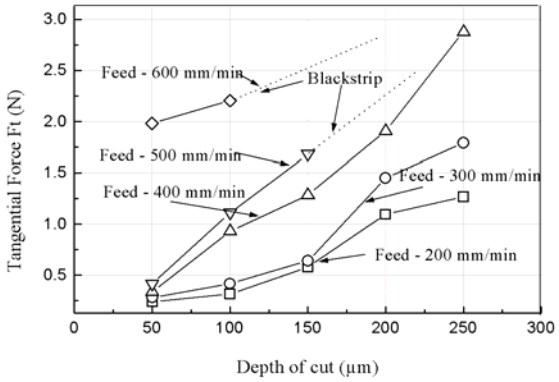

(a) Normal grinding force

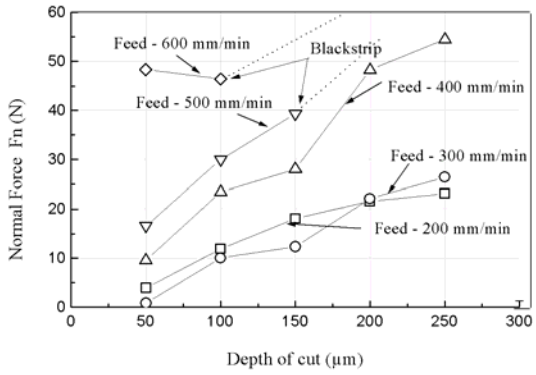

(b) Tangential grinding force

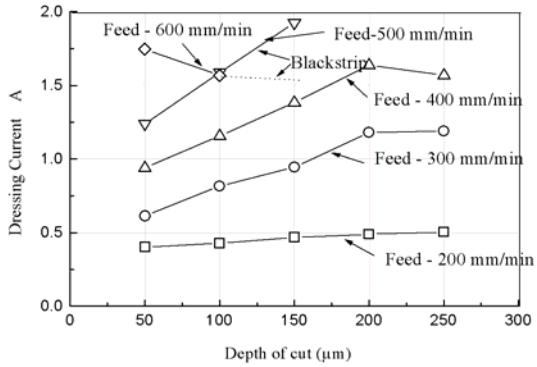

(c) Dressing current

Figure 5.9: Effect of feed rate on the ELID.

Figure 5.9 (c) shows that the dressing current increases with increase of feed rate. At feed rate 200 *mm/min*, the current gradually increased up to 0.468 *A* at a total depth of cut of 150 μm and almost remains constant throughout the process. At feed rates 300 *mm/min* and 400 *mm/min*, the current gradually increased up to a total depth of cut of 200 μm and almost remains constant. However, the dressing current at the beginning of feed rates of 500 and 600 *mm/min* are found to be much higher. It was observed that when the current increases more than 2 *A* the black strips started to appear on the surface of the workpiece.

(a) Clean Surface after using feed rate 200 mm/min

(b) Black strips after using feed rate 500 mm/min

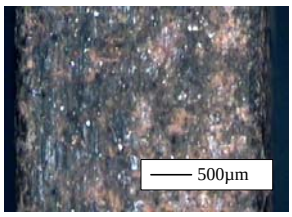

(c) Grinding wheel surface after machining Clean Surface

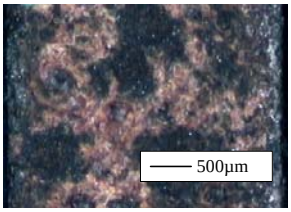

(d) Grinding wheel surface after machining Black strips

Figure 5.10: Microscopic views of ground surfaces and grinding wheels.

Figure 5.10 (a) is a microscopic view of a clean surface ground at feed rate of 200 *mm/min* and figure 5.10 (b) shows the microscopic view of a ground surface with black strips at 500 *mm/min*. Figures 5.10 (c) and 5.10 (d) show the microscopic view of grinding wheels after machining the clean and black strips, respectively. It was found that the grinding wheel surface was more uniform after producing clean surface than the wheel surface after producing the black strip on the workpiece. Black spots were found on the surface of the grinding wheel as can be seen in Figure 5.10 (d).

5.5.2 The effect of the feed rate and current duty ratio on the ELID grinding

The grinding experiments were conducted using feed rates 100 – 600 *mm/min* and the current duty ratio 20 – 60 %. Figure 5.11 shows the correlation between the grinding parameter and the ELID parameter. From the results it is clear that the correlation between the grinding parameters and the ELID parameters have a strong influence on

the surface defects. Increase in feed rate increases the removal rate of oxide layer from the grinding wheel surface and leads to an increase in current. If the removal of oxide layer from the grinding wheel is more than the formation of oxide layer, the work surface has more chances of being ground by a grinding wheel surface containing bonding material and worn diamond grits of the wheel. The nature of the wheel and workpiece contact in grinding has a strong effect on the temperature, force, surface integrity and wheel wear in grinding. The grinding speed, feed rate and the depth-of-cut have strong influences on the energy (heat) conduction to the workpiece. If the work surface is ground by bonding material and worn diamond particles, rubbing takes place rather than grinding. The rubbing action increases grinding forces and the heat passed into the workpiece and for this condition carbon particles from the bonding material may be deposited on the surface of the workpiece and produces the black strips. From the results it is clear that dressing with high current duty ratio increases the possibilities of increasing of the feed rate without producing surface defects.

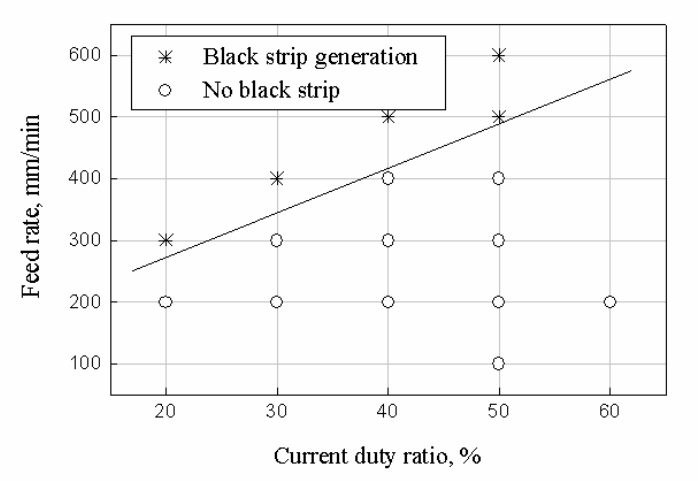

Figure 5.11: Effect of feed rate and the ELID on ground surface.

The equivalent-chip-thickness introduced by Peters [Peters, 1990] is a useful measure of the amount of material removed per unit area of wheel surface. The equivalent-chip-thickness is expressed as

$$h_{eq} = \left(\frac{v_w}{v_s} \right) a \tag{5.2}$$

where h_{eq} – Equivalent-chip-thickness,

v_w – work velocity,

v_s – wheel velocity and

a – depth-of-cut.

The h_{eq} is increases with the increases of feed rate when the spindle speed and the depth-of-cut were unchanged. However, it can be concluded that if the equivalent-chip-thickness increases beyond certain value, the application of the ELID become ineffective.

5.6 Concluding remarks

The application of the ELID is found to be effective in all grinding modes such as brittle, semi-ductile and ductile. The self-protected oxide layer produced on the active-wheel surface breaks at certain condition, which depends on the properties of the oxide layer. The breakage of the oxide layer from the wheel-active-surface increases the conductivity, which stimulates electrolysis and the oxide layer is reformed on the wheel-active-surface. The breakage of the oxide layer makes the wheel surface free from worn grits and loaded chips. The breakage and formation cycle produces some force instabilities, which can be minimized when dressing using high current duty ratio. The surface finish improves when the wheel is dressed using high current duty ratio. However, it can be achieved with the increase of wheel wear, which shows that the active grits are bonded by less harder bonding matrix than the actual bond matrix

(metal). The machining parameters such as feed rate influence the ELID. When the equivalent chip thickness exceeds to a certain condition, the ELID totally fails and produces surface defects. If the removal rate of the oxide layer is more than the formation rate, the possibility of failure of the ELID is more. Therefore care should be taken when grinding with high feed rate, larger depth of cut and larger contact area. The surface defect produced at ductile mode removal was reduced when dressed the wheel using 40 % and more current duty ratios.

The wear mechanism of the grinding wheels dressed using the ELID, the wear reduction strategies and the model for in-process dressing has been presented in the forthcoming chapter.

Chapter 6

Wear mechanism of the ELID-grinding wheels

6.1 Introduction

The ELID-grinding wheels have a conductive bond matrix made of either metals or metal-resin bond. The superabrasives such as diamond and CBN are embedded into the metal/metal-resin matrix. The grains are exposed from the wheel-active-surface when necessary bond matrix is removed. The removal occurs by electrolytic corrosion when the wheel is dressed using low current and voltage, and the process continues until a required grit protrusion is achieved. The dressing current is controlled based on the force ratio during grinding or monitoring the sharpness of the grits [Murata et al., 1985; Karmer et al., 1999]. However, the above control methods are not suitable for superabrasive wheels because of the following reasons:

- The grit protrusion needed (50 % of mean grit size) is less than 1μm for most of the wheels, and
- The wheel life (the time between the dressing intervals) is shorter due to wheel loading.

Therefore, the ELID uses different technique, which produces an oxidized layer on the wheel surface to control the electrolysis which produces non-linearity during electrolysis. The behavior of different bonding materials has been reported based on the thickness of the oxide layer formation by Ohmori et al. [Ohmori et al.., 1997]. However, the wear rate

of the oxide layer during grinding depends on the grinding parameter and hence the wear mechanisms of the ELID-grinding wheels need to be studied carefully in order to control the process efficiently.

6.2 The character of the ELID-grinding wheels

The bond-materials used for the ELID-grinding wheels have been classified in a group as ‘Transition metals’ in the periodic table as shown in Figure 6.1. The 38 elements in groups 3 through 12 of the periodic table are called "transition metals". Among the metals, the transition elements are both ductile and malleable, and conduct electricity and heat. The interesting thing about transition metals is that their valence electrons, or the electrons they use to combine with other elements, are present in more than one shell. The Transition metals are the elements found between the Group IIA elements and the Group IIB elements in the periodic table. The Group IIB is sometimes considered transition elements. The transition elements are also known as the d-block elements, because while the outermost level contains at most two electrons, their next to outermost main levels have incompletely filled d-sub-orbital, which are filled-up progressively on going across the periodic table from 8 to 18 electrons. The filling of the d sub-orbital of the transition elements across a row of the periodic table is not always regular.

The Properties of transition metals are largely dependent on the electronic configuration of the electrons in the outer shell and in the penultimate outer shell. The transition elements readily form alloys with themselves and with other elements. The atomic size is fairly constant since the electrons in the outer most shells have similar environments. The low ionization potentials mean that the elements show variable valency states by loss of electrons from the‘s’ and ‘3d’ orbital. The elements in this group can have different oxidation states which makes them useful as catalysts. The common material used for the ELID-grinding wheels are copper, bronze, cobalt and cast iron, which possesses the above said properties.

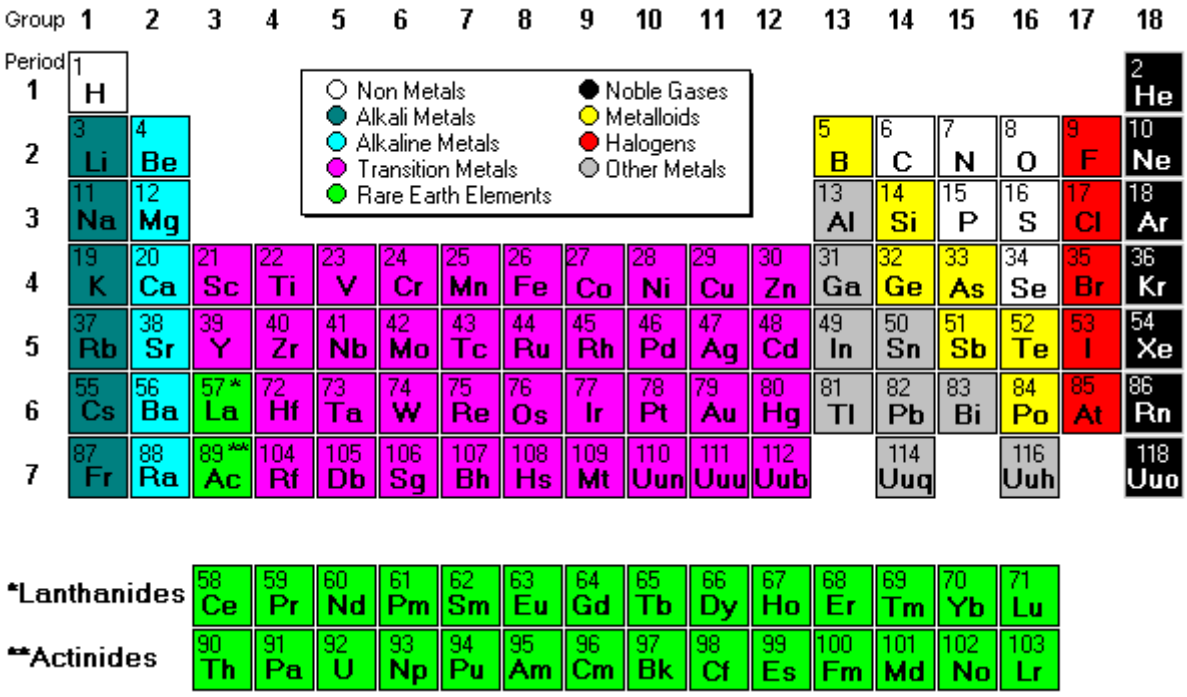

Figure 6.1: Periodic Table.

6.3 Wear mechanisms of the ELID-grinding wheels

Wheel wear is an extremely complex process, which involves the culmination of numerous wear events encountered between many single grits and the workpiece. The conventional way of quantifying wheel wear is to express it as volumetric loss of material, which tells little about the wear mechanism. It is generally recognized that there are three main mechanisms of wheel wear: - attritious wear, grain fracture and bond fracture. Attritious wear involves dulling of abrasive grains and the growth of wear flats by rubbing against the workpiece. Grain fracture refers to removal of abrasive fragments by fracture within the grain, and bond fracture occurs by dislodging the abrasive from the binder. Binder erosion is caused by reduction of bond strength and promotes grain dislodgement, especially with resin and metal-bonded wheels [Malkin, 1987]. Attritious wear has the smallest contribution to the decrease in volume but the wheel life is determined based on the attritious wear. Attritious wear reduces the sharpness and the protrusion height of the grit, and it leads to wheel glazing, which is an indication of the end of wheel life.

Generally the end of wheel life is indicated by excessive forces, or by loss of finish, form, or size of the workpiece. The end of wheel life is deduced by a skilled operator, or with the help of special sensors [Hassui et al..., 1998; Amin et al.., 2000; Gomes et al.., 2001]. During ELID grinding, the wheel is redressed during the grinding operation. The wheel wear must be compensated in order to obtain high accuracy and tolerance. If the wheel is dressed prior to the end of wheel life, the wear rate will increase, and if it occurs later the

workpiece surface will be affected. The dressing intervals should be selected in a way that balances better grinding performance with reasonable wheel wear.

The wear mechanism of the ELID-grinding wheels is classified into two different stages. The first stage of wear occurs during pre-dressing and the second stage is during in-process dressing. The knowledge of wear during both the stages should be essential for precision grinding.

6.3.1 Wear during pre-dressing

The grinding wheel need to be pre-dressed in order to provide enough grit protrusion to facilitates grinding. The transition bond metals sometimes give away two electrons and sometimes three electrons during electrolysis. For example iron gives Fe^{2+} or Fe^{3+} to form oxide or hydroxides during electrolysis. The anodic reaction during the ELID is as follows:

$$Fe \rightarrow Fe^{2+} + 2e^{-} \quad (6.1)$$

$$Fe^{2+} \rightarrow Fe^{3+} + e^{-} \quad (6.2)$$

$$Fe \rightarrow Fe^{2+} + 2e^{-} \quad (6.3)$$

$$H_2O \rightarrow H^{+} + OH^{-} \quad (6.4)$$

$$Fe^{2+} + 2OH \rightarrow Fe(OH)_2 \quad (6.5)$$

$$Fe^{3+} + 3OH \rightarrow Fe(OH)_3 \quad (6.6)$$

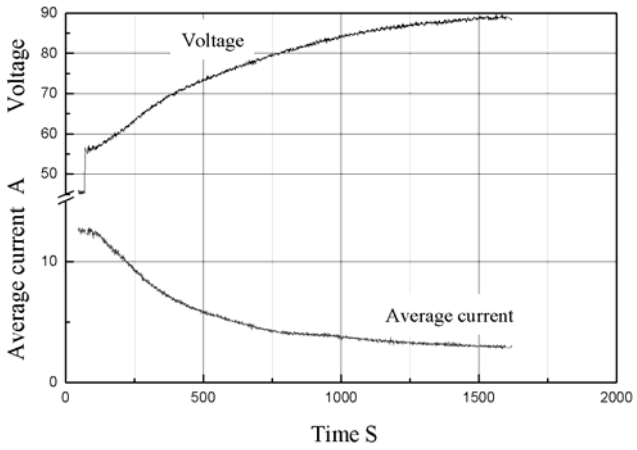

Figure 6.2: Average current and voltage during pre-dressing.

The self-protected oxide layer (iron hydroxide) resists the flow of current and therefore a drop in current and increase in voltage has been reported. Figure 6.2 shows the average current and the voltage recorded during pre-dressing. Figure 6.3 shows the grinding wheel profile measured using the profile-sensor before and after pre-dressing. The pre-dressing conditions were 90 V, 10 A, pulse width of 10 μs (T_{on} - 5 μs, T_{off} - 5 μs) and spindle rotation of 1000 rpm. An increase of wheel diameter of about 250 μm was noticed after pre-dressing. The wheel after dressing was inspected under an optical microscope and it was found that the surface was completely covered by the oxide of the flow out bond material, which covers the active grits and only few grits were exposed on the top layer of the wheel. However, if the layer was formed by the metal oxide deposition, it will be totally removed during grinding and that makes some inaccuracies in the precision grinding process. The reason for the increase of diameter can be due to the oxide produced which is not solvable in the electrolyte. It started growing on the grinding wheel surface, which prevents the bond material from further oxidizing. Hence the wear of

grinding wheels during pre-dressing depends on the bond material and the type of electrolyte used.

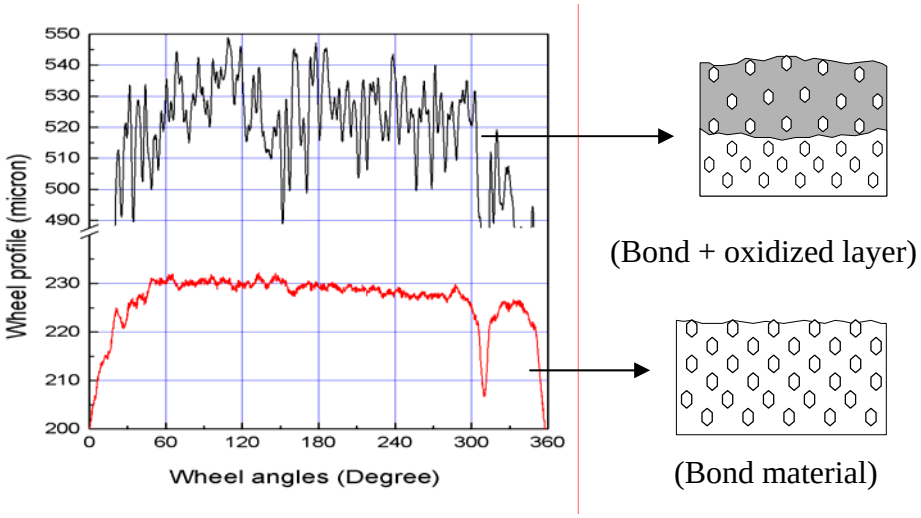

Figure 6.3: Grinding wheel profiles before and after dressing.

The wear rate of the oxide layer was analyzed by comparing the wear rate of the oxide layers on a partially over dressed wheel. A grinding wheel was pre-dressed for 10 *min* with the similar dressing conditions stated earlier and the wheel rotation was stopped for 5 *min* without stopping the dressing current. Figure 6.4 (a) shows a partially over dressed grinding wheel that shows the wheel portion near the electrode was increased by about 25 μm. The eccentric wheel was used to grind BK7 glass using the grinding conditions of feed rate: 200 *mm/min*, depth-of-cut: 1 μm/pass and spindle rotation: 3000 *rpm*. Figures 6.4 (b) and (c) show the wheel profiles after 20 and 40 passes respectively. From the result the following conclusions can be drawn:

- The over dressed portion wears much faster than the dressed portion, which means that the over dressed portion should be less hard than the layer previously formed on the wheel surface during pre-dressing.
- The oxide layer produced is not an oxide deposit on the wheel surface because it withstands the grinding forces unto 40 passes and wears slowly, which shows that the layer has enough strength to hold the active grits.

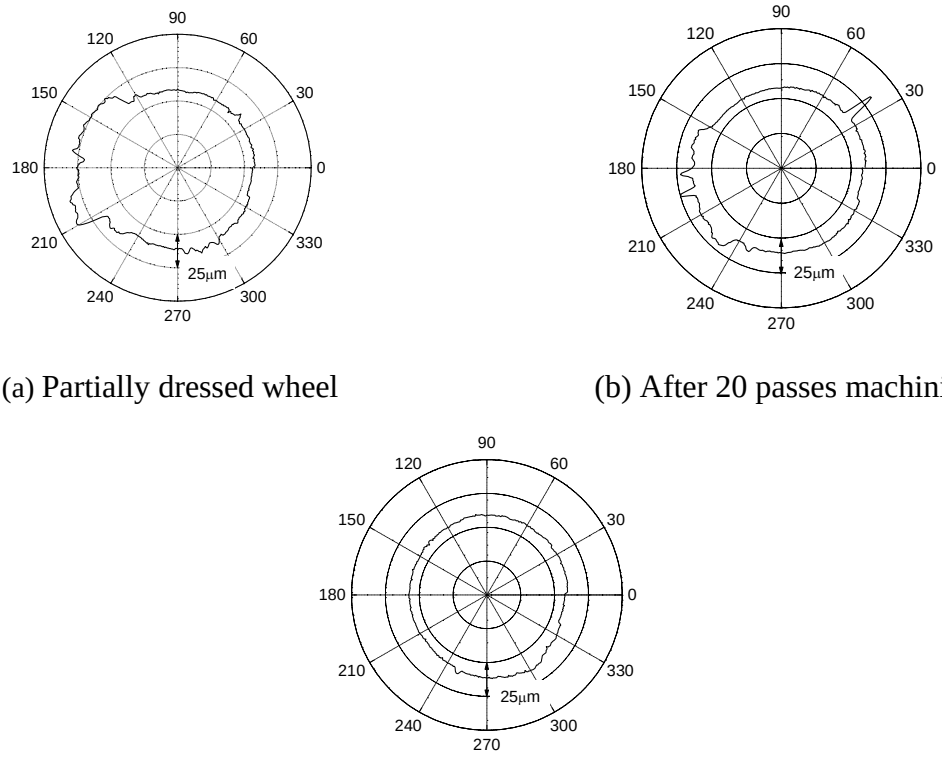

(a) Partially dressed wheel (b) After 20 passes machining

(c) After 40 passes machining

Figure 6.4: Change of wheel profile of an eccentric over dressed wheel.

The phenomena of pre-dressing for wheels other than cast iron-bonded wheels (copper and bronze bonded) were found to be different when dressed at similar dressing conditions. Figure 6.5 shows the copper-bonded grinding wheel profile before and after pre-dressing, and found that there is no change of diameter. However, change of color at the wheel surface due to the deposition of oxide layer was noticed. The bronze bonded wheel wears gradually with the increase of dressing time and there was no oxide layer formed on the grinding wheel (the oxide was soluble in the electrolyte). The above investigations clearly show that there is no bond wear during pre-dressing when the oxide layer is not dissolved by the electrolyte, and this is a process of producing a protective layer on the wheel surface.

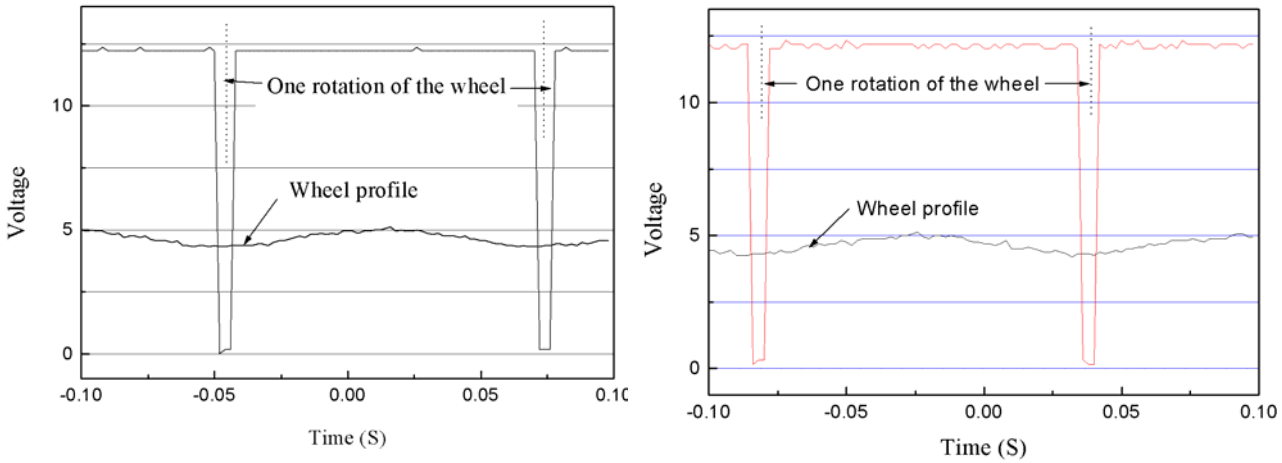

(a) Before dressing (b) After dressing

Figure 6.5: Profiles of a copper bonded grinding wheel before and after pre-dressing.

6.3.2 Wear mechanism during in-process dressing

The pre-dressed cast iron-bonded grinding wheel shows different results when pre-dressed and hence the wear mechanism of the wheel draws attention than other grinding wheels. The mechanisms of wheel wear, the end of wheel life (wheel glazing) and the phenomena of in-process dressing have been analyzed in this section using a simple grinding experiment. A vertical groove was ground on BK7 glass using cast iron-bonded diamond grinding wheel of grade #4000. The force components and the dressing current were recorded with respect to the spindle rotation. The machining conditions were spindle speed: 3000 *rpm*, feed rate: 200 *mm/min* and depth of cut: 1μm/pass. The wheel dressing conditions were 90 V, 10 A and pulse width of 10 μs (T_{on} - 5 μs, T_{off} - 5 μs). The normal force, tangential force and dressing current during ELID grinding are shown in figures 6.6 (a), (b) and (c), respectively.

The drop in dressing current during the air cut region shows that the wheel surface contains thick oxide layer that resists the flow of current. The increase of grinding forces from point A to B shows the condition of instability of the grinding wheel. The pre-dressed wheel surface contains large amount of dislodged grits, which can be identified by larger protrusion from the wheel surface. When the wheel contacts the workpiece, the dislodged grits are removed from the grinding wheel surface that reduces the grit density at the beginning stage and it increases the normal grinding force at the beginning of grinding as seen in Figure 6.6 (a). After the point B, normal force is found to be more stable and it shows that the wheel surface is in a stable condition. After the point C the normal grinding force gradually reduces and started increasing gradually once again. This

kind of phenomena repeats throughout the grinding process, and the cycle time becomes longer or shorter depending upon the material removal/pass. When the normal force starts decreasing, a sudden increase of tangential force is noticed, and it retains only for the few cycles. The increase of dressing current during the above cycle shows the occurrence of electrolytic in-process dressing of the grinding wheel. Similar cycles repeat in between the points D, E and F, which shows the end of wheel lives and the in-process dressing cycles.

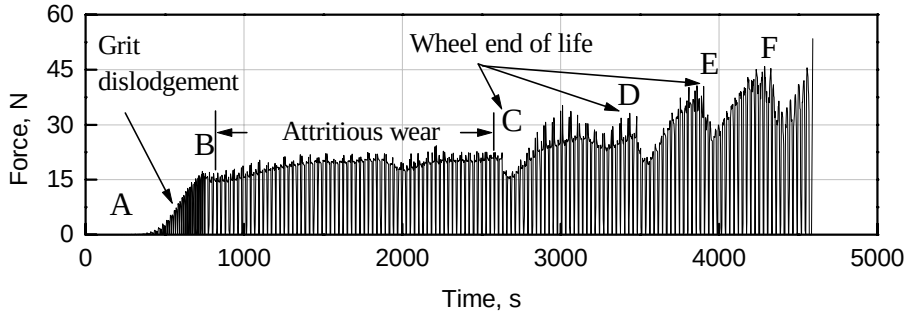

(a) Normal force

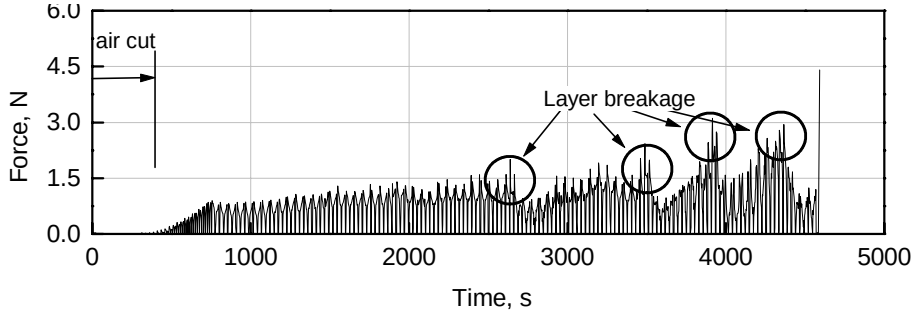

(b) Tangential force

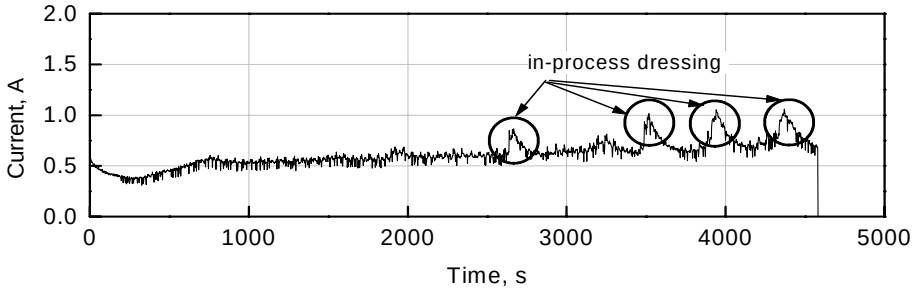

(c) Dressing current

Figure 6.6 Normal force, tangential force and dressing current during ELID grinding

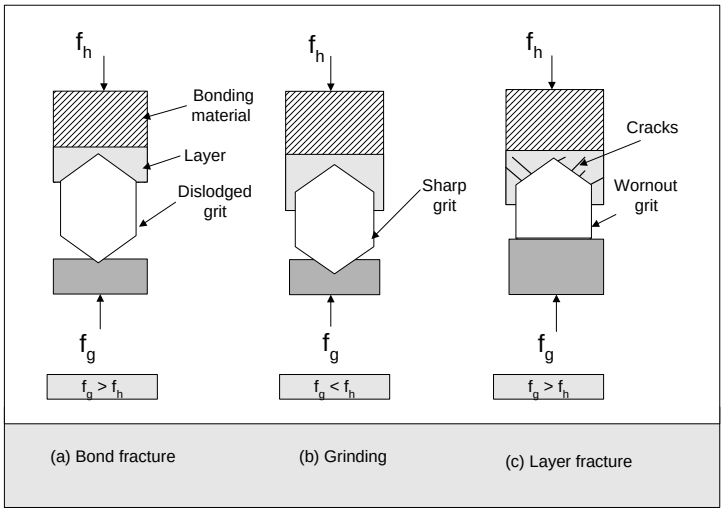

Figure 6.7 Different states of grit-workpiece interaction.

When the diamond grit performs grinding, there are two major forces that are acting opposite to each other on the grit. They are the maximum grit holding force exerted by the bond strength (f_h) and the grinding force per grit (f_g). Figure 6.7 shows the different states of grit-workpiece interaction based on the condition of forces during grinding. Normally the grinding wheel surface consists of diamond grits at different conditions such as dislodged grits, worn out grits and sharp grits. For the dislodged grits, the holding force f_h is lower than f_g, so that the grit cannot penetrate into the workpiece. If the grit cannot penetrate into the work, it is removed from the bond matrix due to the hardness of the workpiece while grinding as illustrated in Figure 6.7 (a). For a sharp grit, f_h is greater than f_g and the grit penetrates and cuts the workpiece material (Figure 6.7 (b)). The depth of penetration depends on the condition of the grit i.e., the sharpness and the size of the grit. Now, the holding force and grinding force for single grit during ELID grinding can be expressed as shown below:

$$f_h = k_1 . \sigma_s . a_g \tag{6.7}$$

$$f_g = k_2 \; S \; h_{\max} \tag{6.8}$$

where,

k_1 – Constant related to wheel topography

k_2 – Constant related to material properties

S – Sharpness factor depends on condition of the grit (size and sharpness),

a_g – Holding area of grit, and

σ_s – Yield strength of the layer.

The grinding force of the grit gradually increases during grinding because of the grit wear. When worn out grit performs grinding, the f_g exceeds f_h and the force exerted on the grit produces cracks on the bonding matrix as seen in Figure 6.8 (c). At this stage, the percentage of grits on active-wheel-surface is dominated by the worn out grits, which promotes the crack propagation throughout the wheel active-surface and creates a macro fracture from the grinding wheel surface. When the insulating outer layer is separated from the wheel-active-surface due to macro fracture, the electrical conductivity of the grinding wheel increases and that stimulates electrolytic in-process dressing.

Assuming that the grinding wheel profile is uniform with equal grit protrusion and that there are N numbers of active grits per unit area, the total holding force can be approximated as,

$$F_h = N \; f_h \; A_g \tag{6.9}$$

When the force per grit is resolved into normal and tangential components, the total normal and tangential forces can be expressed as:

$$F_n = N \ \alpha \ f_g \ \ A_g \tag{6.10}$$

$$F_t = N \ \beta \ f_g \ \ A_g \tag{6.11}$$

where

α, β – The normal and tangential force components of f_g, and

A_g – Total grinding area.

The condition of macro fracture from the wheel or the wheel end of life can be expressed as when,

$$F_n > F_h \tag{6.12}$$

The above grinding experiment was conducted using copper bonded grinding wheel with similar machining and in-process dressing conditions and similar results were obtained. However, the initial wear rate was comparatively smaller than the cast iron-bonded wheel.

6.4 Wear reduction strategies

According to Faradays law of electrolysis, the amount of material removal is proportional to peak current (I_p) and pulse ON-time (T_{on}).

$$m \propto I_p \ T_{on} \tag{6.13}$$

The wheel wear increases with increase in either T_{on} or I_p. If the thickness of layer removed from the wheel surface during macro fracture is more than the grit size of the grinding wheel, the sharp new diamond grits are also removed along with the fractured

layer. This will increase the reduction of wheel diameter and increases the wastage of diamond grits that may cause more form error.

An attempt is made to control the bond fracture by controlling the electrolysis based on the grit size of the grinding wheel. The first step is to control the pre-dressing time of the grinding wheel. If the wheel is pre-dressed for a longer time, it increases more bond fracture at the beginning of grinding. The pre-dressing time for finer grit size wheels (#4000 and more) could be 5 – 10 *min* to produce enough grit protrusion, and courser grit size wheels need to be dressed (# 325 and below) 20 – 30 *min* for better grinding performance.

The second step is controlling the wear during in-process dressing. The simple method of measuring the wheel wear is by measuring the reduction of grinding wheel diameter. Figure 6.8 shows the effect of T_{on} time on wheel wear. The decrease of wheel diameter can be reduced if shorter T_{on} time is used during in-process dressing. Changing the T_{on} time will control the amount of material oxidized or the amount of macro fracture. Courser grit sized wheel needs high grinding efficiency therefore it is recommended that shorter T_{on} (2-4 μs) time is suitable for courser grit size such as #325 and # 1200 which have an average grit size of 46 μm and 12.5 μm respectively. Finer grit size wheels of about an average grit size from 4 μm (#4000) and finer need to be dressed often and a longer T_{on} time is preferable. For finer grits, equal T_{on} and T_{off} time could be selected for better results. Increase of T_{on} time more than T_{off} time, increases the radial wear without any significant improvement in ground surface finish.

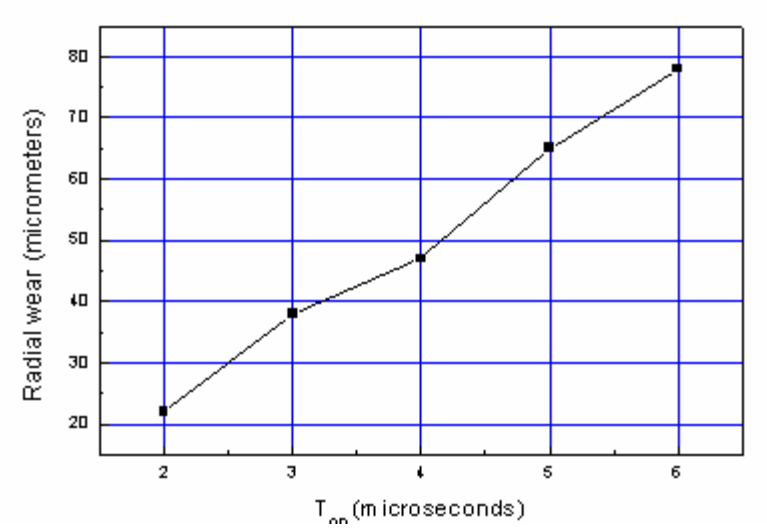

Figure 6.8: Radial wheel wear at different T_{on} time.

6.5 Influence of grinding parameters on wheel-wear

A grinding wheel can be used to perform different operations such as surface grinding, plunge grinding and creep-feed grinding. The operations can be performed using different grinding parameters but, there is no rule for selecting the ELID parameters suitable for different operations. Therefore it is essential to study the behavior of the ELID-wheels at various grinding processes in order to achieve better tolerance. The influence of the combination of the grinding parameter, grinding process (grinding method) and the dressing method has been reverberated in terms of the grinding forces and the surface quality.

The regenerative grinding chatter is mainly influenced by the cutting stability. Grinding hard and brittle materials using grinding wheels with harder binder increases the possibilities of regenerative chatter. The best method of reducing the chatter is by

reducing the wheel hardness [Malkin, 1987]. The application of the ELID reduces the hardness at the wheel active-surface can be more useful to reduce the grinding forces. However, the excessive reduction of bond strength may lead to excessive wheel wear and influences the tolerance of the ground surface. The surface profile traced by the grits and the change of grit density were measured by measuring the surface waviness perpendicular to the grinding direction. Similarly the waviness caused due to the change of wheel profile was also measured and the occurrence of topographical changes was observed using different grinding methods.

Three types of grinding geometry namely a slot, a vertical groove and a flat surface were ground to study the influence of the change of dressing parameters with different machining conditions. The horizontal slot was ground using a larger depth of cut (approximately 3 times of the mean grit size of the wheel) and slower feed rate. The vertical groove was ground by using an increase of contact area for every depth-of-cut/pass and a flat surface was ground using depth-of-cut equal to the resolution of the machine (the allowable minimum depth of cut i.e. 1 μm).

6.5.1 Horizontal slots

The dimensions of the slots were 70 *mm* length, 5 *mm* width and depth of 5 μm. The grinding conditions used were feed rate: 20 *mm/min*, depth of cut: 5 μm/pass and spindle speed: 3000 *rpm*. The dressing conditions were I_p – 10 A, V_p – 90 V and R_c – (20% - 50%). Figure 6.9 (a) shows the average normal and tangential forces measured during machining the slots. The results show that the increase of current duty ratio reduces the

grinding forces. The surface roughness and the waviness of the ground slots measured parallel and perpendicular to the grinding direction are shown in Figure 6.9 (b) and (c) respectively. The surface roughness and waviness increases with the increase of current duty ratio when measured parallel to the grinding direction, but when measured perpendicular to the grinding direction it gradually reduced until it reaches R_c – 30% and then started increasing again. The increase of average surface roughness and waviness measured parallel to the grinding direction shows that higher dressing current changes the wheel profile (due to wheel wear) while grinding. The measurements were perpendicular to the grinding direction which shows that the grit density was higher or grit interaction with the work was found to be better up to 30% current duty ratio. From the results it is found that for better results the grinding wheel should be dressed between 20 – 30% current duty ratio.

The reason for reduction of grinding forces during machining the slots was closely observed. Figures 6.9 (d) and (e) show the grinding forces (digitized using scope) recorded during 20% and 50% current duty ratios respectively. From the results it is clear that the reduction of grinding forces in this case is caused due to the removal of the binder from the grinding wheel due to the hardness of the workpiece.

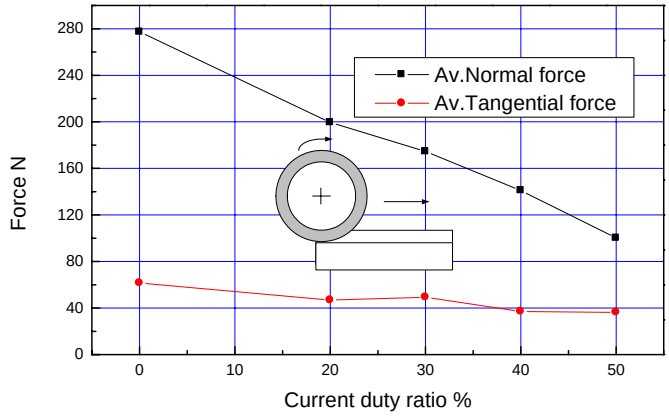

(a) Grinding forces

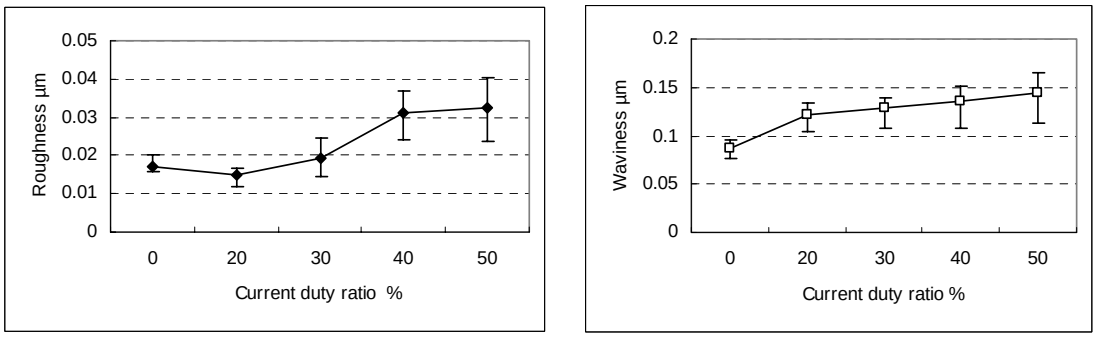

(b) Average surface roughness and waviness measure parallel to grinding direction

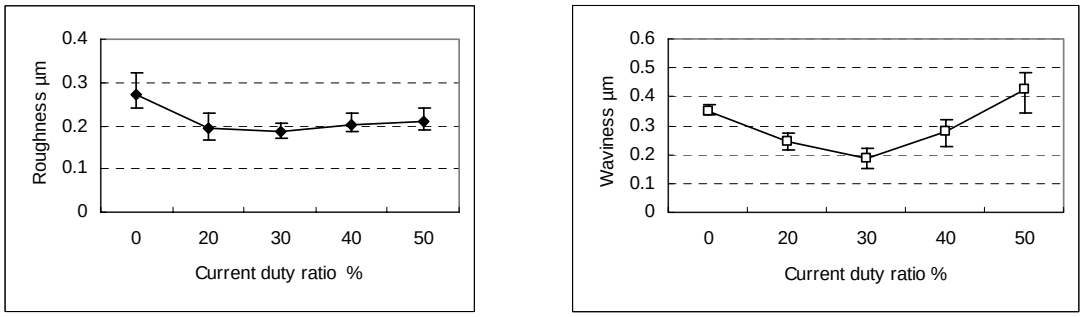

(c) Average surface roughness and waviness measure parallel to grinding direction

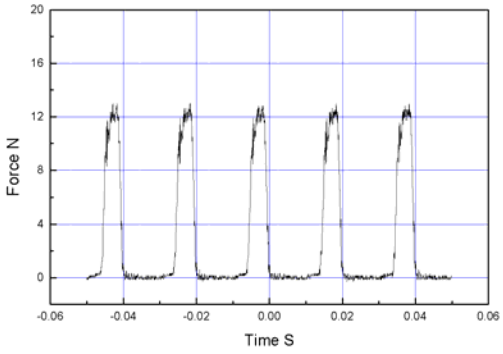

(i) Normal force

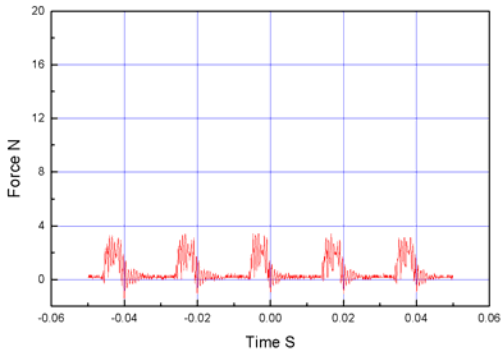

(ii) Tangential force

(d) The normal and tangential forces recorded during R_c – 20%

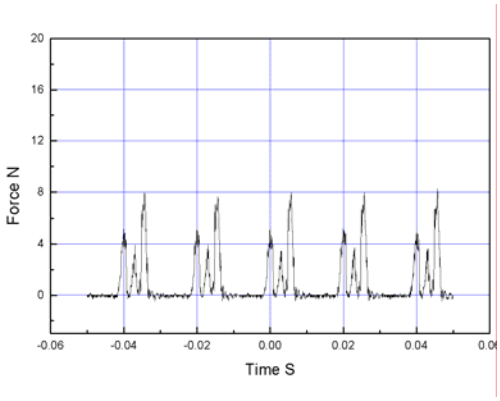

(i) Normal force

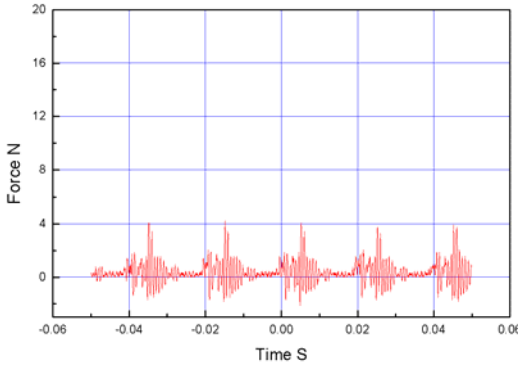

(ii) Tangential force

(e) The normal and tangential forces recorded during R_c – 50%

Figure 6.9: Grinding forces and surface texture during slot grinding.

6.5.2 Vertical grooves

The grit-depth-of-cut or the undeformed chip thickness is a useful measure in grinding. The chip thickness is influenced by the factors such as the properties of the material, the machining parameters and the grinding wheel conditions. The condition for defect free ductile surface was reported by Bifano et al. [Biafano et al., 1991]. The critical-depth-of-cut to produce a defect free surface on hard and brittle material is expressed as shown in Eq. (6.14).

$$d_c \propto \left(\frac{E}{H}\right) \cdot \left(\frac{K_c}{H}\right)^2 \tag{6.14}$$

where d_c is the critical-depth-of-cut

E is the Young's modulus

H is the hardness of the material

K_c is the fracture toughness

The critical depth-of-cut solely depends on the properties of material to be machined. For BK7 optical glass, the critical-depth-of-cut is approximately equal to 45 *nm*. The maximum chip thickness or grit-depth-of-cut, h_{max}, is expressed as:

$$h_{\max} = 2\, L_s \left(\frac{v_w}{v_s}\right) \sqrt{\frac{a_e}{d_s}} \tag{6.15}$$

where, h_{max} – Maximum chip thickness,

L_s – Distance between the active grits,

v_w – Velocity of work,

v_s – Velocity of the wheel,

a_e – Effective depth-of-cut and

d_s – Effective diameter of the grinding wheels.

From the above expression, it is clear that the maximum chip thickness depends on both machining and wheel parameters. If the penetration depth of a single grit is less than the critical-depth-of-cut, the chip deformation takes place plastically and that reduces the subsurface damages. Now the condition for ductile mode grinding can be expressed as shown below:

$$h_{\max} < d_c \tag{6.16}$$

The above condition can be obtained by controlling different machining parameters during grinding. For example, the increase of wheel speed or reduction of depth-of-cut reduces the chip thickness but, it needs special machines or special attachments. Recent studies show that ductile mode could be achieved using the conventional machine with the superabrasive grinding wheels and the ELID. The superabrasive wheels reduce the distance between the adjacent grits (L_s) and minimize the chip thickness. But, there is no explanation about the significance of dressing parameters that influence the grinding wheel topography in a significant amount.

The method of vertical groove grinding is highly useful for determining the grit interaction with the work surface. Each grit cuts as well as scratches the work surface since the grinding wheel is rotating and moving up and down. This method is more efficient to analyze the significance of the dressing effect. The grooves were ground to a length of 70 *mm* and a depth of 250 μm. Figures 6.10 (a), (b) and (c) show the grinding forces, surface roughness and waviness measured parallel and perpendicular to the grinding directions, respectively. The grinding condition were feed rate: 200 *mm/min*,

depth of cut: 1 *μm/pass* and spindle speed: 3000 *rpm*. The dressing conditions were I_p – 10 *A*, V_p – 90 *V* and R_c – 20% to 50%. The grinding forces were found to be reduced with the increase of current duty ratio. The average surface roughness and waviness measured parallel to the grinding direction was found to be almost constant for 30 % and more. The parameters measured perpendicular to the grinding direction shows that the surface roughness and waviness reduces when dressed more than R_c – 30 %. The result obtained using ELID grinding dressed at 30% of current duty ratio shows a *P–V* surface roughness of 27 *nm*, which is less than the critical depth-of-cut of glass material. From the above experimental result, it is clear that the $h_{\max}$ during ELID is also influenced by the bond strength of the grinding wheel. The $h_{\max}$ for the ELID grinding can be written as shown below:

$$h_{\max} = 2\ k L_s \left(\frac{V_w}{V_c}\right)\sqrt{\frac{a_e}{d_s}} \tag{6.17}$$

where *k* – ELID dressing constant and,

$$k \propto I_p,\ V,\ R_c \tag{6.18}$$

(a)

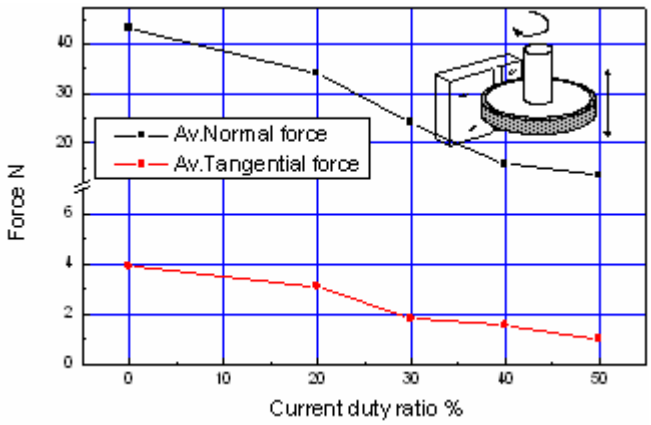

(b)

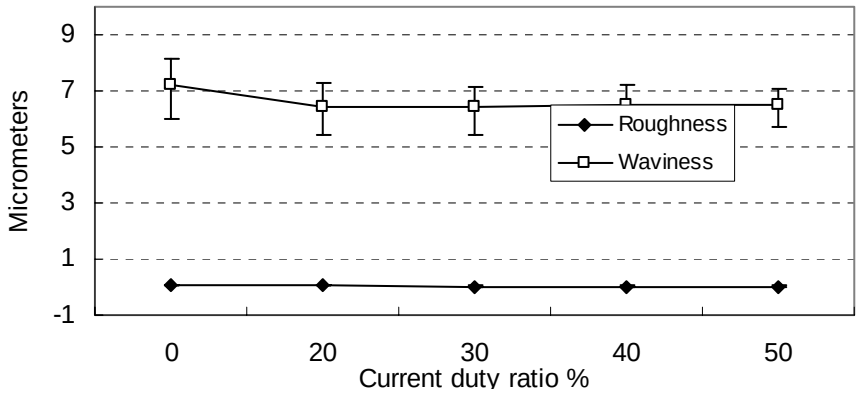

(c)

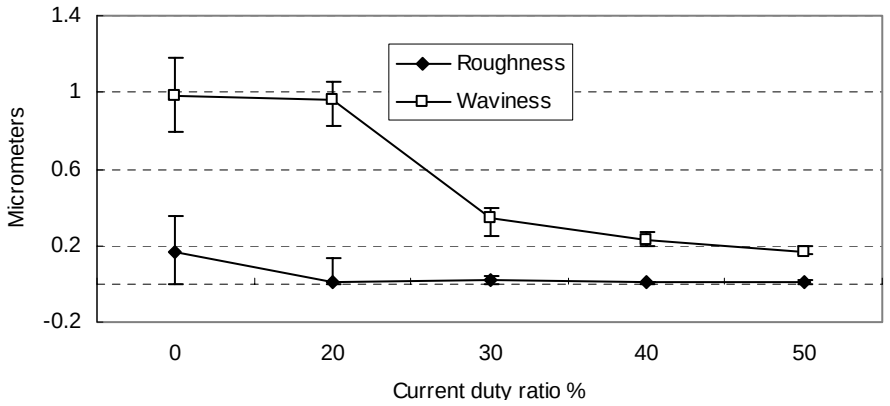

Figure 6.10: Vertical groove grinding (a) grinding forces (b) and (c) surface measurements parallel and perpendicular to the grinding direction.

6.5.3 Surface grinding

From the previous experimental results it is clear that for deeper cut (for geometrical accuracy) the grinding wheel needs to be dressed below R_c – 30 % and for low depth (for mirror surface finish) the wheel needs to be dressed above R_c – 30. However, the Surface grinding experiments were used to study the performance of the dressing methods. Two different methods have been used for finishing the brittle surface. They are in-process dressing and interval dressing. The difference between the processes was described in

Chapter 2. The grinding conditions were feed rate: 200 *mm/min*, depth-of-cut: 1 μm/pass and spindle speed: 3000 *rpm*. The dressing conditions were I_p – 10 A, V_p – 90 V and R_c – 50%. The grinding pitch was 1 *mm* with zigzag direction. The surface was ground to a depth of 250 μm. The dressing interval for the interval dressing was 15 *min*. There is no significant difference in grinding forces and surface roughness. The average surface roughness of the ground surfaces was found to be 3 *nm* and 3.2 *nm*, respectively. However, there was a significant different in grinding marks on the surfaces were reported. Figures 6.11 (a) and (b) show the Normarski interface micrographs of surface obtained from the above conditions. The grinding marks obtained during in-process dressing shows the mode is closer to the plastic scratching mode obtained during polishing [Izumitani, 1986]. Therefore, it is concluded that the in-process dressing method is the most suitable process for finishing brittle surfaces at submicron level.

(a) (b)

Figure 6.11: Normarski micrographs of ground surface using in-process and interval dressing [50 X].

6.6 Model for the in-process dressing

Figure 6.12 (a) shows the change of normal force and dressing current during ELID grinding with the grinding conditions of spindle speed: 3000 *rpm*, depth of cut: 1 μm, feed rate: 200 *mm/min* and 60% of current duty cycle. Figure 6.12 (b) shows the force profile with respect to the wheel angles. The frame numbers are used to relate the normal force in figures 6.12 (a) and 6.12 (b). In this process a breakage cycle starts approximately between 180 – 220 *sec*, which is represented by the frames 10 and 15. This clearly shows the condition of the grinding wheel and the oxide layer breakage from the grinding wheel. From the above example it is clear that the breakage of the oxide layer from the grinding wheel occurs segment by segment.

Based on the experimental results the model for in-process dressing has been proposed. The increase of wheel diameter happens only in cast iron bonded grinding wheels. However, similar mechanism was found when grinding using copper bonded grinding wheels. Even though electrolytic dressing reduces the strength of the bonding material, the layer has enough strength to hold the diamond grits during grinding. Figure 6.12 (c) shows the change of wheel surface while grinding. If the grinding force exceeds a certain value, which depends on the machining conditions, the layer starts breaking. The outer layer contains worn grits and grinding chips are removed along with the layer. The new layer of the grinding wheel beneath the broken layer contains fresh diamond grits that come into cutting action. The new layer is softened by electrolysis and the speed of the electrolysis depends on the duty ratio of the dressing current. If the grits are worn out,

which leads to macro fracture and the crack propagates as shown in Figure 6.12 (c). The whole layer is removed due to the hardness of the workpiece. The breakage of the outer insulating layer increases the electro-conductivity of the grinding wheel, which stimulates electrolysis, causing an increase in dressing current and reducing the normal cutting force. This cycle repeats throughout the grinding process.

(a)

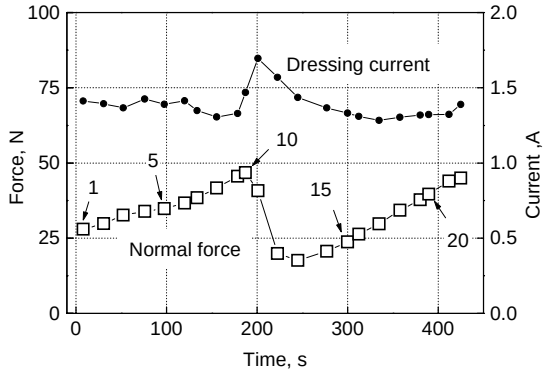

(b)

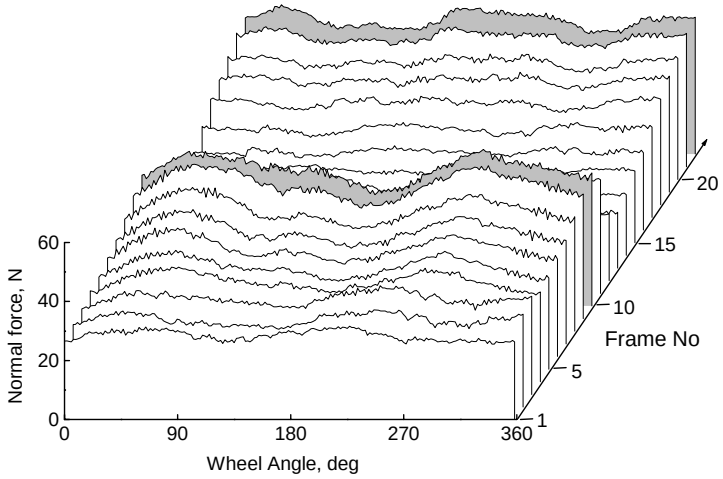

(c)

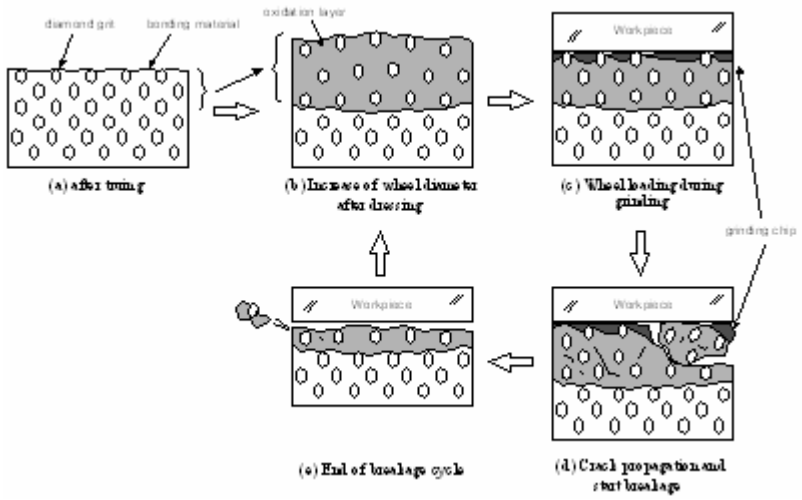

Figure 6.12: Model for in-process dressing.

6.7 Concluding remarks

The wear mechanism of the ELID grinding wheels is different from the conventional grinding wheels. The dressing interval during in-process dressing influences the radial wear/grinding ratio which depends on the layer that holds the grit during grinding. However, the produced ELID-layer strongly depends on the dressing current and the bond material. When the grinding method is different, the requirement of in-process dressing is also different. For deeper cut, the wheel needs to be dressed with lower current duty ratio (20 – 30 %), but the results for smaller depths shows that it is better to dress the grinding wheel about approximately 50 %. It may be concluded that the layer produced on the grinding wheel during in-process dressing is very important when grinding with the aid of the ELID and hence a detailed analysis is necessary to understand the ELID-layer (oxidized layer).

Chapter 7

Investigations on the ELID-layer

7.1. Introduction

The studies conducted in the previous chapters clearly proves that the oxide layer formed on the wheel-active-surface influences the grinding forces, the surface finish and the wheel wear. Therefore, the characterization of the ELID-layer (oxidized layer) becomes inevitable for better control of grinding process, but characterization of the thin layer is a difficult task and hence it is almost overlooked. Recent advances in measuring equipments make it possible to analyze the properties of thin layers. Microhardness testing and nanoindentation are some of the techniques that can be used to investigate the thin layers. A detailed investigation on the ELID-layer has been presented in this chapter. These investigations include the studies on microconstituents and the mechanical properties of the layer. The results obtained are more helpful for better understanding about the layer, and measurement of mechanical properties such as microhardness and modulus of elasticity are useful because the layer acts as the binder for the active grits.

7.2 Analysis on the pre-dressed wheel

Pre-dressing is the process of producing ELID-layer on the active-surface of the wheel using electrolysis as discussed in the previous chapter. The idea behind the pre-dressing is

producing high resistance to current in order to make the wheel suitable for in-process dressing. The conductivity of the wheel should be very low for in-process dressing in order to reduce the radial wheel wear while grinding. From the previous chapters it found that the grinding performance is found to be better when the grinding wheel is dressed at high current densities. Therefore, the layer produced at high current densities has been chosen for the analysis, and almost full thickness of the layer has been produced on the wheel surface for the purpose of analysis. A cast iron-cobalt bonded grinding wheel of 100 mm diameter, 5 mm width, 3 mm diamond layer thickness and mesh #4000 was pre-dressed with an electrode that covers ¼th of the perimeter of the grinding wheel. The wheel was pre-dressed using the ELID condition of I_p – 10 *A*, V_p – 90 *V*, T_{on} – 5 μs, T_{off} – 5 μs and the spindle rotation of 1000 *rpm*. The increase of average current and decreases of voltage at the beginning of pre-dressing indicates the good electrical conductivity of the wheel surface [Please refer Figure 6.2]. During electrolysis, voltage increases gradually with the decrease of current, and the process was stopped after 30 *min* because of the voltage and current remains almost constant. The current drops to a small value of 1.3 *A* and the voltage was approximately equal to the applied voltage (V_p). An increase of wheel radius about 200 μm was measured after pre-dressing. Figures 7.1 (a) and (b) show the EDX test results of the wheel surfaces before and after pre-dressing, respectively. The EDX test on wheel surfaces before and after dressing conforms that the wheel active-surface is covered by the oxidized layer that contains the metal oxides.

(a)

(b)

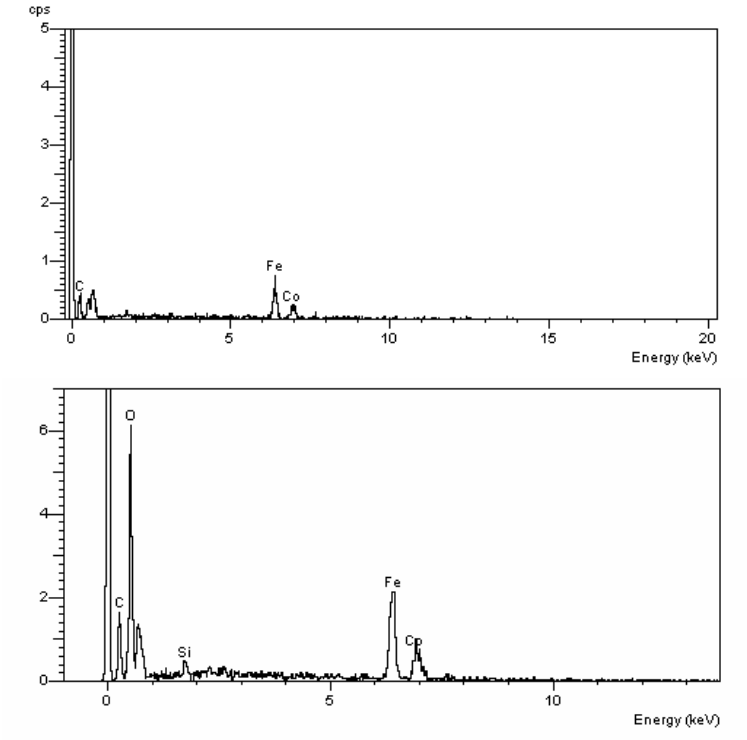

Figure 7.1: The EDX test results of an ELID grinding wheel before and after pre-dressing.

The active-surface of the grinding wheel is important because it contains the active grits that perform grinding. When the metal-bond is oxidized, the properties of the layer such as hardness and Young's modulus are important because if the wheel surface is not hard enough to hold the grits while perform grinding, almost the whole thickness is removed from the wheel surface due to the hardness of the work. Therefore, a comparative study has been performed on the active-wheel-surface. The microhardness of the ELID-layer (pre-dressed wheel) and the metal-bond (wheel without layer i.e. after truing or new grinding wheel) at different points was measured using Matsuzawa MXT50 digital microhardness tester. The behavior of the active-wheel-surfaces has been experimented by measuring the

microhardness of the surfaces at a series of loads from 20 *g* to 200 *g* with the dwelling period of 15 *sec*. Figure 7.2 shows the behavior of the active wheel surfaces under various loads. From the observations it is clear that the microhardness of ELID-layer is much lower than the metal-bond. However, the above experiment does not provide information about the whole layer. Therefore a detailed analysis on the whole layer is necessary in order to know the properties of the layer.

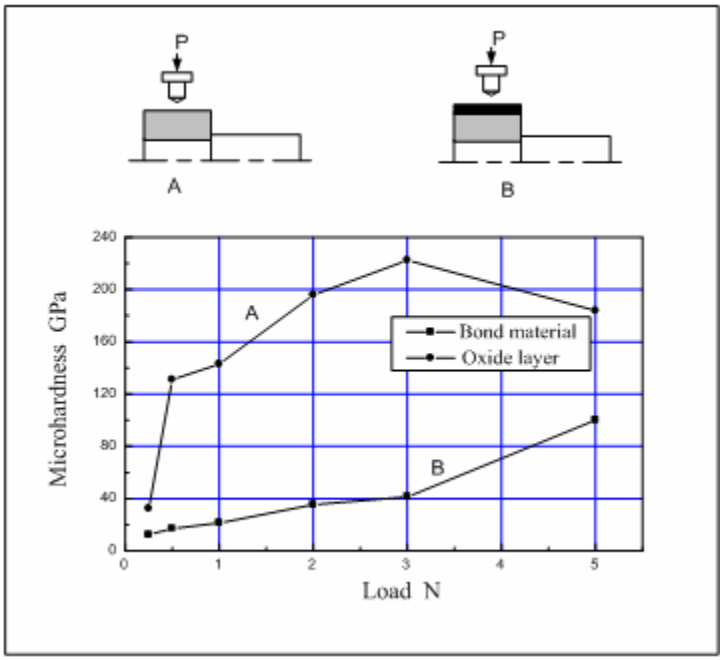

Figure 7.2: Microhardness of the actual bond and the layer at different loads.

7.3 Microconstituents of the ELID layer

The samples were taken from grinding wheels at different conditions for the purpose of microstructural analysis. The samples were taken from an undressed wheel and dressed wheel with different ELID conditions. Sample A was taken from the grinding wheel before

dressing, and samples B and C were from dressed grinding wheels dressed at current densities of 1 A/cm^2 and 3.25 A/cm^2, respectively. The samples were taken from grinding wheels (all samples from FCI-X wheels) of diameter 8 *mm*, diamond layer 10 *mm* and mesh #4000. The grinding wheel specimens were sliced to a thickness of 3 *mm* using wire-EDM. The molded specimens were ground to flat and then polished using slurry containing abrasive size of 1 μm. After polishing, the specimens were etched in order to reveal the microstructural difference between the real bond and the oxide layer. For cast iron bonded grinding wheels, the specimens were etched using an etchant Nital – 2%. There was a clear microstructural difference as observed at the wheel edges in samples B and C after etching, which shows the actual thickness of the oxidized layer. Figures 7.3 (a), (b) and (c) show SEM micrographs of the grinding wheel samples A, B and C, respectively. The thicknesses of the oxidized layers at the wheel edges were found to be 50 μm and 200 μm for samples B and C.

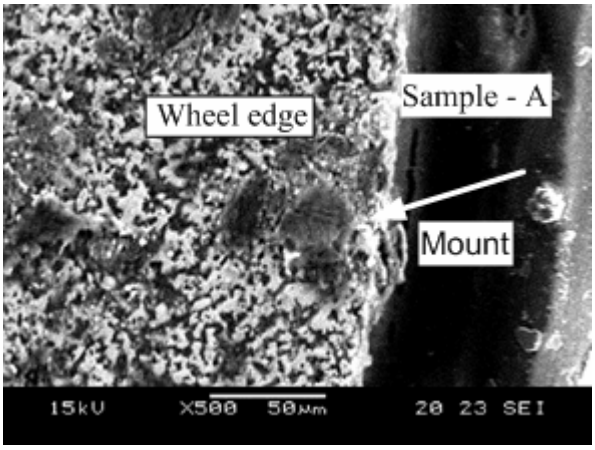

(a) Sample – A (undressed wheel)

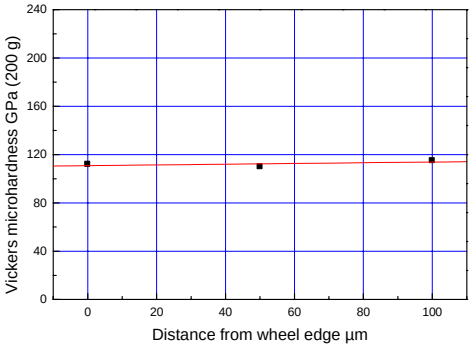

(d) Microhardness of the Sample - A

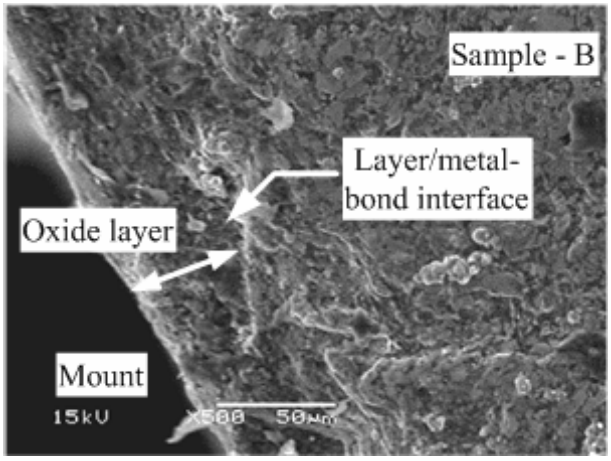

(b) Sample – B (dressed at 1 A/cm^2)

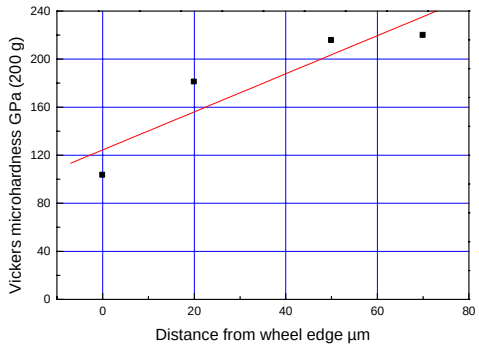

(e) Microhardness of the Sample - B

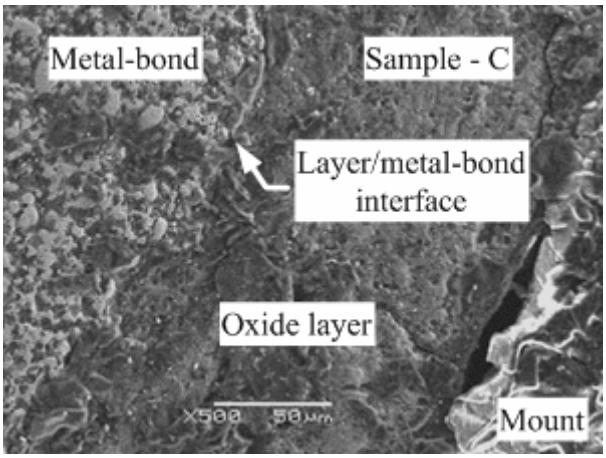

(c) Sample – C (dressed at 3.25 A/cm^2)

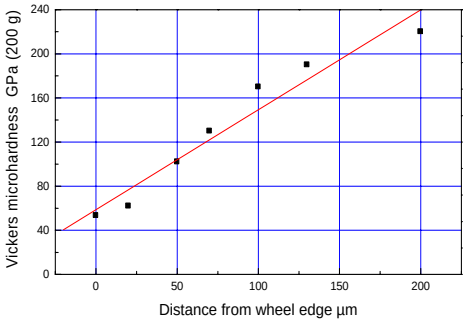

(f) Microhardness of the Sample - C

Figure 7.3: SEM micrographs of grinding wheel samples and the microhardness of the samples.

The microhardness of the samples was measured at a load of 200 *g* with the dwelling period of 15 *Sec*. The actual microhardness of the bonding material (sample-A) was measured as 110 *GPa* (200 *g*) (Figure 6.3 (d)). The microhardness of the layer was measured at different points on the oxide layer from the edge to towards the layer/metal-bond interface. Figures 7.3 (e) and (f) show the microhardness measured at different points on the layers of the samples

B and C, respectively. The microhardness of the oxidized layer on both the wheel surfaces increases from the wheel edge to towards the layer/metal-bond interface. The hardest layer on the grinding wheel surface was found at the interface, which has microhardness of 220 *GPa* (200 *g*).

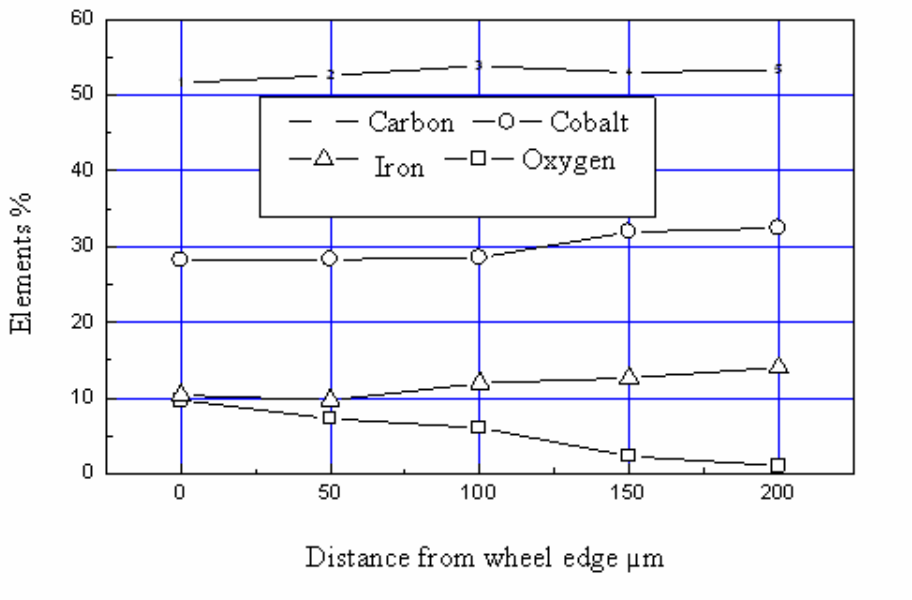

Figure 7.4: Microconstituents of the layer at different points from wheel edge to the layer/bond interface.

The reason for the change of microhardness of sample C (after etching) has been investigated using EDX testing of the layers at different points. Figure 7.4 shows the EDX testing results, which shows the difference in the microconstituents and the amount of oxygen present in the layer. These variations of microhardness and microconstituents confirm that the layer is not the oxide film produced during electrolytic corrosion, but it seems a resistive layer that grows from the surface of the grinding wheel. The oxidized layer obtained during the ELID resembles a layer that consists of number of small layers with different microconstituents. The step etching method was used for further analysis of microstructure at different layers.

Figure 7.5 shows the SEM micrographs of the layers at different levels. The microstructure of the outer layer and the layer beneath are found to be different. Based on the experimental results, the model for the ELID-layer is represented schematically as shown in Figure 7.6.

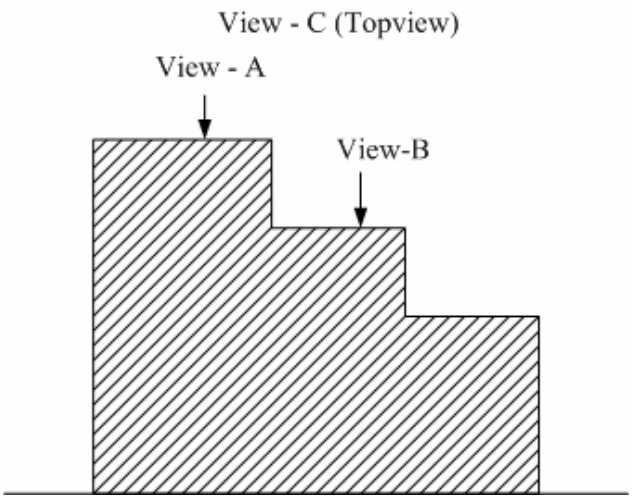

(a) Schematic illustration of the etched wheel

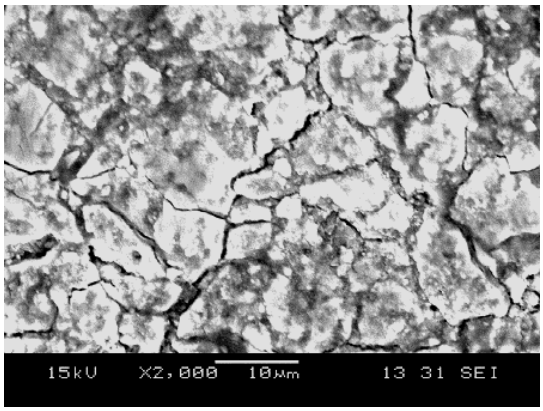

(b) Microstructure of outer layer (View A)

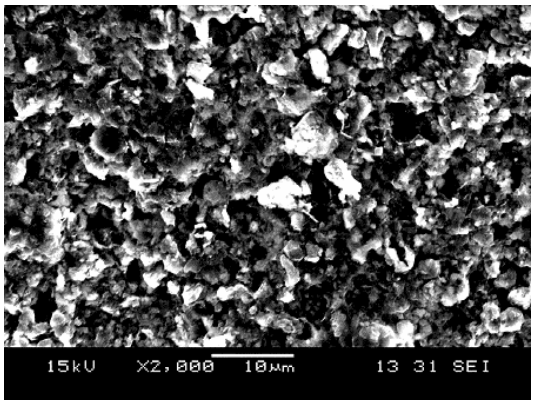

(c) Microstructure of the inner layer (20 µm beneath) View B

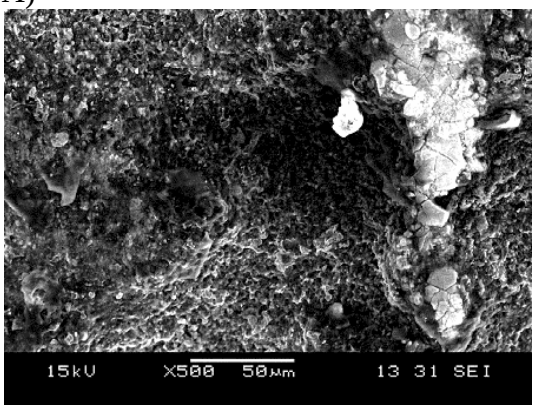

(d) Different layers at View C

Figure 7.5: SEM micrographs of barrier oxide layer showing different layers.

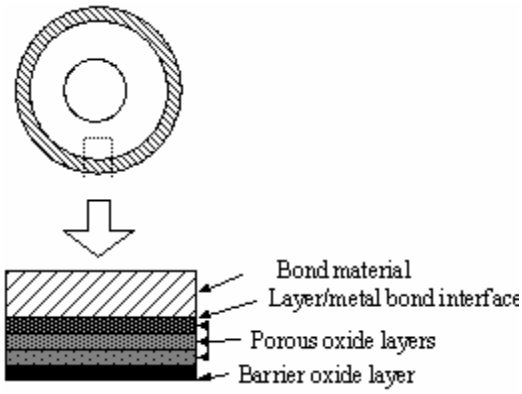

Figure 7.6: Schematic illustration of the anodized ELID-layer.

7.4 Analysis on the ELID-layer

The investigations conducted on the ELID-layer confirm that the wheel is being anodized during in-process dressing because of the similarity of the properties of the anodized layer. An oxide film can be grown on certain metals (chromium, iron and nickel) by an electrochemical process called anodizing. When a metal is anodically polarized in an aqueous solution, the metal ions combined with electrolyte anions and formed oxide/hydroxide films on the metal surface. A thin, dense barrier oxide film of uniform thickness was formed on the metal surface. The barrier oxide layer stabilizes the surface against further reaction with the environment because it is an excellent electrical insulator. The electrolytes are selected in which the oxide is insoluble, or dissolves at a slower rate than it deposits, and then an adherent oxide layer grows. The layer formed on the surface on the anodic metals is classified into either conductive type or nonconductive type. Conductive type oxide layers conduct electrons through the film but the non-conductive layer has no electro-conductivity. However, the ions can transfer into and from the nonconductive layer.

The oxide layer of nonconductive type is classified into barrier type and porous type. The barrier type layer is very common in the transition metals and its thickness is about few nanometers. However, when the anode potential is raised, barrier or porous layers of several hundred nanometers are formed. The thickness of the oxide layer increases linearly with the voltage. After reaching a critical value, the arc discharge stats that crease the film thickness. When anodizing is performed at constant voltage, the current reduces exponentially and finally attains a very small value, which is known as leakage current. But, prolonged anodizing improves the quality of the oxidize layer [Konno, 1986]. The above phenomena is verified using the relation between the current and voltage recorded during pre-dressing as shown in Figure 7.7.

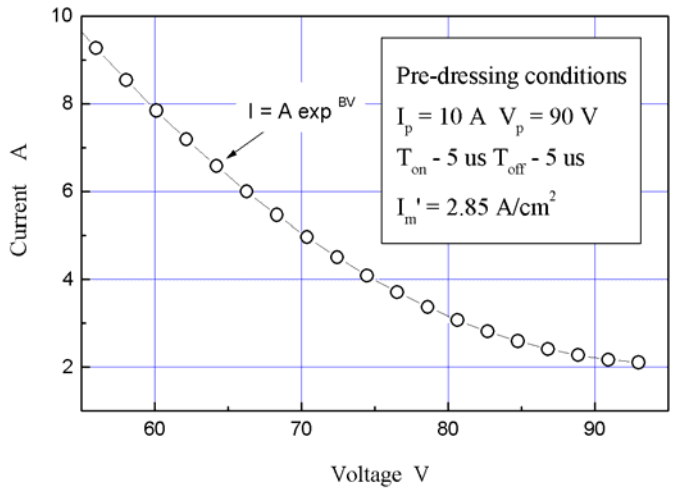

Figure 7.7: Relation between the average dressing current and the voltage during pre-dressing.

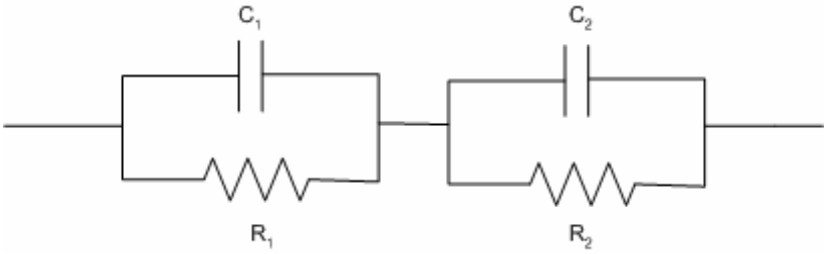

Figure 7.8: Equivalent circuit diagram of the ELID-layer.

During the formation of the barrier type layer, the oxide/hydroxide ions migrate through the barrier oxide film and formed oxide/hydroxide films to the metal/oxide layer interface. The new oxide layers are formed at both interfaces depending on the transport number of the ions, which provide high electrical insulation and corrosion resistance. Therefore, the microhardness and the microconstituents at every micrometer are found to be different, which resembles the property of a dielectric material. Therefore, the anodic oxide layer can be approximated as a capacitance and a resistance in parallel. Figure 7.8 shows the schematic illustration of the anodized ELID layer. The anodized layer formed on the grinding wheel provided strong corrosion resistance to the bonding material. The anodic oxide layer grows towards the metal/oxide interface while the outer barrier layer is removed by the work/wheel interface. Then the oxide layer grows on the surface until a steady state is attained (this phenomenon is verified by observing the dressing current during in-process dressing). When the in-process dressing is performed with high anodic potential, there is no chance of the actual bonding material to come in contact with the workpiece during ELID grinding.

7.5 Investigation of the mechanical properties of the ELID layer

Nanoindentation has been used to evaluate the mechanical properties of the surface layers and thin films in the recent years. Nanoindentation involves an instrument that continuously monitors the depth of the indent relative to sample surface during indentation. The load – displacement characteristics are used to determine the mechanical properties such as hardness and Young's modulus [Bharat Bhushan, 1999, Wolf and Richter, 2003].

7.5.1 Principle of nanoindentation

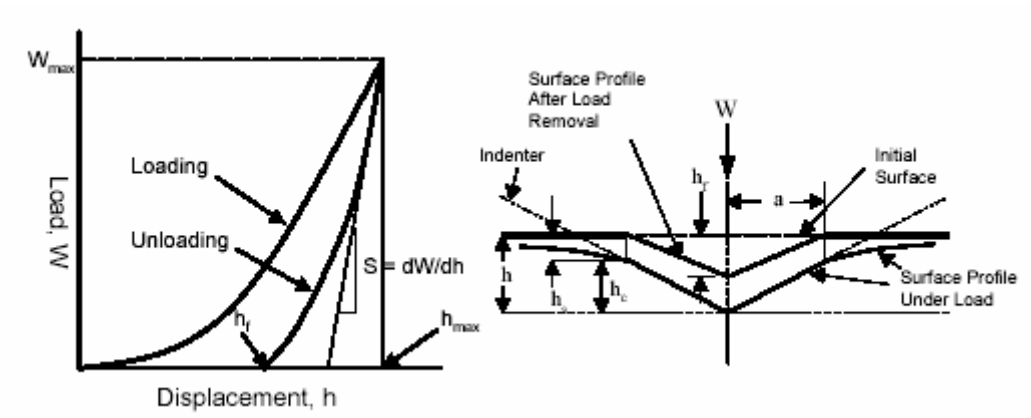

Figure 7.9: Schematic illustrations of the load – displacement curve and the indentation process [Bharat Bhushan, 1999].

The development of depth-sensing indentation techniques has increased in the recent years. Therefore, the nanoindentation technique has been used to evaluate the mechanical properties of surface layers and thin films. However, the procedures used for nanoindentation are based on simplified assumptions about the material behavior during unloading and empirical relations of the contact area with little input from analytical and numerical solutions. Figure 7.9 shows the schematic illustration of the load – displacement curve and the indentation

process. At peak load, the load and displacements are W_{max} and h_{max}, respectively. The depth measured during indentation h is the summation of h_s and h_c. The depth h_f represents the final depth of the residual hardness when the intender is fully withdrawn. Figure 7.10 shows the typical load – displacement curve during nanoindentation of the ELID layer. The change of mechanical properties has been evaluated by the nanoindentation on the metal-bond and the ELID-layer. Figures 7.11 (a) and (b) show the AFM picture of the metal-bond before and after nanoindentation. The Young's modulus and the Poison ratio of the indenter were 1140 *Gpa* and 0.07, respectively.

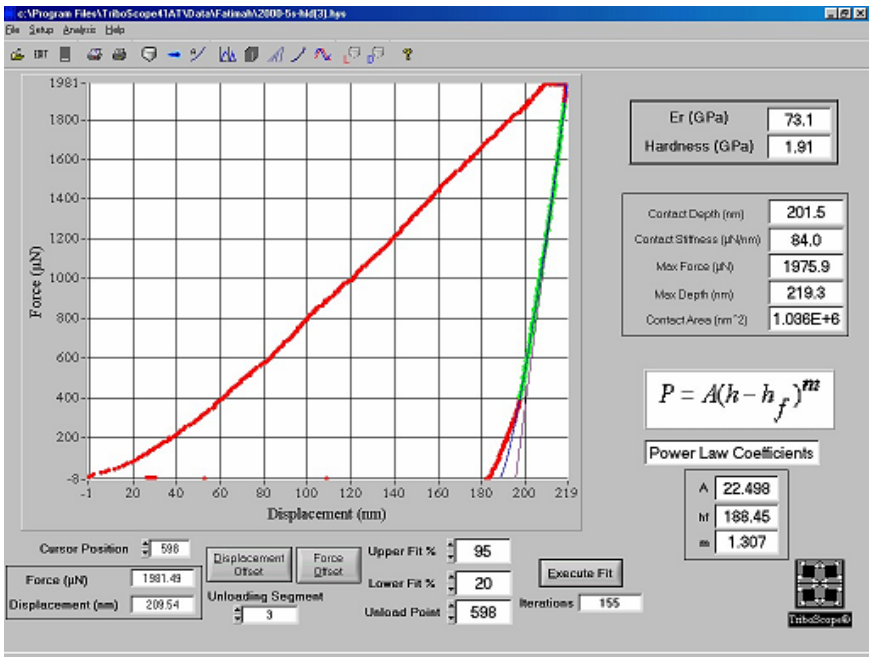

Figure 7.10: A typical load – displacement curve during nanoindentation.

Figures 7.11 (c) and (d) show the AFM picture of the oxide layer before and after nanoindentation. The Young's modulus of the layer at a distance 180 μm from the wheel edge can be calculated using equation (7.1). The results obtained from the nanoindentation

for the actual bond and the ELID-layer is shown in Table 7.1. From the nanoindentation results, it is clear that the Young's modulus of the layer is lower than the actual metal-bond. Therefore, the hardness and the Young's modulus of the layer at the active-wheel surface were found to be lower than the actual metal-bond. The increase of hardness from the wheel edge towards the layer/metal-bond interface reduces the radial wheel wear to a remarkable amount because the grit is bonded by different layers with varying hardness.

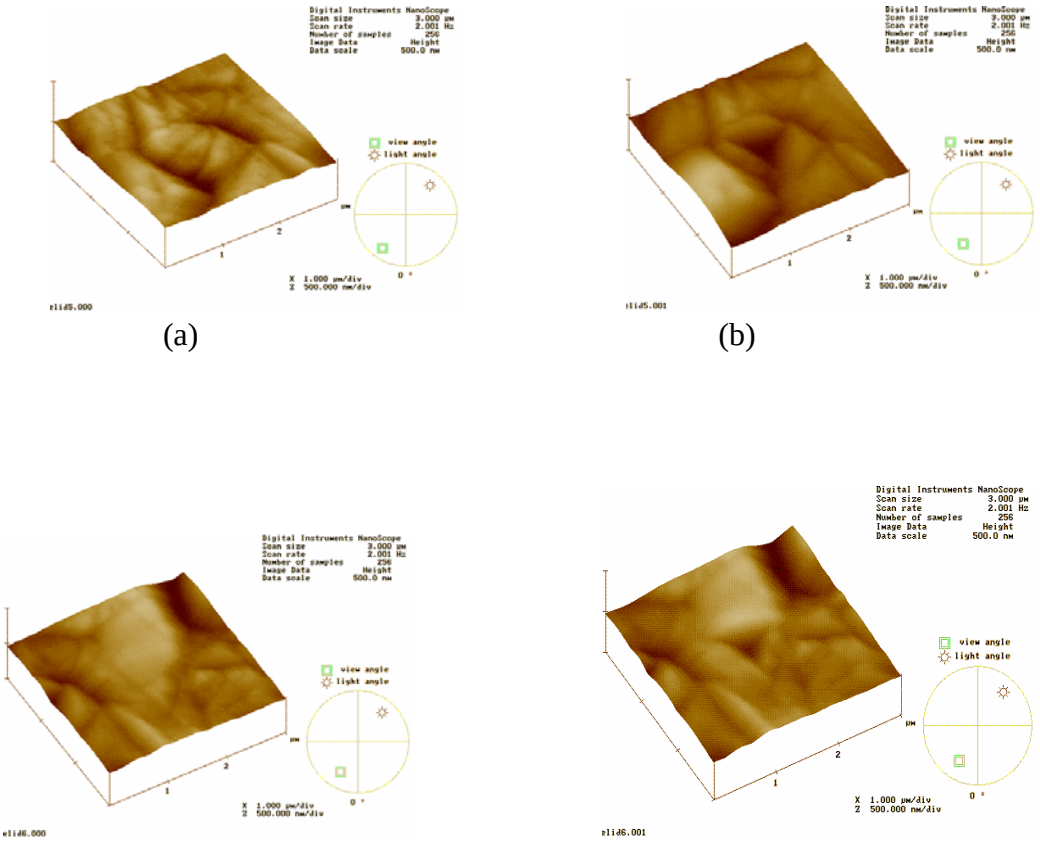

(a) (b)

(c) (d)

Figure 7.11: AFM views of Nanoindentation on the ELID-layer and the actual bond material.

Table 7.1 Nanoindentation results

Parameters/ Properties	Bond material	ELID-layer
Stiffness (k) $\mu N / nm$	44.34	16.34
Er *GPa*(measured)	63.78	23.36
H *GPa*	5. 22	5.13
Er *Gpa* (actual)	82.00	31.00

7.6 Grit size and the anodized wheels

The investigations on the ELID-layer show that the performance of the grinding wheel is found to be better when the active-wheel-surface contains the anodic layer that is generated during the ELID. Grinding wheels with bond materials such as cast iron and copper can be easily anodized using the ELID. The advantages of grinding with the anodized ELID-layer have been experimented by wheels with different mesh sizes. Three different grinding wheels of mesh sizes of #325, #1200 and #4000 have been anodized using the ELID.

Figures 7.12 (a), (b) and (c) show the grinding wheel-active-surfaces of grinding wheels of grade #325, #1200 and #4000, respectively. The actual bond strength for the diamond grits is different since the anodic layer was made of different layers with varying mechanical properties. Therefore, the bond matrix for the above grinding wheels at wheel-active-surface was found to be different. The grit-depth-of-cut depends on the grinding parameters and the

binder properties [Sharp, 2000]. The radial wheel wear of a FCI-X wheel of grade #325 was measured after ground a glass workpiece of 80 *mm* diameter to a depth of 200 μm. The grinding conditions were spindle speed: 3000 *rpm*, feed rate: 200 *mm/min* and depth-of-cut: 5 μm/pass. The wheel was dressed with the current density of 3.25 A/cm^2 (pulse width 4 μs). When comparing the grinding wheel profile before and after machining no radial wear was observed.

The radial wheel wear of FCI-X wheels of grade #1200 and #4000 was measured after ground the workpiece to a depth of 50 μm and 10 μm, respectively. The grinding conditions were spindle speed: 3000 *rpm*, feed rate: 200 *mm/min*. The depth-of-cuts were 2 and 1 μm/pass for the above wheels. The grinding wheels were dressed with similar current density with pulse width of 10 μs. The radial wheel wear of the above grinding wheels were found to be approximately 23 μm and 75 μm respectively. From the results it is found that the wheel wear depends on the grit size of the grinding wheel.

From the above experimental results, it is clear that grinding with anodic ELID-layer was very effective for the grinding wheels of grit size more than 10 μm. However, the advantage of grinding with anodic ELID-layer for grit size less than 4 μm was found to be more useful because there was no bond metal exist in the surface and hence the grinding scratches were very much reduced. Therefore the work surface was ground in the similar way as abrasive pad used in polishing.

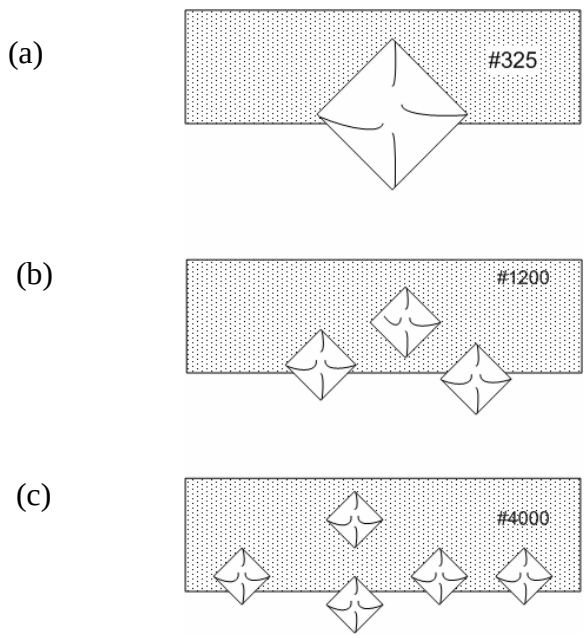

Figure 7.12: Active-surfaces of grinding wheels with different grades.

7.7 Advantages of grinding with anodized ELID layer

7.7.1 The profile of the grinding wheel

Maintaining the grinding wheel profile throughout the grinding process is an essential factor in precision grinding. Though the grinding wheel is trued and dressed before starting grinding, the wheel is redressed while performing grinding with the aid of the ELID. The investigations have shown that the oxide layer breaks and reforms on the wheel surface in order to promote in-process dressing. Hence the investigation on the wheel profile during ELID grinding becomes necessary.

The wheel profile with anodized ELID-layer has been monitored at equal intervals. A grinding wheel with eccentric profile was dressed and used for the grinding experiments. It is found that the wheel profile improved with the increase of grinding time. The experiment conducted using a over dressed eccentric grinding wheel discussed in Section 6.3.1 shows that the wheel profile is improved with the increase of grinding time. Figure 7.13 also shows that the grinding wheel profiles are also better after grinding approximately 15 mm^3.

7.7.2 Control of the wear rate of ELID-layer (Effect of pulse ON-time and OFF-time)

The ELID uses square pulses which are separated by interval with zero current. The main advantage of using pulsed electrolysis is the versatility. The pulse ON-time and OFF-time are very important parameters since it affects the damping and the concentration gradient of the electrolyte. In pulsed electrolysis, the T_{on} time is known as the reaction time and the T_{off} time is known as the relaxing time, which is considered as the most important factor for nucleation and crystallization. In pulse electrolysis, instead of one parameter three parameters - the pulse density, the T_{on} time and the T_{off} time can be varied independently over a broad range. The experiments conducted on pulsed electroplating show that the change of T_{off} time has a strong influence on the surface produced [Ibl et al., 1978]. There is no reported result explaining the influence of T_{on} and T_{off} time during electrolytic dressing.

The simplest way of studying the influence of double layer and the diffusion layer effect is by varying the T_{on} and T_{off} during in-process dressing. There are two methods adopted in this study. The first method used is keeping the peak current and the pulse width as constants, and

varying the T_{on} and T_{off} times. The first method varies the average current densities. The influence of the change of average current density on the grinding forces, the surface finish and the wheel wear were reported in the previous chapters. The second method is keeping the peak current and the average current as constants and varying the pulse frequency. A set of experiments were conducted by using pulsed current at different frequencies. The lowest and the highest frequency obtained using the ELID power supply are 50 (T_{on} = 1 μs and T_{off} = 1 μs) *Hz* and 250 (T_{on} = 10 µs and T_{off} = 10 µs) *Hz*, respectively. The I_p value of 10 *A*, voltage 90 *V* and I_m of 3.25 A/cm^2 were chosen for the above experiments with similar machining conditions.

Figure 7.13 shows the effect of pulse frequencies on the ELID-layer at 50 *Hz* and 250 *Hz*. The wheel profiles after pre-dressing (Figure 7.13 (b) and (e)) show that the wheel radius increased about 25 μm after dressing using pulse frequency 50 *Hz*, but the wheel radius was found to be reduced by about 10 μm while pre-dressed using 250 *Hz*. The radial wheel wear observed was approximately 25 μm and 250 μm for the above pulse frequencies. The radial wear increased when dressing with high frequency pulse current without any significant improvement in the surface roughness (R_a – 3 *nm* for both). Therefore at similar peak and average current densities, low frequency pulse reduces the wear rate of the ELID-layer to a significant amount. When grinding with superabrasives, it is recommended to dress the wheel using pulse frequency not less than 100 *Hz*.

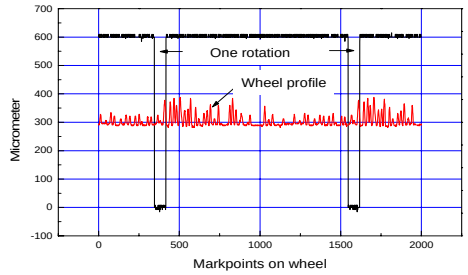

(a) Wheel profile before pre-dressing (50 *Hz*)

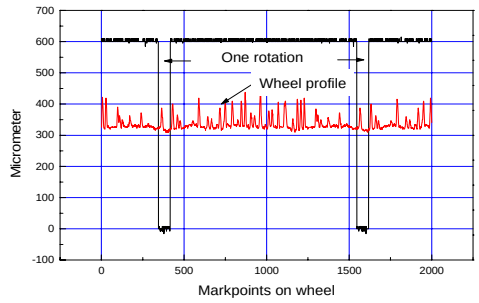

Wheel profile after 10 *min* of pre-dressing (50 *Hz*)

(b)

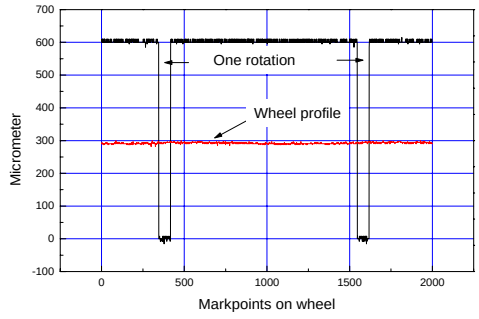

(c) Wheel profile after grinding (50 *Hz*)

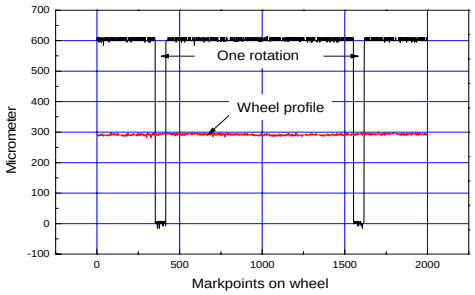

(d) Wheel profile before pre-dressing (250 *Hz*)

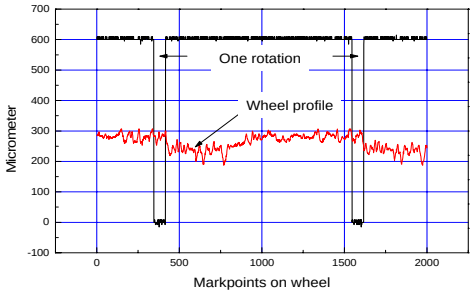

(e) Wheel profile after 10 *min* of pre-dressing (250 *Hz*)

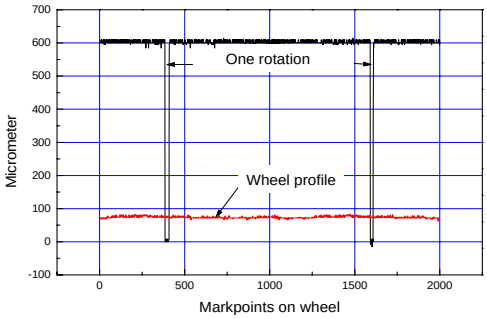

(f) Wheel profile before pre-dressing (250 *Hz*)

Figure 7.13: Effect of pulse frequency on the ELID-layer.

7.8 Concluding remarks

When a cast-iron bonded grinding wheel is dressed with the current density above 2 *A/cm2* and voltage 60 – 90, an anodized layer was formed on the wheel-active-surface. This thickness depends on the bond material of the grinding wheel. This layer has a strong corrosion resistance to the electric current and makes the grinding wheel suitable for in-process dressing. The mechanical properties such as hardness and Young's modulus are found to be different from the actual bond material. The layer hardness is different and that depends on the thickness of the layer. The hardest layer is at the bond/layer interface and the hardness reduced towards the wheel edge. The bond matrix of the active grits is influenced by the layer properties such as hardness and Young's modulus and the grit size.

The wear rate of the ELID-layer is influenced by the frequency of the pulse, higher the frequency more will be the wear of the oxide layer. When grinding with the ELID-layer, the profile is improved or maintained throughout the grinding process.

Chapter 8

Modeling of micro/nanoELID grinding

8.1 Introduction

Grinding is known as a complex machining process because it is influenced by numerous parameters. The early grinding models developed [Tonshoff et al., 1992; Malkin, 1989; Kun Li and Liao, 1997; Chan, 1999] are based on the parameters such as wheel and work velocities, depth-of-cut and the grit size of the grinding wheel. The early models show that the grits penetrate and cut the material from the work surface, and the grinding forces generated are proportional to the material removal. However, those models are not suitable for micro/nanoscale grinding because the mode of material removal and the method of contact between the surfaces (wheel and work) are different from the macroscale material removal. In macrogrinding, there may not be any direct contact between the bond material and the work material because the depth-of-cut chosen is relatively smaller than the abrasive size. The abrasives on the wheel surface penetrate and cut the work, and the material removal has been obtained by propagation of cracks. However, during micro/nanoELID grinding, the contact between the oxidized layer and the work surface is unavoidable since the sizes of the abrasives are very small.

Apart from the machining parameters the role of several other parameters such as the mechanical properties of the oxidized layer formed on the grinding wheel surface during the ELID, surface topographies of the wheel/work, and the contact made between the

surfaces are also play a vital role during micro/nanoELID grinding. Therefore, a new grinding model for micro/nanoELID grinding is necessary in order to predict closer correlations with the actual results produced during grinding, which may reduce the expensive and cumbersome grinding experimental trials. The grinding forces are the result of the cumulative effect obtained from the process and hence they are widely used as the performance measures. Therefore, a force model for micro/nanoELID grinding has been proposed in this chapter, the simulated results are compared with the experimental results in order to evaluate the developed grinding model.

8.2 Principle and modeling of micro/nanoELID grinding

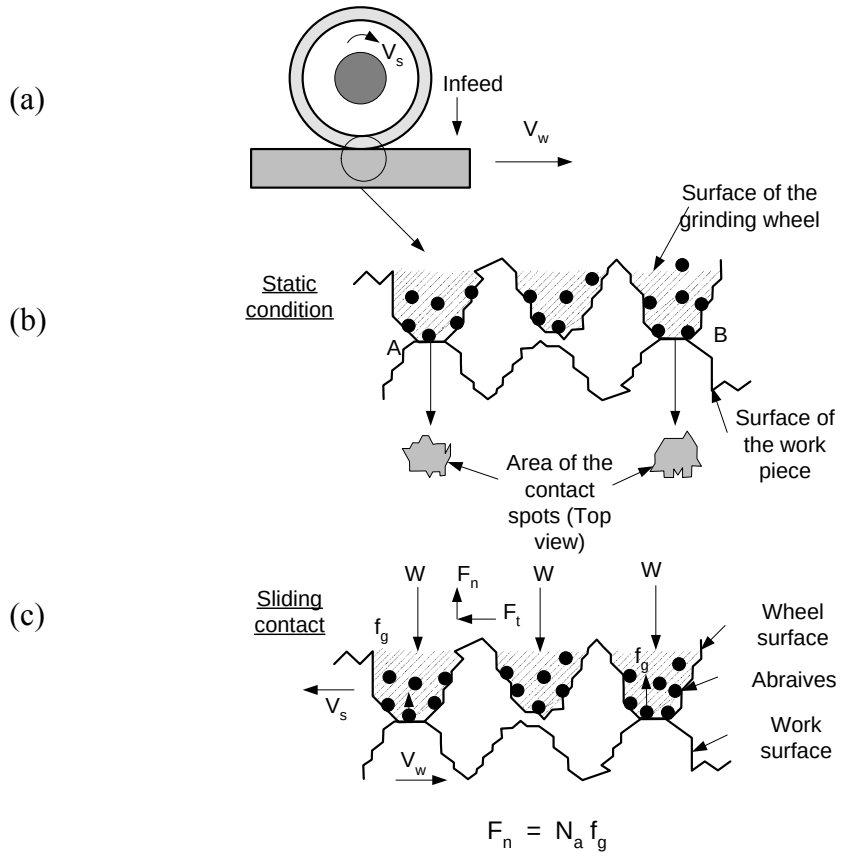

Figure 8.1: Micro/nanoELID grinding.

For achieving nanosurface finish, the ground surface should be free from microcracks and grinding marks. Grinding and polishing processes are widely used for producing nanosurface finish on brittle materials. Though, the processes are using fine abrasive particles for the material removal there is a definite difference between the processes. The main difference between the micro/nanoELID grinding and the polishing processes is the method of contact created between the surfaces (wheel and work). The contact between the surfaces during polishing is made by the application of known down pressure. The pressure has been chosen in such a way that the asperities are in plastic contact. The abrasive grits entrapped by the polishing pad removes the material from the work surface and the volume of material removal is proportional to the applied pressure. Unlike polishing, the contact between the surfaces has been achieved by the downward (infeed) movement of the grinding wheel as illustrated in Figure 8.1 (a). Different techniques have been adopted for establishing nanocontact between the surfaces during grinding. Using smaller infeed in steps of few nanometers is one of the methods to achieve nanocontact.

No surface is perfectly flat in nature and hence the asperities of the surfaces are in real contact when a pair of surfaces in nanocontact. The asperities are deformed plastically when the applied load is very small. However, it is difficult to know the type of contact (plastic or elastic) would be made between the asperities during grinding. If the load exceeds a certain value the deformation becomes elastic, which should be avoided during nanogrinding. The downward movement of the wheel ensures the contact between the asperities and the grits embedded on the wheel asperities are indent into the work asperities (Figure 8.1 (b)), the material removal has been performed by the relative movement between the wheel and work surfaces as illustrated in Figure 8.1 (c).

The grinding force generated during micro/nanoELID grinding is a useful measure to know the contact zone was made between the surfaces. However, the grinding forces are generated during micro/nanoELID grinding depending on the real contact between the wheel/work surfaces. The real contact area between the surfaces is comparatively very small as illustrated in Figure 8.1 (b). The real contact area during grinding depends on the following:

1. The surface micro/nanotopography of the wheel and work surfaces,
2. The micro/nanomechanical properties of the wheel and work surfaces, and
3. The machining (grinding) parameters.

The model proposed in this thesis has been developed by considering all the above listed parameters. However, some assumptions are also necessary in order to simplify the task of modeling of complicate machining processes such as grinding. In real grinding environment, the surfaces are in hydrodynamic contact because there is a possibility of thin film of coolant could be present between the contact surfaces. The sizes of the asperities are very small and hence the contact between the asperities is assumed as solid-solid contact in this model. The contact between the asperities is also assumed in plastic contact that obeys the Heritizian law. The main objective of the model developed in this study is to develop a force model for micro/nanoELID grinding in order to know the method of contact and contact zone created during grinding. The simulated grinding forces represented at pure plastic deformation of the material, and the simulated results are used as a threshold value for the micro/nanoELID grinding process.

The force model considers two types of contact as shown below:

- The contact between the wheel and work asperity: Modeling of wheel and work surfaces, the contact between the asperities and the real contact between the surfaces.
- The contact between the grit and work: The force per grit.

The normal force generated during the ELID grinding is related with the actual area of contact between the surfaces, grit density and the force generated per grit. The model development consists of several steps, which are listed below:

1. Modeling of the work surface
2. Modeling of the wheel surface
3. Modeling the contact between the asperities
4. Estimation of real area of contact and
5. Modeling of the grinding forces.

Each step is described and discussed in the following sections.

8.2.1 Modeling of the work surface

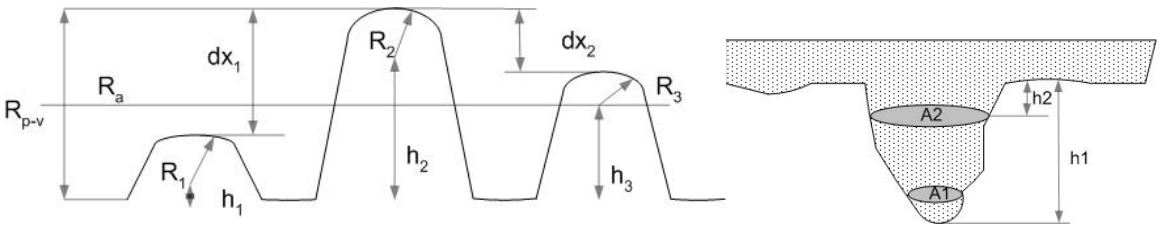

Figure 8.2: (a) Illustration of rough surface (b) Shape of an asperity.

The micro/nanoELID grinding usually performed on a brittle/semi-ductile surfaces. A rough surface consists of summits distributed throughout the surface. The information of

the size of the summits and their distribution have a great influence on the area of contact during grinding. Figure 8.2 (a) shows a schematic illustration of a rough surface. Consider three asperities with radii R_1, R_2 and R_3 in the sampling length at distances h_1, h_2 and h_3 from a reference level. Figure 8.2 (b) shows the shape of an asperity. The cross-sectional area of the asperity is gradually increases towards the base. Let A_1 be the area of the summit and A_2 be the area near the base of the asperity. When consider $A_1 << A_2$, the radius of the summits R_1, R_2 and R_3 are comparatively very small. For a rough surface, if $R_a \approx R_t$, the height difference between the asperities Δx_1 and Δx_2 are ignorable and hence the asperities are assumed as spheres of similar sizes.

The distribution of asperities on the work surface can be estimated using Greenwood-Williamson model [Bharat Bhushan, 1999] that assumes the work surface composed of hemispherical asperities of radius of curvature that contacts a flat plane. Assuming the asperity distribution is under Gaussian distribution with standard deviation of σ_s. Now the probability of distribution is

$$\int_{d/\sigma s}^{\infty} g(\overline{h_s})\ d\overline{h_s} \tag{8.1}$$

where $\overline{h_s}$ - The summit height normalized by summit rms height σ_s,

d – Distance between the contact planes

Now assuming the surface density of summits is D_{sum}, and the number of contact, N_{cont}, per area, can be calculated as

$$N_{cont} = D_{sum} \int_{d/\sigma s}^{\infty} g(\overline{h_s})\ d\overline{h_s} \tag{8.2}$$

The increase in number of contact between the surfaces increases the grinding forces generated during grinding.

8.2.2 Modeling of the ELID-grinding wheel surface

The surface of the ELID-grinding wheel consists of oxidized layer and abrasive grits. The dressed grinding wheel surface is covered by the oxidized layer, and the grits become active when the oxide around the grits is removed while rubbing on the work surface. Therefore, the conventional methods such as profile measurement and imprint method are difficult to implement on the ELID grinding wheel. The mesh size stamped on the grinding wheel is used to estimate the mean grit size (d_g) of the grinding wheel as shown below

$$d_g = \frac{15000}{mesh\ size\ of\ the\ grinding\ wheel} \tag{8.3}$$

The abrasive grits are generally irregular in shape and they are assumed as spheres of diameter d_g, and the volume of grit is calculated as shown below

$$v_g = \frac{4\pi}{3}\left(\frac{d_g}{2}\right)^3 \tag{8.4}$$

The number of diamond particles in the diamond layer (metal bond and diamond mix) per unit volume can be calculated as

$$N_v = \frac{f_v V_l}{v_g} \tag{8.5}$$

where f_v is the volume percentage of the diamond grits, and

V_l is the volume of the diamond layer

The grit density per unit area of diamond layer can be estimated by using the formula given below:

$$N_g = N_v^{\,2/3} \tag{8.6}$$

The active grit density for macroabrasive wheels can be estimated by the grit protrusion from the wheel surface [Fuji Die Catalog]. However, the active grit density for

micro/nanoabrasives depends on the actual contact between the asperities and hence the total grits present on the wheel-active-surface consists of active and inactive grits. Therefore, the grit density obtained from the equation (8.6) can be written as the sum of active and inactive grits as shown below;

$$N_g = N_a + N_i \quad \text{and} \tag{8.7}$$

$$N_a = N_g \, A_c \tag{8.8}$$

$$N_i = (A_o - A_c) N_g \tag{8.9}$$

where N_g is the number of grits per unit area,

N_a is the number of active grit per unit area,

N_i is the number of inactive grits per unit area of the grinding wheel,

A_o is the apparent area of contact, and

A_c is the actual area of contact.

Grits on the wheel-active-surface becomes either active or inactive depending on the contact between the wheel-work asperities. Increase in area of contact increase the number of grits in action. The advantage of micro/nanoELID grinding is the grit density per unit area remains constant throughout the process, which can produce more uniform material removal from the work surface. The grit concentration on the grinding wheel surface can be increased or decreased by choosing suitable wheel concentration.

8.2.3 Modeling the contact between the asperities

During grinding, the surfaces with dissimilar properties are brought into contact, and one of the surfaces is slowly fed into the other surface in order to remove the material from the other surface. For every in-feed (depth-of-cut), the wheel is fed into the work and the contact was made between the asperities. The contact radius and the contact

displacement can be derived using contact mechanics (assuming the asperities as spheres) [Johnson, 2000]. According to Hertz, when two spherical surfaces are in plastic contact, the contact-radius (r_c) is

$$r_c = \left(\frac{3WR}{4E^*}\right)^{1/3} \tag{8.10}$$

where W is the load applied on perpendicular to the surface in contact, and

R is the composite or effective curvature, which can be expressed as

$$\frac{1}{R} = \frac{1}{R_w} + \frac{1}{R_s} \tag{8.11}$$

where R_w – the radius of the asperity on the work surface and

R_s – The radius of the asperity on the wheel surface.

The E^* is known as the effective modulus which can be written as

$$\frac{1}{E^*} = \frac{1-\gamma_w^{\,2}}{E_w} + \frac{1-\gamma_s^{\,2}}{E_s} \tag{8.12}$$

where γ_w is the Poisson ratio of the work material,

γ_s is the Poisson ratio of the ELID layer,

E_w is the Modulus of elasticity of the work material and

E_s is the Modulus of elasticity of the ELID layer.

Now the area of contact (a_c) is expressed as

$$a_c = \pi r_c^{\,2} = \pi\left(\frac{3WR}{4E^*}\right)^{2/3} \tag{8.13}$$

The displacement within the contact, δ, is expressed as

$$\delta = \left(\frac{9W^2}{16R\,E^{*2}}\right)^{1/3} \tag{8.14}$$

The depth of plastic zone for a hard and brittle material is depending on the material properties such as hardness, elastic modulus and the fracture toughness. When the contact between the asperities is assumed in plastic contact, the total displacement δ should be within the maximum plastic deformation of the brittle material. Assuming $\delta \approx R_p$, then the maximum load required to cause the asperities in contact can be written as

$$W = \frac{4}{3} R_p^{3/2} R^{1/2} E^* \tag{8.15}$$

where R_p is the radius of plastic zone.

The load 'W' is the load applied on the grits embedded into the wheel surface. The grits penetrate and plow the work during grinding and generate grinding forces, which can be described latter part of the modeling.

8.2.4 Estimation of the real area of contact

Estimation of the real area of contact between the wheel and work surfaces is an important task because it provides the number of active grits within the area of contact. The real surface contains hills and valleys and the equation of a rough surface can be expresses as a mathematical function as shown below

$$z = f(x, y) \tag{8.16}$$

where x and y are the co-ordinates of a point on the two dimensional plane, and

z is the vertical height

Assuming a hard flat plan is in contact with the surface, the ratio of real contact and the apparent area can be written as

$$\frac{A_r}{A_a} = \int_d^{\infty} g(z)\, dz \tag{8.17}$$

where A_r is the real area of contact,

A_a is the apparent area of contact and

$g(z)$ is the probability of height distribution.

The height distribution is assumed as Gaussian distribution,

$$g(\bar{z}) = \frac{1}{\sqrt{2\,\pi}} \exp\left[-\frac{(\bar{z} - \bar{z}_m)^2}{2} \right] \quad -\infty < \bar{z} < +\infty \tag{8.18}$$

where $\bar{z}$ is the non-dimensional surface height ($\bar{z} = z/\sigma$)

σ is the standard deviation and

$\bar{z}_m$ is the non-dimensional mean height

Now the above equation can be written as

$$\frac{A_r}{A_a} = \int_{d/\sigma}^{\infty} g(\bar{z})\, d\bar{z} \tag{8.19}$$

The apparent contact between the wheel-work can be written as

$$A_a = l_c\, b \tag{8.20}$$

where l_c is the arc length between the wheel and work and b is the grinding wheel. The apparent contact length is

$$l_c = \sqrt{D_w\, a} \tag{8.21}$$

D_w is the diameter of the grinding wheel and

a is the depth-of-cut.

8.2.5 The development of force model for micro/nanoELID grinding

The grinding forces generated can be predicted from the grinding action of grits. The grinding forces generated during grinding are proportional to the real contact area, the active grit concentration and the co-efficient of friction.

8.2.5.1 Force per grit model

The shape of a single grit is assumed as an indenter (the shape of the indenter is either pyramid or sphere), and the load applied on grit is derived using the Equation 8.5. Now, the radius of impression during indentation of grit can be estimated as

$$r_{\text{int}} = \sqrt{\frac{1.854\,W}{H_w}} \quad \text{for grits assumed as pyramids} \tag{8.22}$$

$$r_{\text{int}} = \sqrt{\frac{2\,W}{\pi\,H_w}} \quad \text{for spherical shape} \tag{8.23}$$

When the load W is applied on grit, the material displaced by the indentation is assumed as a hemisphere of radius r_{int} as shown in Figure 8.3 (a). The volume of material replaced by the grit depending on the grinding parameter as illustrated in Figure 8.3 (b). The relative movement between the wheel and work is expressed as

$$\overline{V}_{ratio} = \frac{v_w}{v_s} = \frac{v_w}{\pi\,D_w\,N} \tag{8.24}$$

where N is the spindle rotation in *rpm*.

The volume of material displaced by grit during grinding can be written as

$$V_{grit} = \frac{2}{3}\,\pi\,r_{\text{int}}^{\,3}\,\overline{V}_{ratio} \tag{8.25}$$

The force generated per grit while removing V_{grit} of material from the work asperity can be written as the product of the hardness of the work and the area of contact during sliding. Now the force per grit can be expressed as

$$f_g = H_w * r_{\text{int}}\,\overline{V}_{ratio} \tag{8.26}$$

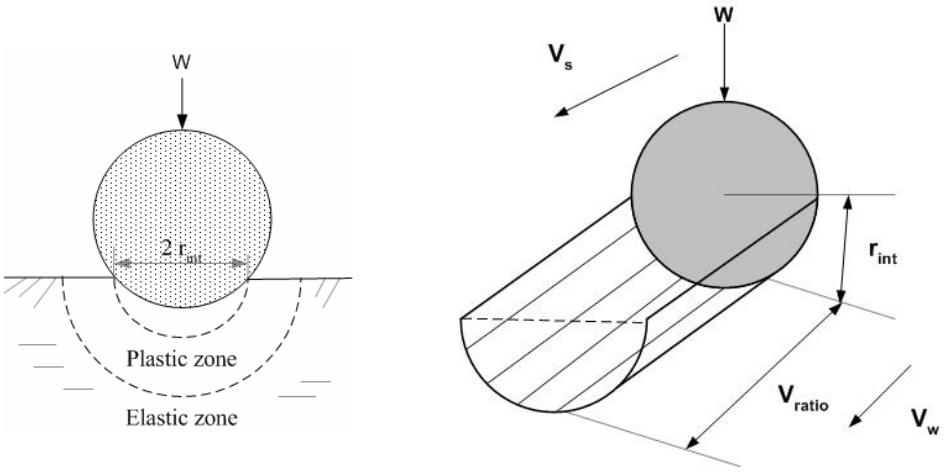

(a) Indentation of grit (b) Plowing of grit

Figure 8.3: Grinding action of single grit.

8.2.5.2 Normal and tangential grinding forces

The normal force generated during grinding is the cumulative effect of force generated by the active grits on the wheel surface. The number of active grits depends on the grit concentration of the grinding wheel and the real contact area between the wheel and work. Now the normal grinding force generated is

$$F_N = f_g \quad N_g \quad A_r \tag{8.27}$$

The specific frictional or tangential force can be estimated from the equation given below

$$F_T = \mu \; F_N \tag{8.28}$$

where μ – Frictional co-efficient depends on the work/bond material, and

F_N, F_T – Normal and tangential forces during grinding.

The normal and tangential grinding forces given in Equations (8.27) and (8.28) are simulated and used as a measure to the grinding process.

8.3 Simulation and verification of the model

The developed model for micro/nanoELID grinding is simulated and compared with the experimental results. The simulation of the developed model consists of the following steps:

- Selection of the grinding method, grinding parameters and dressing parameters,
- Simulating the actual contact area and the grit density and
- Simulation and verification of the grinding forces.

The above steps are explained in the following sections.

8.3.1 Selection of grinding method, grinding parameters and dressing parameters

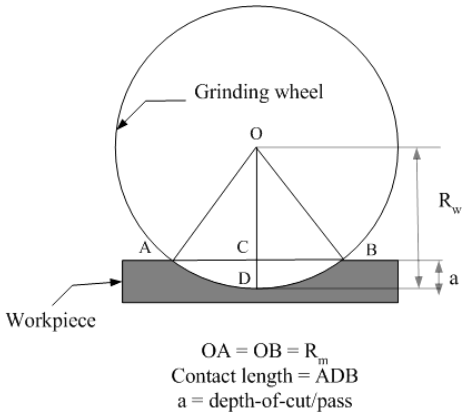

Figure 8.4 Schematic illustration of the contact length between the wheel and work.

The model developed for micro/nanoELID grinding claims that the grinding forces generated are proportional to the actual contact between the asperities of the wheel-work surfaces in contact, and hence the vertical grooving method (described in Chapter 3) is found to be more suitable for the verification. The method for prediction the theoretical contact area between the wheel and work during the vertical groove method is illustrated in figure 8.4. The main objective of the experiment is to produce nanosurface finish on

the brittle surface. Hence the grinding parameters and the ELID dressing parameters have been chosen based on the investigations conducted in Chapter 5. The grinding parameters chosen for the simulation are the spindle rotation of 3000 *rpm*, the feed rate of 200 *mm/min* and the depth-of-cut of 1 $\mu m/pass$. Then the pre-dressing and in-process dressing conditions have been chosen in such a way that it could work good association with the grinding parameters chosen. The dressing conditions chosen for the simulation are $I_p - 10\ A$, $V_p - 90\ V$, $T_{on} - 5\ \mu s$ and $T_{off} - 5\ \mu s$.

8.3.2 Simulation of the actual contact area and the grit density

The mechanical properties of BK7 glass (workpiece material) have been used for the simulation. The optical glass was ground using macrogrinding (#325) in order to produce a flat and brittle surface for the experiments. The brittle surface with an average surface roughness of 1.432 μm has been characterized in order to obtain the parameters such as the size of the asperity, distribution of the asperity and the ratio between the real and apparent contact areas. The replica of the brittle surface was used for the characterization. From the results, the size of the asperity, D_{sum} and A_r/A_0 for the brittle surface were found to be 500 μm, 28 */mm* and 0.15, respectively. The bond properties such as Poisson ratio and the Young's modulus for various bond materials are tabulated in Table 8.1. The mean grit size and abrasive grit concentration of different mesh sized grinding wheels have been simulated using Equations (8.3) – (8.6) and tabulated in Table 8.2. A cast iron-bonded grinding wheel with dimensions diameter 100 *mm*, thickness 3 *mm* and grade #4000 has been chosen for the simulation. From the Table 8.1 the mean grit size and the grit concentration of the wheel are found to be 3.75 μm and 45839 */mm*^{2}, respectively. A copper electrode of 1/4th of perimeter of the wheel with the

true area of the electrode of 2.35 cm^2 has been chosen for the purpose of simulation. The current density for the in-process dressing condition was calculated as 2.15 A/cm^2. The above data are used to simulate the grinding forces.

Table 8.1 Properties of various bond materials

Material	Poisson ratio (bond)	E(b) *Gpa*
Bronze	0.34	104
Cast iron	0.28	173
Copper	0.35	117
Layer (on cast iron)	0.3 (assumed)	31

Table 8.2 Mean grit size and the grit density on the wheel surface

Grade	d_g μm	V_g / mm^3	N_g / mm^2	N_g / mm^2
# 4000	3.75	27.597	9058740	45839
#8000	1.875	3.449	72469922	184631
#12000	1.25	1.022	2.45E+08	417108
#30000	0.5	0.065	3.82E+09	2630925

8.3.3 Simulating and verification of the grinding forces

Substituting the values of the mechanical properties of wheel and work in Equations 8.10 – 8.15 provide the contact radius, contact modulus and the load W on the asperities under plastic contact. The contact modulus obtained for different bond materials and the BK7 glass are tabulated in Table 8.3. From the table it is found that the oxide layer

produced on the grinding wheel surface (cast iron) produced very lower contact modulus of 24.29 *GPa* and the highest contact modulus was produced by the cast iron bonded wheel (58.38 *GPa*).

Table 8.3 The contact modulus obtained for various bond materials.

Material	E* *Gpa*
Bronze	49.248
Cast iron	58.382
Copper	51.810
Layer (on cast iron)	24.297

The grinding forces were simulated using Equations 8.27 and 8.28 for two different conditions stated below:

- The grinding wheel was pre-dressed and then used without the application of the ELID (can be considered as without ELID condition).
- The grinding wheel is pre-dressed and then used with the application of the ELID. The pre-dressing and the in-process dressing conditions were chosen as 2 A/cm^2.

The simulated results for the above conditions were tabulated in the appendix tables Table C.1 and Table C.2 (Appendix C), respectively. The value of friction-co-efficient was found to be 0.09 and 0.05 for without ELID and ELID with 2 A/cm^2, respectively.

Figures 8.5 (a) and (b) show a comparison of the simulated and experimental normal and tangential grinding forces for the above prescribed conditions. Figure 8.5 (a) shows the simulated and experimental grinding forces. The grinding forces were simulated

using the properties of the cast iron, and the experiment was conducted using a pre-dressed cast iron wheel. The normal and the tangential grinding forces are found to be much lower than the simulated results until the apparent contact length reaches 4 *mm*. After that the grinding forces were raised and almost have a good correlation with the simulated results. From the results, it is clear that the oxide layer present on the surface after pre-dressing was the reason for the reduction of forces at the initial stage, and after the wear of the layer the forces were behaved as similar with the simulated results.

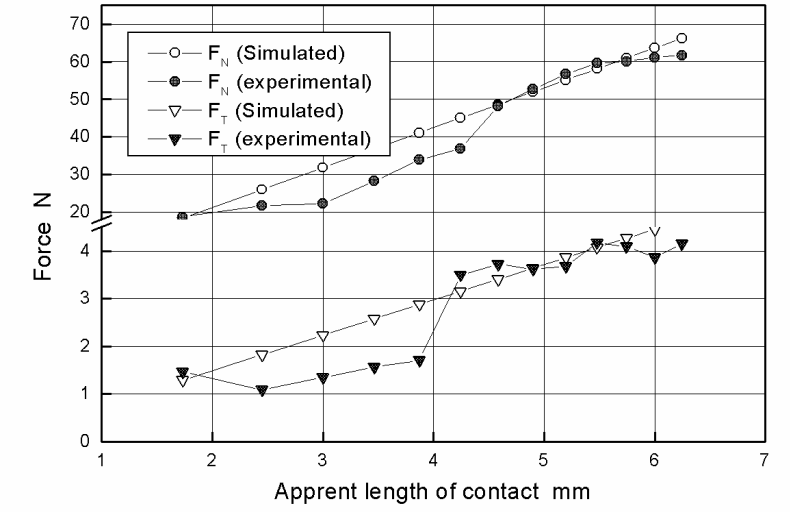

(a) Pre-dressed wheel (without ELID)

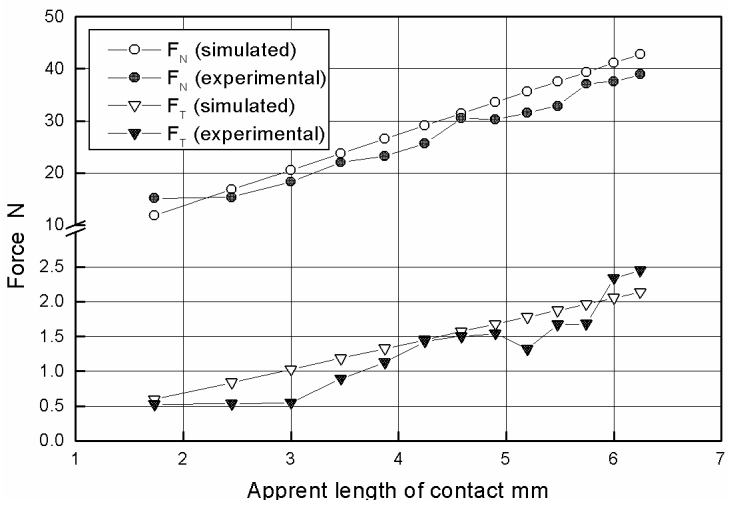

(b) Pre-dressed wheel with the application of the ELID

Figure 8.5: Comparison between the simulated and experimental results.

Figure 8.5 (b) was simulated using the micro/nanomechanical properties of the oxide layer from Table 8.3. The experimental and the simulated results show good correlation with each other. The surface roughness was found to be 0.034 μm and 0.007 μm for without ELID and with ELID processes, respectively. From the verification it is very clear that the properties of the oxide layer play a vital role in micro/nanoELID grinding.

8.4 Concluding remarks

From the compatibility found between the simulated and the experimental results the following conclusions are achieved:

- The results obtained from the verification of the model clearly evident that the application of ELID reduce the grinding forces to a significant amount and improves the quality of the ground surface.

- Grinding with ELID produces a soft oxide layer at the wheel-active-surface, which reduces the friction between the surfaces.

- Selection of suitable ELID parameters helps to produce an oxidized layer with certain micro/nanomechanical properties and facilitate a defect free surface.

- The developed model would be more useful for choosing the suitable bond material and the in-process dressing conditions for a particular work material.

Chapter 9

Conclusions, contributions and recommendations

This chapter includes the conclusions obtained from the fundamental analysis of the ELID grinding, the contributions of the thesis in the field of precision finishing and future recommendations.

9.1 Conclusions

The conclusions obtained from the fundamental analysis of the ELID grinding are grouped under the following headings:

1. The grinding forces
2. The surface finish
3. The wheel wear
4. Conclusions about the ELID-layer (oxidized layer)
5. Conclusion obtained from the developed grinding model

9.1.1 The grinding forces

The conclusions obtained regarding the grinding forces during ELID grinding are listed as follows:

- At similar grinding conditions, the application of the ELID reduces the grinding forces to a significant amount (when compared to the conventional grinding).

- The grinding forces generated during the ELID grinding are generally found to be unstable due to the breakage and formation of the oxidized layer on the grinding wheel surface.

- The increase of current duty ratio reduces the grinding forces and improves the stability of the forces.

- The tangential grinding forces are found to be unstable throughout the grinding process irrespective of the current duty ratio. The macrofracture of the oxidized layer from the grinding wheel causes the instability, which is an essential phenomenon for stimulating the electrolysis.

- The grinding forces are gradually increased during ELID grinding until the normal force reached a certain value. After the value, certain thickness of the layer was separated from the grinding wheel, which causes a drop in normal and tangential grinding forces. The separation of the oxidized layer from the surface helps the wheel free from loaded chips and worn grits and allows the fresh layer beneath comes in contact with the work surface.

9.1.2 The surface finish

The conclusions drawn related to the surface finish and the surface defects are listed below:

- The application of the ELID shows significant improvement on surface finish in all grinding modes.

- A comparison between the surfaces obtained from in-process dressing and interval dressing shows that better surface finish could be obtained by the in-process dressing.

- The surface finish obtained from the ELID grinding depends on the current duty ratio chosen for the in-process dressing. The higher the dressing current duty ratio the finer the surface finishes.

- The surface defects and surface cracks have been reported when grinding with dressing current duty ratio from 20 % - 40%. The defect free surface has been reported when grinding with current duty ratio 50% and more.

- For deeper cuts (depth-of-cut greater than the mean grit size of the wheel), the surface roughness and waviness are found to be better while grinding with current duty ratio of 30%. Grinding with more than 30% current duty ratio increases the roughness and waviness of the ground surfaces.

- For smaller depth-of-cuts (the depth-of-cut less than the mean grit size of the grinding wheel) the surface roughness and waviness are found to be improved with the increase of current duty ratio. Average surface roughnesses of 3 *nm* and 7 *nm* (for #4000 grade wheels) have been achieved from the surface grinding and vertical groove grinding processes, respectively.

9.1.3 The wheel wear

The conclusions obtained from the wheel wear mechanism of the ELID grinding wheels are listed below:

- The wear mechanism of the ELID grinding wheels is different from the wear mechanism of the conventional grinding wheels. The oxidized layer on the grinding wheel surface undergoes grit wear, microfracture and finally macrofracture of the layer. The macrofracture of the oxidized layer is the indication of the wheel end-of-life. The grinding wheels are dressed after every macrofracture while performing grinding.

- The wear ratio of the grinding wheels is increasing with the increase of the current duty ratio. When the current duty ratio increases beyond 50%, the wear rate of the grinding wheels increases without showing any significant improvement on the surface finish.

- The oxidized layer wears faster than the actual bond material, but the wheel diameter was found to be increased after pre-dressing.

- The radial wear rate of the grinding wheel is influenced by ON-time of the pulse. The wheel wear rate increases for shorter pulse ON-time.

- The radial wear increases with the frequency of current pulses without significant improvement on the grinding parameters.

9.1.4 ELID-layer (oxidized layer)

The characterization of the ELID-layer can be concluded as follows:

- The ELID-grinding wheels are made of transition materials, and they can produce an oxidized layer during the electrolytic dressing, which prevents the bond material from further oxidization. The oxidized layer formed on the grinding wheel surface has been produced in two different phases. The first phase of the layer produced during pre-dressing and the second phase of the layer formation occurs during in-process dressing.

- The thickness of the oxidized layer produced by the ELID depends on the dressing current density. The thickest oxidized layer of 250 μm was formed on the cast iron-bonded grinding wheels when dressed using current density of about 3 A/cm^2. The layer formed on the other bond materials such as copper and bronze are not as thick as the layer formed on the cast iron-bonded grinding wheels.

- The microconstituents and the microhardness of the oxidized layer show that the layers have different micro/nanomechanical properties. The hardness of the layer increases from the wheel edge towards the layer-bond interface, which reduces the excessive layer wear.

- The microhardness of the layer produced at 3 A/cm^2 has a hardness of 60 GPa (200 g) and the layer produced at 1 A/cm^2 was found to be 110 GPa

(200 *g*). The lower hardness improves the self-sharpening effect and reduces the depth of grit penetration and produces good surface finish.

- According to the pulse electrolysis, the selection of ON-time and OFF-time of the pulse should be greater than the charging and discharging time of the electrical double layer. If the above condition is not satisfied, heavy damping occurs and it leads to larger wear of the oxidized layer.

- Among the grinding wheels the cast iron-bonded grinding wheel shows the most non-liner character during the ELID. The non-liner character shows high resistance to bond wear and also produces good self-sharpening effect.

9.1.5 Conclusion obtained from the developed grinding model

The model developed for micro/nanoELID grinding fetch the following conclusions:

- The developed model shows that the grinding forces produced during micro/nanoELID grinding depends on the micro/nanomechanical properties of the work surface, the ELID-layer and the topography of the surfaces in contact.

- The actual grit density during micro/nanoELID grinding depending on the actual area of contact between the asperities and the grit density of the ELID-layer.

- The simulated grinding forces are used as a threshold value for the plastic deformation of the work material. The developed model would be more useful for selecting suitable bond material and the dressing parameters for the micro/nanoELID grinding.

9.2 The research contributions

The contributions of this thesis in the field of precision grinding have been classified and discussed in the following headings:

9.2.1 The approaches and analyses on ELID grinding

- The approaches used in this thesis for the prediction of effectiveness of the ELID technique are never been reported earlier. The analytical studies and investigations conducted in this thesis will be certainly helpful for the ELID users to understand the importance of choosing dressing parameters that works in good association with the grinding parameters, and to utilize the full effectiveness of the ELID for precision finishing.

- The analyses conducted in this thesis on the wear mechanisms, wear rate of the ELID grinding wheels and the wear reduction strategies are new and never been reported. The relation between the dressing current and the wear ratio of the grinding wheels, the influence of the pulse frequency on the wheel wear are entirely new and useful analyses, which are more essential for wear compensation. The relation between the dressing current and the depth-of-cut given by the grinding wheels for different geometrical shapes will be more helpful for precision finishing of non-axis-symmetrical components using the ELID.

- The investigations conducted on the ELID-layer reveals the characters and behavior of the ELID. The knowledge of the micro/nanomechanical properties of the ELID-layers promotes the importance of selection of suitable bond material for finishing a particular workpiece.

9.2.2 Proposal of new grinding model

The grinding model proposed in this thesis for micro/nanoELID grinding has a different approach from the conventional grinding models. It depends more on the real environment factors such as the topographies of the wheel and work surfaces. The substantiated results show that the model will be more useful in nanoscale finishing. The developed model will be useful to examine the effectiveness of the grinding process when the micro/nanomechanical properties of the ELID-layer have been supplied.

The research contributions described are certainly useful for increasing the robustness of the ELID grinding for precision grinding.

9.3 Recommendations for Future research

The ELID is a new technique need to be analyzed and improved further. This chapter covers few directions

- Optimization of the ELID grinding process

  Proper guidance is essential for the ELID user to select the suitable parameters in order to avoid the malfunction of the ELID process.

Optimization of the grinding process reduces the ambiguities and increases the robustness of the process in the field of precision manufacturing.

- Wear monitoring and wear compensation

  On-line wheel wear monitoring and compensation are the essential steps to be performed in order to maintain the geometrical accuracy of the machined components.

- The improvement of the ELID cell

  The power supply, grinding wheel materials and the electrolyte are the importance factors in the ELID-cell. For better performance of the ELID-cell, the following recommendations are proposed:

  - A programmable power supply is much essential for ELID, which reduces the risk of malfunctioning of the ELID-cell.

  - Though different materials have been used as bond material for the wheels, a unique bond material will reduce the ambiguity of selecting the in-process dressing parameters since different bond materials respond to the ELID in a different way.

  - Though the ELID electrolyte contains rust preventing additives, the problem of rusting was reported. A rust free electrolyte improves the grinding environment and reduces the maintenance difficulties.

References

Amin A, Mokbel, Maksoud T M A, Monitoring of the condition of diamond grinding wheels using acoustic emission technique, Material processing technology, Vol. 101, pp. 292 – 297, 2000.

Bandyopadhyay B P, Ohmori H, Takahashi I, Ductile regime mirror finish grinding of ceramics with electrolytic in-process dressing (ELID) grinding, Materials and Manufacturing Processes, Vol. 11, Issue 5, pp. 789–801, 1996.

Bandyopadhyay B P, Ohmori H, The effect of ELID grinding on the flexural strength of silicon nitride, International Journal of Machine Tools and Manufacturer, Vol. 39, pp. 839–853, 1999.

Bifano T G, Dow T A, Scattergood R O, Ductile –Regime Grinding: A new technology for machining brittle materials, ASME, Journal of Engineering for Industry, Vol.113, pp. 184-189, May 1991.

Chan Xun, Brian Rowe W, Allanson D R, Mills B, A grinding power model for selection of dressing and grinding conditions, Transaction of the ASME, Vol. 121, November, 1999.

Fujihara K, Ohshiba K, Komatsu T, Ueno M, Ohmori H, Bandyopadhyay B P, Precision surface grinding characteristics of ceramic matrix composites and structural ceramics

with electrolytic inprocess dressing, Machining Science and Technology, Vol. 1, pp. 81–94, 1997.

Fuji Die Catalog, Fuji Die Co., Japan.

Gomes de Oliveria J F, Dornfeld D A, Application of AE contact sensing in Reliable Grinding Monitoring, Annals of the CIRP,50/1/ 2001, pp.217-220.

Hans H, Gatzen, Chris Maetzig J, Nanogrinding, Precision Engineering, Vol. 21, pp. 134 – 139, 1997.

Hassui A, Diniz A E, Oliverira J F G, Felipe J, Gomes J JF, Experimental evaluation on grinding wheel wear through vibration and acoustic emission, Wear, Vol. 217, pp. 7 – 14, 1998.

Ibl N, Puippe J Cl and Angerer H, Electrocrystallization in pulse electrolysis**,** Surface Technology, Vol. 6, Issue 4, pp. 287- 300, 1978.

Ibl N, Some theoretical aspects of pulse electrolysis, Surface Technology, Vol. 10, Issue 2, pp. 81-104, 1980.

Itoh N, Ohmori H, Moriyasu S, Kasai T, Toshiro K, Bandyopadhyay B P, Finishing characteristics of brittle materials by ELID-lap grinding using metal-resin bonded wheels, International Journal of Machine Tools and Manufacturer, Vol. 38, pp. 747–762, 1998.

Karmer D, Rehseteiner F, Agathon AG, ECD (Electrochemical In-process Controlled Dressing), a new method for grinding of modern high-performance cutting materials to high quality, Annals of the CIRP, Vol. 48/1/1999, pp. 265 – 268.

Kato T, Ohmori H, Zhang C,Yamazaki T, AkuneY, Hokkirigawa K, Improvement of friction and wear properties of CVD-SiC films with new surface finishing method 'ELID-grinding', Key Engineering Materials, Vol. 196, pp. 91–101, 2001.

Kun Li, Warren Liao T, Modelling of ceramic grinding processes Part I. Number of cutting points and grinding forces per grit, Journal of Material processing technology, Vol. 65, pp. 1 – 10, 1997.

Lee E S, study of the development of an ultraprecision grinding system for mirror-like grinding, International Journal of Advanced Manufacturing Technology, Vol. 16, pp. 1–9, 2000.

Lim H S, Ohmori H, Lin W, Qian J, High productivity and high accuracy electrode-less ELID grinding on die material, RIKEN Review, 24, pp. 136–137, 2000 (in Japanese).

Lim H S, Ohmori H, Lin W, Qian J, High productivity and high accuracy electrode-less ELID grinding on die material, Journal of Society of Grinding Engineer, 45: 298–303, 2001 (in Japanese).

Matsuzawa T, Ohmori H, Zhang C, Li W, Yamagata Y, Moriyasu S, Makinouchi A, Micro-spherical lens mold fabrication by cup-type metal-bond grinding wheels applying

ELID (Electrolytic In-process Dressing), Key Engineering Material, 196, pp. 167–176, 2001.

Murata R, Okano K, Tsutsumi C, Grinding of structural ceramics, Milton C Shaw Grinding Symposium PED 16, pp. 261–272, 1985.

Ohmori H, Nakagawa T, Mirror surface grinding of silicon wafers with electrolytic in-process dressing, Annals of the CIRP, Manufacturing Technology, 39/1/1990, pp. 329–333.

Ohmori H, Nakagawa T, Analysis of mirror surface generation of hard and brittle materials by ELID (electronic in-process dressing) grinding with superfine grain metallic bond wheels, Annals of the CIRP, Manufacturing Technology, 44/1/1995, pp. 287–290.

Ohmori H, Nakagawa T, Utilization of nonlinear conditions in precision grinding with ELID (Electrolytic in-process dressing) for fabrication of hard material components, Annals of the CIRP, Manufacturing Technology, 46/1/1997, pp. 261–264.

Ohmori H, Moriyasu S, Li W, Takahashi I, Park KY, Itoh N, Bandyopadhyay B P, Highly efficient and precision fabrication of cylindrical parts from hard materials with the application of ELID (Electrolytic In-process Dressing), Materials and Manufacturing Processes, Vol. 14, pp. 1– 12, 1999.

Ohmori H, Li W, Makinouchi A, Bandyopadhyay B P, 2000 Efficient and precision grinding of small hard and brittle cylindrical parts by the centerless grinding process combined with electro-discharge truing and electrolytic in-process dressing, Journal of Material processing technology, Vol. 98, pp. 322–327, 2000.

Ohmori H and Qian J, ELID-II grinding of micro spherical lens RIKEN Review, Vol. 23, pp. 140, 2000.

Okuyama S, Yonago M, Kitajima T, Suzuki H, A basic study on the combination machining of ELID-grinding and EDM-experiments of combination machining using a pulse power-source. Journal of the Japan Society of Precision Engineering, 67/3/2001, pp. 407–412.

Qian J, Wei L, Ohmori H, Cylindrical grinding of bearing steel with electrolytic in-process dressing, Precision Engineering, Vol. 24: pp. 153–159, 2000.

Qian J, Ohmori H, Lin W, Internal mirror grinding with a metal/metal-resin bonded abrasive wheel, International Journal of Machine Tools and Manufacturer, Vol.41, pp. 193–208, 2001.

Shimada S, Ikawa N, Inamura T, Takezawa N, Ohmori H, Sata T, Brittle-ductile transition phenomena in microindentation and micromachining, Annals of the CIRP, Manufacturing Technology , 44/1/1995, pp. 523–526.

Stephenson D J, Veselovac D, Manley S, Corbett C, Ultra-precision grinding of hard steels, Precision Engineering, Vol. 25, pp. 336 – 345, 2001.

Stephenson D J, Hedge J, Corbett C, Surface finishing of Ni–Cr–B–Si composite coatings by precision grinding, International Journal of Machine Tools and Manufacturer, Vol. 42, pp. 357–363, 2002.

Suzuki K, Uematsu T, Nakagawa T, On-machine truing/dressing of metal-bonded grinding wheels by electro-discharge machining, Annals of the CIRP, Manufacturing Technology, 36/1/1987, pp. 115–118.

Tonshoff, H.K. Peters, I. Inasaki, Paul T, Modelling and simulation of grinding processes, Annals of the CIRP, Manufacturing Technology, 41/2/1992, pp. 677-688.

Uehara Y, Ohmori H, Yamagata Y, Moriuasu S, Makinouchi A and Morita S, Microfabrication grinding by ultraprecision microform generating machine employed with plasma discharge truing and ELID technique, RIKEN Review, Issue 34, pp. 25–28, 2001.

Venkatesh V C, Inasaki I, Toenshof H K, Nakagawa T, Marinescu I D, Observations on polishing and ultraprecision machining of semiconductor substrate materials, Annals of the CIRP, Manufacturing Technology, 44/2/1995, pp. 611–618.

Wang P, Shi Z, Xin Q, Optical surface grinding of optical glasses with ELID grinding technique, Proceedings of the SPIE- The International Society for Optical Engineering, Vol. 4231, pp. 509–514, 2000.

Wolf B, Richter A, The concept of differential hardness in depth sensing indentation, New Journal of Physics 5 (2003) Pages 15.1–15.17.

Yoshioka J, Hashimoto F, Miyashita M, Kanai A, Abo T, Daito M, Ultraprecision grinding technology for brittle materials: Application to surface and centerless grinding processes, Milton C. Shaw Grinding Symposium, PED 16, pp. 209 – 227, 1985.

Zhang F, LiW, Qiu Z, Ohmori H, Application of ELID grinding technique to precision machining of optics, Proceedings of the SPIE- The International Society for Optical Engineering, Vol. 4231, pp. 218–223, 2000.

Zhang Bi, Yang F, Wang J, Zhu Z, Monahan R, Stock removal rate and workpiece strength in multi-pass grinding of ceramics, Journal of Material processing technology, Vol. 104, pp. 178–184, 2000.

Zhang C, Ohmori H, Li W, Small-hole machining of ceramic material with electrolytic interval dressing (ELID-II) grinding, Journal of Material processing technology, Vol. 105, pp. 284–293, 2000.

Zhang C, Ohmori H, Kato T, Morita N, Evaluation of surface characteristics of ground CVD-SiC using cast iron bond diamond wheels, Precision Engineering, Vol. 25, pp. 56 –62, 2001.

BOOKS

Bharat Bhushan, Handbook of Micro/Nanotribology, CRC Press, Washington D.C., Chapter 4, pp. 187 – 246, 1999.

Blaedel K L, John S T, Evans C J, Ductile-Regime Grinding of Brittle Materials, Machining of ceramics and composites, Edited by Said Jahanmir, M. Ramulu and Philip Koshy, Marcel Dekker, New York, Chapter 5, pp. 139 – 176,1998.

Izumitani T S, Optical Glass, American Institute of Physics, New York, Chapter 4, pp. 106-114, 1986.

Johnson K L, Contact mechanics, Cambridge University Press, New York, 1985.

Kanno H, Pulsed anodic reactions, Theory and practice of pulse plating, Edited by Jean-Claude Puippe and Frank Leaman, American Electroplaters and Surface Finishers Society , Orlando, Chapter 12, Pages 209 – 217, 1986.

Malkin S, Grinding Technology: Theory and applications of machining with abrasives, Ellis Horwood, Chichester, UK, 1989, Chapter 8, pp. 197-221.

Puippe J Cl, Theory and practice of pulse plating, Edited by Jean-Claude Puippe and Frank Leaman, American Electroplaters and Surface Finishers Society , Orlando, 1986.

Shaw M C, Principle of abrasive processing, Oxford University Press, New York, 1996.

List of publications

A fundamental study on the mechanism of electrolytic in-process dressing (ELID) grinding, H. S. Lim, K. Fathima, A. Senthil Kumar and M. Rahman, International Journal of Machine Tools and Manufacture, Volume 42, Issue 8, June 2002, Pages 935-943.

A Study on the Grinding of Glass Using Electrolytic In-Process Dressing, A. Senthil Kumar, H. S. Lim, M. Rahman and K. Fathima, Journal of Electronic Materials, Volume 31, Issue 10, October 2002, Pages 1039-1046.

A study on wear mechanism and wear reduction Strategies in grinding wheels used for ELID grinding, K. Fathima, A. Senthil Kumar, M.Rahman, Lim H.S, Wear, Volume 254, 2003, Pages 1247 – 1255.

ELID grinding technique for nano finishing of brittle materials, M. Rahman, A. Senthil Kumar, H. S. Lim, K. Fathima , SADHNA, Journal of Engineering Sciences, Indian Academy of Sciences, Volume – 28, Part 5, October 2003, Pages 1 -18.

International Conference

1. Nano-surface finish using Electrolytic In-process Dressing (ELID) grinding, M. Rahman, A. Senthil Kumar, H. S. Lim, K. Fathima. (Published as a **Keynote paper** in the proceedings of the second international conference on Precision Engineering and Nano Technology (ICPN2002), Changsha, Hunan,China. Oct.28-30, 2002 Pages 29-43).

Article in book

A study on some factors affecting the mechanism of ELID grinding, K.Fathima, M.Rahman, A.Senthil Kumar and H.S.Lim, International Progress on Advanced Optics and Sensors, Edited by Ohmori H and Shimizu H M, Universal academy press, 2003, ISBN 4-946443-76-2,Pages 283 – 298.

Table A.1 Properties of the bond materials

Material	Young's Modulus (E) GPa	Shear Modulus(S) GPa	Poisson's ratio (γ)
Bronze	104	44.9	0.34
Cast iron	173	86.3	0.28
Copper	117	43.5	0.35

Table A.2 Electromotive series

Material	Standard potential (Eo)
Zn/Zn^{2+}	- 0.76 mV
Cr/Cr^{3+}	- 0.74 mV
Fe/Fe^{2+}	- 0.56 mV
Fe/Fe^{3+}	- 0.44 mV
Co/Co^{2+}	- 0.28 mV
Ni/Ni^{2+}	- 0.23 mV
$H_2/2H^+$	**± 0.00 mV**
Cu/Cu^+	+ 0.34 mV
Au/Au^+	+ 0.1.50 mV

Table A.3 Properties of BK7 glass

Properties	Values
Density (g /cm^3)	2.51
Glass transition temperature (˚ C)	559
Co-efficient of thermal expansion (10^{-6} C^{-1})	7.1
Young's modulus (GPa)	81
Poisson ratio	0.21
Vickers Hardness (GPa)	5.1
Fracture toughness (MPa $m^{½}$)	0.82

Fick's law of diffusion

The assumptions during the pulsed electrolysis are listed below:

1. The concentration of the electrolyte is independent of the time and the distance.

2. The limiting current in pulse electrolysis could be higher when compared with that of DC electrolysis.

3. The distance between the poles is larger than the diffusion layer, so that the cathode can be assumed to be located as for away from the electrode.

According to the Fick's second law of diffusion,

$$\frac{dC(x,t)}{dt} = D\,\frac{d^2C(x,t)}{dx^2} \quad (4.4)$$

The boundary conditions are

$C(x,t) = Co$ for $t = 0$ and for all the x values

$C(x,t) = Co$ for $t > 0$ and $x = 0$

$$\frac{D(dC(x,t))}{dt} = \frac{I}{nF} \text{ for t >0 and } x = dl$$

While $I = I_p$, for all T_{on} time, and

$I = 0$ for all T_{off} time.

Table C.1 Simulated grinding forces for the conventional grinding process

Cumulative depth-of-cut in *mm*	Contact length in *mm*	F_N in *N*	F_t in *N*
0	0	0	0
0.01	1.7320893	18.3792	1.286544
0.02	2.449598622	25.99269	1.819488
0.03	3.000200036	31.83512	2.228459
0.04	3.464409609	36.76085	2.57326
0.05	3.873413807	41.10079	2.877056
0.06	4.243206576	45.02466	3.151727
0.07	4.58328884	48.63328	3.404329
0.08	4.899850834	51.99232	3.639462
0.09	5.197192215	55.14741	3.860318
0.1	5.478443467	58.13176	4.069223
0.11	5.745967801	60.97046	4.267933
0.12	6.001601153	63.68299	4.457809
0.13	6.246803518	66.28483	4.639938
0.14	6.482758624	68.78855	4.815199
0.15	6.710442015	71.2045	4.984315
0.16	6.930668959	73.54133	5.147893
0.17	7.144129057	75.80635	5.306445
0.18 0.18	7.351411795	78.00583	5.460408

Table C.2 Simulated grinding forces for ELID grinding

Cumulative depth-of-cut in *mm*	Contact length in *mm*	F_N in *N*	F_t in *N*
0	0	0	0
0.01	1.7320893	11.80679	0.590339
0.02	2.449598622	16.69769	0.834884
0.03	3.000200036	20.45086	1.022543
0.04	3.464409609	23.61515	1.180757
0.05	3.873413807	26.40313	1.320156
0.06	4.243206576	28.92382	1.446191
0.07	4.58328884	31.24199	1.562099
0.08	4.899850834	33.39983	1.669992
0.09	5.197192215	35.42666	1.771333
0.1	5.478443467	37.34381	1.86719
0.11	5.745967801	39.16739	1.958369
0.12	6.001601153	40.90991	2.045496
0.13	6.246803518	42.58134	2.129067
0.14	6.482758624	44.18972	2.209486
0.15	6.710442015	45.74173	2.287086
0.16	6.930668959	47.2429	2.362145
0.17	7.144129057	48.69796	2.434898
0.18	7.351411795	50.1109	2.505545